AN ABSTRACT OF THE DISSERTATION OF

Emily S. Bellis for the degree of Doctor of Philosophy in Integrative Biology presented on June 1, 2017.

Title: Evolutionary Insights into Cnidarian-Dinoflagellate Symbiosis from Natural Variation in *Aiptasia* Sea Anemones.

Abstract approved: _____

Dee R. Denver

Mutualistic associations between corals and symbiotic microalgae of the genus *Symbiodium* power tropical reef ecosystems, hotspots of marine biodiversity that buffer coastlines, support tourism- and fisheries-based economies, and offer untapped potential for discovery of novel pharmaceutical compounds. However, reef ecosystems are declining at an alarming rate, in large part due to severe episodes of coral bleaching, or breakdown of the coral-*Symbiodinium* symbiosis. The sea anemone *Aiptasia* has emerged as a laboratory model system for understanding coral-*Symbiodinium* interactions at multiple biological levels. To further develop *Aiptasia* as an evolutionary model system, the goal of my dissertation work was to characterize natural variation in *Aiptasia*-*Symbiodinium* symbioses by (1) examining genome-wide polymorphism among global anemone lineages, (2) experimentally evaluating natural variation in bleaching response, and (3) investigating patterns of genetic variation in natural populations across diverse abiotic environments. In Chapter 2, I use low-coverage genome skimming to investigate polymorphism in well-studied laboratory strains hosting diverse *Symbiodinium*, revealing that higher genetic diversity exists in *Aiptasia* from the Western Atlantic compared to a more globally distributed lineage. I further compare polymorphisms in sliding windows across the genome to identify candidate genes under balancing and positive selection

based on patterns of heterozygosity, nucleotide diversity, and Tajima's D. In Chapter 3, I characterize bleaching of *Aiptasia* lab strains to different stressors and discover significant variation in responses to acute heat stress but not to cold-shock. In Chapter 4, I examine potential relationships between abiotic environmental variation and genetic variation of anemone-*Symbiodinium* assemblages in the wild, at four locations in Caribbean Panama where long-term environmental datasets are available. High-throughput genotyping of anemone populations revealed the presence of a closely related cryptic species, *Exaiptasia brasiliensis,* and striking differences in anemone abundance, distribution, and patterns of symbiont association across environments. An *Aiptasia* sub-population specific to the Bocas del Toro Archipelago is described, with strong differentiation compared to the global population at several loci predicted to be important for mediating interactions with *Symbiodinium.* Analyses further suggest that the spatial extent of clonal reproduction in natural populations could be somewhat limited. Overall, Chapters 2-4 support a widespread global *Aiptasia* population distributed throughout tropical and subtropical latitudes with one or more diverged lineages, diversity of both host lineages and holobiont assemblages centered in the tropical Western Atlantic, and holobiont distribution patterns that may be strongly influenced by abiotic environment. Future studies leveraging natural variation in the *Aiptasia* model system described here hold great promise for advancing our fundamental knowledge of the evolution of symbiotic interactions in the sea.

Evolutionary Insights into Cnidarian-Dinoflagellate Symbiosis from Natural Variation in *Aiptasia* Sea Anemones

by
Emily S. Bellis

A DISSERTATION

submitted to

Oregon State University

in partial fulfillment of
the requirements for the
degree of

Doctor of Philosophy

Presented June 1, 2017
Commencement June 2017

Doctor of Philosophy dissertation of Emily S. Bellis presented on June 1, 2017.

APPROVED:

Major Professor, representing Integrative Biology

Chair of the Department of Integrative Biology

Dean of the Graduate School

I understand that my dissertation will become part of the permanent collection of Oregon State University libraries. My signature below authorizes release of my dissertation to any reader upon request.

Emily S. Bellis, Author

ACKNOWLEDGEMENTS

This work would truly not have been possible without the support of my mentors, colleagues, friends, and family. First and foremost, I am so profoundly grateful to my advisor, Dr. Dee Denver, for giving me the opportunity to pursue this research and a strong foundation in evolutionary biology that I will build upon the rest of my career. I thank Dee for so many years of sage advice (that never actually came in the form of a direct answer), for creating a training environment in which I took risks and made mistakes, and for the freedom to explore different systems and ways of thinking.

I would also like to thank my committee members for their thoughtful mentorship and for a supportive and challenging environment to grow as a scientist. Many thanks to Dr. Eli Meyer for sharing RAD-Seq and bioinformatics expertise, lab space, and equipment for multiple dissertation chapters and for conversations about the quantitative genetics of corals that greatly developed my thinking. I thank Dr. Virginia Weis for sharing her deep wisdom and her wonderful model system with me and always making me feel like part of the cnidarian research community. I am grateful to Drs. Aaron Liston and Joey Spatafora for insights that have altered my research and training trajectories on several occasions. Several graduate courses continue to influence my thinking about evolution, photosynthesis, scientific writing, data analysis, and the process of teaching and learning, and I thank Drs. Steve Arnold, Michael Behrenfeld, Shawn O'Neil, and Jessica White for their exceptional contributions to those courses.

I owe a huge debt of gratitude to the Denver lab members past and present for their support over the years. I thank Dr. Amanda Brown for frank conversations about symbiosis evolution and life in general and Dana Howe, whom I will greatly miss getting to see in the lab every day, for preparing so many genomic libraries with me. Four undergraduate students were instrumental in the care and maintenance of anemones over

the years, and I would like to especially thank Reid Edlund for his hard work and endless enthusiasm (and for coming all the way to Panama to help me collect sea anemones).

As part of the Integrative Biology Department, I have been so lucky to interact with a bright and engaging community of fellow graduate students who have become my dearest friends and closest colleagues along the way. In particular I thank Dr. Riana Wernick, my academic twin sister, for being one of the most fiercely loyal and supportive people I know. I would not have made it through the past few months without the friendship of Holland Elder and several much-needed swimming and coffee breaks. In addition, I do not believe I would have ever finished writing this dissertation without the support of my Friday writing group – a big thank you to Dr. Hannah Tavalire for comedic interludes and for getting us organized every week and to Trang Dang for her sunny and unfaltering confidence in us all throughout many rainy afternoons at Imagine. I am grateful to Katherine Denemark, for everything, and for reading through my entire dissertation to share her poetic perspective.

Finally, I am immensely appreciative of my family for their humor, love, and support along the way. I would like to thank my parents, for teaching me to marvel at the world and encouraging an early curiosity about the ocean and its inhabitants. Thank you to Kevin for always being there for me, my rock, my love.

CONTRIBUTION OF AUTHORS

Chapter 2: Dr. Dee Denver helped conceive of the project, assisted with writing, provided valuable advice for data analysis, and support for sequencing. Dana Howe assisted with experimental design, genomic library preparation, and contributed valuable feedback to writing.

Chapter 3: Dr. Dee Denver helped conceive of the project, provided advice for experimental design, and contributed integral assistance to writing.

Chapter 4: Reid Edlund helped with data collection and designed and performed the *Symbiodinium* genotyping assay. Hazel Berrios helped with data collection and provided advice for the sampling protocol. Dr. Harilaos Lessios helped conceive of the project and with logistical planning of the experiments in addition to providing laboratory space in Panama City for sample processing. Dr. Dee Denver helped conceive of the project and contributed invaluably to data interpretation, writing, and support for sequencing.

TABLE OF CONTENTS

TABLE OF CONTENTS (Continued)

LIST OF FIGURES

LIST OF TABLES

LIST OF APPENDIX FIGURES

LIST OF APPENDIX TABLES

In loving memory of
Grant Risch, Ellie Risch, Anthony Hiscocks,
and Olivia Bellis

Evolutionary Insights into Cnidarian-Dinoflagellate Symbiosis from Natural Variation in *Aiptasia* Sea Anemones

CHAPTER 1 – Introduction

Many marine organisms depend on mutualistic relationships with photosynthetic microalgae. Examples include reef-building corals, sea anemones, jellyfish, sponges, molluscs, and foraminaferans (Pochon *et al.* 2006). These mutualisms, however, are often sensitive to high ocean temperatures, and increased symbiosis breakdown is occurring in response to global climate change. How marine symbioses will evolve in response to rapid climate change remains unknown. A major obstacle in understanding these crucial symbiosis systems is the challenge of complementing ecological studies with basic insights from laboratory-based approaches (Weis *et al.* 2008). For many marine species, it is impossible to maintain large laboratory populations, propagate genetically controlled lines, or create different host-symbiont combinations. The dissertation research presented here seeks to connect laboratory and ecological approaches by studying natural variation in the sea anemone *Aiptasia*, a laboratory model for coral symbiosis. This work explicitly combines multiple perspectives that include field-based studies of *Aiptasia* populations in Caribbean Panama, laboratory investigations of bleaching variation, and *in silico* analyses of genome-wide polymorphism and evolutionary patterns. By illuminating the genetic landscape of *Aiptasia-Symbiodinium* interactions across genome, organism, and population levels, this body of work contributes to improved understanding of the mechanisms through which symbiotic cnidarians respond to environmental change.

SYMBIOSIS: THE FOUNDATION OF CORAL REEF ECOSYSTEMS

Intimate symbiotic relationships between coral animals and photosynthetic microalgae of the genus *Symbiodinium* serve as the foundation for coral reef ecosystems. Corals are marine invertebrates that produce the calcareous architecture of critically important reef ecosystems. Diverse species with different growth forms create branching, table-like, and foliose structures of calcium carbonate that together provide habitat complexity for over 25% of known marine species, despite covering less than 1% of the ocean floor (Moberg & Folke 1999). By harboring such tremendous biodiversity, coral reefs support fisheries- and tourism-based coastal economies, provide nutrition for

local communities, and are a promising source of discovery for novel therapeutic compounds (Moberg & Folke 1999; Brañа *et al.* 2015). Almost 40% of the world's population live within 100 km of the coast; the homes of approximately 200 million of these people are protected by coral reefs, valuable natural barriers that dissipate wave energy and mitigate erosion, flooding, and storm damage (Ferrario *et al.* 2014). While their full value is difficult to estimate, coral reef ecosystems may provide global economic benefit of more than $375 billion USD annually (Costanza *et al.* 1997).

Interactions with *Symbiodinium* facilitate the success of corals in oligotrophic tropical waters. This symbiosis funnels energy from photons of sunlight through algal photosynthesis and into cnidarian metabolism to generate the calcium carbonate framework of coral reef ecosystems (Gattuso *et al.* 1999; Lipschultz & Cook 2002). *Symbiodinium* living inside host endodermal cells receive access to carbon dioxide, inorganic nutrients, protection from herbivory, and a fixed position in the water column to access sunlight (Davy *et al.* 2012). In return, the coral host receives fixed carbon compounds produced through algal photosynthesis that support a large portion of host metabolic demands (Muscatine *et al.* 1984). Translocated compounds may include glucose, glycerol, organic acids and/or amino acids (Muscatine *et al.* 1984; Yellowlees *et al.* 2008; Davy *et al.* 2012; Burriesci *et al.* 2012). In reef-building corals, the presence of *Symbiodinium* also enhances calcification and net accretion of the coral skeleton, perhaps by altering the inorganic chemical environment of host tissues or producing high-energy compounds and precursors needed to synthesize the skeletal organic matrix (Gattuso *et al.* 1999; Davy *et al.* 2012).

Symbiotic relationships with *Symbiodinium* have facilitated the success of reef-building corals in tropical waters, but may also render reef ecosystems particularly susceptible to global climate change (Six 2009; Kiers *et al.* 2010). Elevated temperatures just 1-2°C above summer maxima can trigger bleaching, or breakdown of the symbiosis resulting in loss of *Symbiodinium* cells or pigments from coral host tissues (Hoegh-Guldberg 1999; Weis 2008). Widespread bleaching in natural coral populations is most commonly attributed to elevated temperature, through other stressors such as excessively cold temperature, changes in salinity, high solar irradiation, disease, and nutrient

enrichment also induce or exacerbate bleaching (Brown 1997; Weis 2008; Vega Thurber *et al.* 2014). At the molecular level, elevated temperature and light are thought to increase production of harmful reactive oxygen species (ROS) in *Symbiodinium* chloroplasts through back-up of excitation energy at photosystem II; this may occur through damage to the water-splitting D1 protein of photosystem II, reduced photosystem repair, or inhibition of the dark reactions of photosynthesis (Douglas 2003; Takahashi *et al.* 2004; Weis 2008). Damage to thylakoid membranes could also lead to energetic uncoupling whereby electrons are harvested and O_2 is generated by photosystem II, but proton leak prevents production of ATP needed for photosynthesis (Tchernov *et al.* 2004). Host cell mitochondria are another important though sometimes neglected source of ROS production in cnidarians under thermal stress, and differences in heat tolerance of *Acropora* corals from the Great Barrier Reef may be partly attributable to genetic variation in nuclear-encoded mitochondrial membrane components (Nii & Muscatine 1997; Dunn *et al.* 2012; Dixon *et al.* 2015). Ultimately, oxidative stress that overwhelms ROS-scavenging responses of the holobiont leads to loss of symbionts through cellular mechanisms including exocytosis, host cell detachment, *in situ* degradation, apoptosis, and/or necrosis (Weis 2008). Severe bleaching without re-establishment of the symbiosis is associated with increased coral mortality and degradation of reef ecosystems (Hoegh-Guldberg 1999).

MECHANISMS OF RESILIENCE

The question of whether corals have the capacity to adapt in pace with global climate change remains a topic of utmost concern (Glynn 1991; Brown 1997; Pandolfi *et al.* 2011; Hughes *et al.* 2017). Four mechanisms have been proposed that could contribute to the resilience of coral reef ecosystems in the coming decades. These mechanisms include physiological acclimatization, host-symbiont partner switching, range shifts, or evolutionary adaptation via genetic change in either or both partners (Weis 2010; Pandolfi *et al.* 2011; Hoegh-Guldberg 2012). As ocean temperatures continue to rise, a unified framework for understanding the relative importance of each of these mechanisms in shaping holobiont responses to long-term environmental change will

be crucial for developing effective strategies to conserve and manage invaluable reef ecosystems (Kiers *et al.* 2010; van Oppen *et al.* 2015).

Physiological Acclimatization

The most rapid of the four mechanisms described here, acclimatization refers to a process through which an organism can respond to environmental change within its lifetime and includes alterations in behavior, morphology, and physiology (Gates & Edmunds 1999; Edmunds & Gates 2008). Previous studies support substantial capacity for acclimation (in experimental lab conditions) or acclimatization (in natural environments) for both symbiosis partners. For example, short-term thermal preconditioning decreased bleaching in experimental studies of two *Acropora* species and was correlated with differential expression of host genes (Middlebrook *et al.* 2008; Bellantuono *et al.* 2012a; b). Decreased mortality under experimental heat stress was observed for a coral population that naturally experiences variable temperature regimes relative to a population from a more stable, cooler site (Oliver & Palumbi 2011). Though the two populations hosted distinct *Symbiodinium* communities, a large proportion of differences in thermal tolerance are attributable to changes in gene expression rather than host genetic adaptation or symbiont type, suggesting populations from the highly variable site are naturally acclimatized (Barshis *et al.* 2013; Palumbi *et al.* 2014). Experimental acclimation also reduces heat stress in *Symbiodinium* grown at elevated temperatures (Takahashi *et al.* 2013), though strong transcriptional responses to heat stress can be conspicuously absent (Barshis *et al.* 2014; but see Levin *et al.* 2016). These and other studies suggest that long-lasting epigenetic alterations, phenotypic plasticity, and other acclimatory mechanisms will help modulate coral responses to environmental stress (Brown 1997; Gittins *et al.* 2015; Putnam & Gates 2015). However, the extent to which acclimatization will contribute to long-term resilience relative to other processes remains uncertain (Edmunds & Gates 2008).

Partner shifts

The second mechanism, partner shifting, has important consequences for both

short-term persistence and long-term evolution because association with different symbiont types impacts host fitness through reproduction, growth rate, and bleaching susceptibility (Sampayo *et al.* 2008; Abrego *et al.* 2008; Cantin *et al.* 2009; Jones & Berkelmans 2010, 2011). Partner shifts may occur by increasing abundance of tolerant algae types previously present at low concentration (symbiont "shuffling") or acquiring new algae from the environment (symbiont "switching") (Buddemeier & Fautin 1993; Baker 2001). Analysis of ancient DNA from dried coral tissue revealed remarkable stability in octocoral-associated *Symbiodinium* over the past century, consistent with other studies suggesting that partner switches to completely novel symbiont types may be unlikely (Berkelmans & van Oppen 2006; Coffroth *et al.* 2010; Baker *et al.* 2013).

Acquisition of compatible symbionts from the environment involves a complex process of recognition, entry into host cells, and symbiosis maintenance (Davy *et al.* 2012). During onset of the symbiosis, host cells must first detect presence of the algae, which may involve interactions between microbe-associated molecular patterns on the surface of the *Symbiodinium* cell and pattern recognition receptors either secreted by host cells or integrated into host cell membranes. Glycan-lectin interactions, involved in activating the complement pathway of the innate immune system, have received particular attention in studies focused on cnidarian-dinoflagellate symbiosis onset (Wood-Charlson *et al.* 2006; Davy *et al.* 2012; Poole *et al.* 2016). However, other pattern recognition receptors including toll-like receptors, scavenger receptors, and nod-like receptors may also play an important role in cnidarian-dinoflagellate recognition (Meyer & Weis 2012; Neubauer *et al.* 2016). Following recognition, *Symbiodinium* are able to enter host cells through phagocytosis, and phagosomes with healthy, compatible symbionts manage to avoid lysosomal fusion to persist in the host cell as symbiosomes (Fitt & Trench 1983; Chen *et al.* 2003). Post-phagocytotic sorting may then occur through selective apoptosis of host cells containing incompatible symbiont types (Dunn & Weis 2009).

This 'winnowing' process contributes to a certain level of specificity in cnidarian-*Symbiodinium* symbioses, however, partner shifts have been observed in natural populations of cnidarians following bleaching and in transplant experiments (Berkelmans

& van Oppen 2006; Baird *et al.* 2007; Jones *et al.* 2008; Dimond *et al.* 2013; Cunning *et al.* 2015b). *Symbiodinium* exhibit striking diversity and are classified into 9 subgeneric clades designated A-I (Pochon *et al.* 2006; Pochon & Gates 2010). In the absence of prolonged stress, most sampled colonies form stable associations with a dominant *Symbiodinium* type, though many cnidarian species can associate with representatives of multiple clades and several types within the same clade (Baker 2003; Baird *et al.* 2007). Advances in molecular techniques have also revealed greater flexibility in many cnidarian-dinoflagellate symbioses than previously appreciated and the potential functional importance of low-abundance background populations (Fabina *et al.* 2012; Silverstein *et al.* 2012; Cunning *et al.* 2013). The identity of the dominant type can be strikingly correlated with environmental variation across the host range and even within a single colony (Rowan *et al.* 1997; Yang *et al.* 2012; Keshavmurthy *et al.* 2012). Correspondingly, association with different *Symbiodinium* genotypes has been shown to confer elevated thermal tolerance and may contribute to remarkable ecological flexibility in cnidarian-dinoflagellate symbioses (Herre *et al.* 1999). Increased thermal tolerance is often linked to trade-offs in host growth rate or reproduction, though these trade-offs may be highly context-dependent (Little *et al.* 2004; Jones & Berkelmans 2010; Cunning *et al.* 2015a). The costs and benefits associated with hosting different *Symbiodinium* in different environments will likely change as oceans warm.

Range shifts

Coral species could also respond to rising temperatures by shifting their geographic ranges poleward (Greenstein & Pandolfi 2008). Observations of two cold-susceptible *Acropora* species, *A. cervicornis* and *A. palmata,* suggest their ranges may have contracted in response to climactic cooling during the Holocene but are currently re-expanding northward along the Florida peninsula (Precht & Aronson 2004). Population genomic analyses of *A. millepora* from the Great Barrier Reef provided some evidence for preferential survival of larvae from warm-adapted populations migrating southward, though no recent increase in southward migration was detected (Matz *et al.* 2017). Based on a predictive model including 12 coral species, most corals could lose 25-50% of their

current habitat by the year 2100, though some species may avoid substantial habitat loss given a moderate capacity to adapt to elevated temperature (Cacciapaglia & van Woesik 2015). Loss of susceptible species may facilitate colonization by thermotolerant competitors, resulting in marked changes in the community structure of future coral assemblages (Greenstein & Pandolfi 2008; Cacciapaglia & van Woesik 2015; Prada *et al.* 2016). Poleward migration may need to occur at an unreasonably rapid rate (~40-70 km per decade by 2070) to mitigate ecological and economic losses associated with large-scale degradation of reef ecosystems (Hoegh-Guldberg 2012; Couce *et al.* 2013).

Adaptation

Adaptation via standard evolutionary-genetic mechanisms would be expected on longer timescales than acclimatization or symbiont switching (Hoegh-Guldberg *et al.* 2007; Baird & Maynard 2008; Hoegh-Guldberg 2012). With long generation times and limited gene flow from warm-adapted populations in some cases, many coral host species may have limited capacity for rapid adaptation (Babcock 1991; Hoegh-Guldberg 2009). *Symbiodinium* may have much greater potential for rapid adaptation facilitated by large population sizes, higher heritability of thermal tolerance traits, and generation times on the order of days to months (Smith & Muscatine 1999; Rowan 2004; Császár *et al.* 2010; Howells *et al.* 2012; but see Thornhill *et al.* 2017). Whether or not this disparity in adaptive rates could promote genetic conflict between partners likely depends on symbiont transmission mode and local population dynamics (Sachs & Wilcox 2006; Fabina *et al.* 2012; Lesser *et al.* 2013). In contrast to broadcast-spawning corals, most brooding corals transmit symbionts vertically, which promotes cooperation and host-symbiont specificity generally associated with decreased environmental sensitivity (Putnam *et al.* 2012). Brooders may also have more limited capacity for dispersal (Underwood *et al.* 2007). Therefore, the contribution of local host genetic adaptation to variation in bleaching susceptibility may be greater in brooding compared to spawning corals as suggested by Kenkel *et al.* (2013). Broadcast-spawning corals with greater amounts of gene flow among populations may depend more so on horizontal acquisition of locally adapted symbionts or acclimatization (Barshis *et al.* 2013). Importantly, genetic

adaptation, acclimatization capacity, symbiont shifts, and changes in geographic range are not independent processes (Bay & Palumbi 2014; Palumbi *et al.* 2014). For instance, degree of phenotypic plasticity in thermal tolerance traits can evolve via genetic change and is influenced by interactions among particular symbiont types and their hosts (Via & Lande 1985).

UNIFYING RESEARCH FROM CELLS TO ECOSYSTEMS

A complete understanding of climate change impacts on cnidarian-*Symbiodinium* interactions requires integration of knowledge from both partners in the symbiosis across molecule and ecosystem levels. However, strong divisions of labor have historically persisted within the field, with ecology and molecular biology or host-centric and symbiont-centric work often performed separately. For example, a great deal of our knowledge of cnidarian-*Symbiodinium* interactions at the cellular level comes from studies of the laboratory model anemone *Aiptasia* (Weis *et al.* 2008; Davy *et al.* 2012). Yet natural populations are rarely studied, and only recently have researchers begun to explore the evolutionary history of *Aiptasia*, despite half a century of laboratory studies utilizing this important model system (Blanquet 1968; Thornhill *et al.* 2013; Grajales & Rodríguez 2016). Conversely, the majority of field studies on cnidarian-*Symbiodinium* interactions have focused on ecologically important reef-building corals, though corals present particular challenges for further study of the symbiosis at the molecular level (Weis *et al.* 2008). Research focused on biology of *Symbiodinium* and cnidarian host species has also remained somewhat disconnected. For example, only a limited number of studies have simultaneously investigated population genetic variation in both host cnidarians and their associated *Symbiodinium* (Santos 2014). This lack of information regarding natural genetic variation hinders our ability to accurately determine the adaptive potential of cnidarian symbioses and increases uncertainty of predictive models, since including adaptive responses can significantly alter projections of coral reef futures (Parkinson & Baums 2014; Logan *et al.* 2014). With ever-improving analytical methods and advances in genome sequencing technology, we are poised for a breakthrough in our understanding of the extent and mechanisms through which cnidarian symbioses could

adapt to climate change (Meyer & Weis 2012). This invaluable knowledge will require an integrated approach that leverages methods from diverse disciplines and synthesizes information across levels of biological organization.

Aiptasia *as a model system*

Tropical sea anemones in the genus *Aiptasia* have a rich history as a laboratory model system for cell biology studies of cnidarian symbiosis and show great potential as an evolutionary model system (Hoegh-Guldberg *et al.* 2007; Weis *et al.* 2008). Like most broadcast-spawning corals, *Aiptasia* transmits symbionts horizontally and reproduces both asexually or sexually by releasing gametes into the water column (Clayton 1985). Asexual reproduction through pedal laceration allows large, genetically homogeneous populations of anemones to be maintained and propagated in the laboratory. Both the algal endosymbiont and the anemone host can be cultured separately, and aposymbiotic hosts and larvae can be infected with cultured symbionts (Belda-Baillie *et al.* 2002; Wolfowicz *et al.* 2016). Gene knockdown can be performed via RNA interference (Dunn *et al.* 2007a) and use of morpholinos (P. Cleeves, pers. comm.), and lack of a calcium carbonate skeleton facilitates application of additional molecular biological techniques (Weis *et al.* 2008). *Aiptasia* naturally associate with representatives of *Symbiodinium* clades A and B, including *S. psygmophilum* (clade B2) and geographically distinct populations of *S. minutum* (clade B1) (Belda-Baillie *et al.* 2002; Goulet *et al.* 2005; Lajeunesse *et al.* 2012; Thornhill *et al.* 2013; Grajales *et al.* 2016). Natural associations with *Symbiodinium* clade C have also been observed (Lajeunesse *et al.* 2012; Grajales *et al.* 2016). Sixteen *Aiptasia* species have been described, though recent molecular and morphological evidence supports unification as a single species (Thornhill *et al.* 2013; Grajales & Rodríguez 2014). Grajales and colleagues also described a cryptic sister species, *Exaiptasia brasiliensis*, that was restricted to the Southwestern Caribbean Sea and Southwestern Atlantic Ocean and associated with only clade A *Symbiodinium* (Grajales & Rodríguez 2014, 2016). The first population genetic analysis of *Aiptasia* suggested that specificity of *Aiptasia* symbioses could be linked to host genotype based on the presence of two genetically

distinct populations: a globally widespread population that naturally harbored only *S. minutum* and a separate population from Florida that formed associations with diverse *Symbiodinium* clades (Thornhill *et al.* 2013). With numerous transcriptomic and genomic resources available for both *Aiptasia* and *S. minutum* and considerable variation in symbiotic associations observed in the wild, *Aiptasia* is a promising model system for investigating evolutionary dynamics of marine symbioses (Shoguchi *et al.* 2013; Lehnert *et al.* 2014; Baumgarten *et al.* 2015; Xiang *et al.* 2015).

Dissertation outline

To better understand eco-evolutionary dynamics of cnidarian-dinoflagellate symbioses, the work presented here examines natural variation across genomes, individuals, and populations of the model sea anemone *Aiptasia*. First, I present a general introduction to the importance of cnidarian symbiosis and an overview of four interacting mechanisms through which symbiotic cnidarian species could respond to environmental change. In Chapter 2, I use low-coverage genome sequencing to examine evolutionary relationships among well-studied laboratory strains of the sea anemone *Aiptasia* from globally widespread locations, including representatives of *A. pulchella* and *A. pallida.* Analyses are performed to evaluate the hypothesis that geographically separate populations are genetically distinct, with the prediction that lineages with similar geographic origins or patterns of symbiont association will share evolutionary history. This study provides important evolutionary context for interpretation of results from the later data chapters and previous studies utilizing the *Aiptasia* model system. Functional differences among laboratory strains are then explored in Chapter 3 by comparing natural variation in bleaching in response to two distinct stressors: acute heat stress and pulsed cold-shock. I examine the hypothesis that trade-offs exist in bleaching responses to different stressors, corresponding with the prediction that heat-tolerant lineages will exhibit significantly higher susceptibility to cold stress. The potential for thermal environment to influence distribution and diversity of natural host-symbiont assemblages is explored in the final data chapter (Chapter 4). In this study, anemone populations of *Aiptasia* and *E. brasiliensis* are investigated from thermally stressful and stable

environments in Caribbean Panama. By comparing abundance, distribution, and genetic diversity of both host and symbiont populations, I evaluate three hypotheses: (i) population structure of anemone holobionts is consistent with isolation by distance; (ii) different host and symbiont populations are specialized for particular habitats; and (iii) stressful environments promote antagonistic evolutionary dynamics. Finally, in Chapter 5, I synthesize findings from the data chapters presented here and discuss future prospects of the *Aiptasia* model system for contributing to our understanding of the evolution of marine symbioses.

CHAPTER 2 – Genome-wide polymorphism and signatures of selection in the symbiotic sea anemone *Aiptasia*

Emily S. Bellis, Dana K. Howe, and Dee R. Denver

Published in:
BMC Genomics
Volume 17, page 160
BioMed Central Ltd.,
New York, NY

ABSTRACT

Coral reef ecosystems are declining in response to global climate change and anthropogenic impacts. Yet patterns of standing genetic variation within cnidarian species, a major determinant of adaptive potential, are virtually unknown at genome-scale resolution. We explore patterns of genome-wide polymorphism and identify candidate loci under selection in the sea anemone *Aiptasia*, an important laboratory model system for studying the symbiosis between corals and dinoflagellate algae of the genus *Symbiodinium*.

Low coverage genome sequencing revealed large genetic distances among globally widespread lineages, novel candidate targets of selection, and considerably higher heterozygosity than previously reported for *Aiptasia*. More than 670,000 single nucleotide polymorphisms were identified among 10 *Aiptasia* individuals including two pairs of genetic clones. Evolutionary relationships based on genome-wide polymorphism supported the current paradigm of a genetically distinct population from the US South Atlantic that harbors diverse *Symbiodinium* clades. However, anemones from the US South Atlantic demonstrated a striking lack of shared derived polymorphism. Heterozygosity was an important feature shaping nucleotide diversity patterns: at any given SNP site, more than a third of individuals genotyped were heterozygotes, and heterozygosity within individual genomes ranged from 0.37–0.58%. Analysis of nonsynonymous and synonymous sites suggested that highly heterozygous regions are evolving under relaxed purifying selection compared to the rest of the *Aiptasia* genome. Genes previously identified as having elevated evolutionary rates in *Aiptasia* compared to other cnidarians were found in our study to be under strong purifying selection within *Aiptasia*. Candidate targets of selection, including lectins and genes involved in Rho GTPase signalling, were identified based on unusual signatures of nucleotide diversity, Tajima's D, and heterozygosity compared to genome-wide averages.

This study represents the first genome-wide analysis of Tajima's D in a cnidarian. Our results shed light on patterns of intraspecific genome-wide polymorphism in a model for studies of coral-algae symbiosis and present genetic targets for future research on evolutionary and cellular processes in early-diverging metazoans.

INTRODUCTION

Intimate mutualistic associations between photosynthetic algae and invertebrates are integral to the ecology of marine environments. Perhaps the most well-studied invertebrate-algal symbiosis is that between reef-building corals and unicellular photosynthetic algae of the genus *Symbiodinium,* though endosymbioses with *Symbiodinium* are pervasive throughout the phylum Cnidaria, which includes corals, jellyfish, and sea anemones. In these nutritional symbioses, algal symbionts reside inside cells of the cnidarian gastroderm, where they can access CO_2 and other host metabolic byproducts containing nitrogen and phosphorus (Davy *et al.* 2012). In return, the cnidarian host receives compounds derived from algal photosynthesis that support host growth, reproduction, and metabolism (Muscatine *et al.* 1984). The impact of this relationship extends beyond the cnidarian host and algal symbiont to influence the tremendous biodiversity harbored by coral reefs, the cycling of nutrients in oligotrophic marine environments, and fisheries and tourism-based economies that depend on healthy reef ecosystems.

Rising ocean temperatures disrupt invertebrate-algal symbioses, causing expulsion of symbiotic algae from cnidarian host tissues, or "bleaching" (Douglas 2003; Weis 2008). Yet, the processes through which corals might respond to ocean warming in the long-term remain unclear (Pandolfi *et al.* 2011). Potential responses range from short-term physiological changes to those occurring on evolutionary timescales. Physiological acclimation has been increasingly shown to play a crucial role in the thermal tolerance of corals (Barshis *et al.* 2013; Palumbi *et al.* 2014). Others have suggested that corals may respond to elevated temperatures on rapid timescales by harboring more thermally resistant *Symbiodinium* communities, either increasing abundance of background genotypes or establishing symbioses with new symbiont genotypes altogether (Buddemeier & Fautin 1993; Baker 2001; Berkelmans & van Oppen 2006). Characterized by expansive, uniquely structured genomes of ~1.5–5 Gbp (Lajeunesse *et al.* 2005; Shoguchi *et al.* 2013), *Symbiodinium* are a hyperdiverse genus organized into nine distinct subgeneric clades (clades A-I) (Pochon *et al.* 2006; Pochon & Gates 2010). Decreased bleaching has been demonstrated in corals following shifts to putatively more

thermotolerant clade D *Symbiodinium* communities (Berkelmans & van Oppen 2006; Silverstein *et al.* 2015), but symbiotic associations with more thermotolerant partners may be short-lived or come at the cost of reduced host growth (Thornhill *et al.* 2005; Coffroth *et al.* 2010; Jones & Berkelmans 2010). Nevertheless, the diversity of cnidarian-*Symbiodinium* associations regionally, temporally, and even spatially across areas of a single colony underscores the complex nature of cnidarian responses to changing environments (Rowan *et al.* 1997; Jones *et al.* 2008; Keshavmurthy *et al.* 2012).

Previous studies have revealed insights into short-term responses of corals to climate change, such as acclimation and symbiont switching, but a great deal less is known about long-term evolutionary dynamics (Hoegh-Guldberg 2012; Logan *et al.* 2014). The pattern and structure of genetic variation within cnidarian species, a crucial determinant of evolutionary adaptive potential, is virtually unknown at genome-scale resolution. Genome sequences for the non-symbiotic sea anemone *Nematostella vectensis* (Putnam *et al.* 2007), the reef-building coral *Acropora digitifera* (Shinzato *et al.* 2011), and the freshwater hydrozoan *Hydra magnipapillata* (Chapman *et al.* 2010) provide important resources for comparing evolution of early-diverging metazoan genomes. Still, few studies consider intraspecific genome-wide polymorphism in cnidarians. The exceptions include a phylogeographic study of *N. vectensis* based on several hundred SNPs identified through restriction-site-associated DNA sequencing (RAD-Seq) (Reitzel *et al.* 2013) and an analysis of polymorphism based on transcriptomes of the coral *Acropora hyacinthus* (Bay & Palumbi 2014).

A major challenge of high-throughput genome-wide surveys in corals is the limited potential for experimental follow-up studies on identified targets of interest. With long generation times and slow growth rates, corals are difficult to maintain in the laboratory and their calcium-carbonate skeletons hinder many microscopy-based molecular techniques. For these reasons, the fast-growing sea anemone *Aiptasia* has a rich and growing history as a model for cell biology studies of cnidarian-dinoflagellate symbiosis due to its rapid growth and ease of laboratory culture (note: to promote consistency with the previous literature, we use the genus name *Aiptasia* here, though

unification of several *Aiptasia spp.* as *Exaiptasia pallida* was recently proposed) (Weis *et al.* 2008; Grajales & Rodríguez 2014). Unlike many corals, both *Aiptasia* anemones and their dinoflagellate symbionts can be easily cultured in isolation, and symbiont-free hosts can be experimentally bleached and re-infected with exogenous *Symbiodinium* (Belda-Baillie *et al.* 2002). Reproduction by pedal laceration results in relatively rapid clonal generation times and enables laboratory experiments to be carried out under uniform genetic backgrounds, though *Aiptasia* also reproduce sexually through broadcast spawning (Clayton 1985).

With the recent publication of its ~260 Mbp genome, *Aiptasia* also now possesses some of the strongest genomic and transcriptomic resources currently available for a symbiotic cnidarian (Baumgarten *et al.* 2015). Sequencing of a reference transcriptome has facilitated comparison of global gene-expression differences in symbiotic versus aposymbiotic anemones, building on expressed sequence tag (EST) resources previously generated for *Aiptasia* (Sunagawa *et al.* 2009; Lehnert *et al.* 2012, 2014). Transcriptome resources exist for a clade B *Symbiodinium* strain originally isolated from *Aiptasia* strain H2, and a draft genome is available for a related clade B *Symbiodinium* isolated from the coral *Montastrea faveolata* (Lajeunesse *et al.* 2012; Shoguchi *et al.* 2013; Xiang *et al.* 2015). Host genomic and transcriptomic resources were developed using anemones from the clonal strain CC7, which naturally harbors clade A *Symbiodinium*, though *Aiptasia* associates with clade B *Symbiodinium* across much of its tropical and sub-tropical range (Grajales *et al.* 2016).

Recent studies provide some clarification on *Aiptasia*-*Symbiodinium* evolutionary dynamics (Thornhill *et al.* 2013; Grajales & Rodríguez 2016; Grajales *et al.* 2016). Thornhill et al. reported that natural *Aiptasia* populations comprise two distinct lineages with specificity for different *Symbiodinium* genotypes (Thornhill *et al.* 2013). Populations sampled in Florida hosted a diversity of symbiont genotypes, including *Symbiodinium* from three different clades (A, B, and rarely, C) (Thornhill *et al.* 2013). *Aiptasia* from all other sampled localities were more likely to associate only with *Symbiodinium* clade B (Thornhill *et al.* 2013). More recently, Grajales and Rodriguez described a new cryptic species, *Exaiptasia brasiliensis,* that co-occurs with *Aiptasia (*a.k.a. *Exaiptasia pallida)* in

Panama and Brazil but hosts a clade A *Symbiodinium* sub-type distinct from that harbored by Florida *Aiptasia* populations (Grajales & Rodríguez 2014; Grajales *et al.* 2016). Grajales et al. also discovered *Aiptasia* harboring clade A *Symbiodinium* at two other sites in the Caribbean (Grajales *et al.* 2016). However, patterns of variation among representatives of this important model species at genome-scale resolution remain unexplored.

We analyzed the genomes of 10 *Aiptasia* individuals and their associated *Symbiodinium* using a low-coverage (~10x) genomic sequencing approach. This 'genome skimming' strategy surveys a large portion of each genome at shallow coverage, including coding and noncoding nuclear DNA sequence and organelle genome sequences (Straub *et al.* 2012). We utilized data from genome skimming to assess diversity of host-associated *Symbiodinium* and investigate patterns of natural genome-wide variation among *Aiptasia* host strains, some of which have been studied in the laboratory for more than 30 years. Particular attention was paid to single nucleotide polymorphisms (SNPs) in nuclear and mitochondrial genomes, patterns of shared polymorphism among anemone hosts, and the frequency of heterozygous SNPs within and among genomes. In addition, we identified loci in the host genome that displayed unusual patterns of polymorphism based on average pairwise nucleotide diversity, Tajima's D test for neutrality, and heterozygosity. By providing a genome-scale view into patterns of genetic polymorphism in *Aiptasia,* we hope to shed light on evolutionary processes in an early diverging metazoan that is an important laboratory model for understanding cellular mechanisms of cnidarian bleaching and symbiosis.

RESULTS

Sequence yield and mapping

We sequenced 10 strains of *Aiptasia* using Hi-Seq Illumina technology and mapped the reads to a reference genome sequence from the CC7 strain (see Methods) (Baumgarten *et al.* 2015). Sequence read yield and quality varied among samples (Table 2.1). Proportions of mapped reads varied among the 10 samples, with average depth of read coverage ranging from 7x to 14x. Only 51 % of reads mapped to the

genome from UN2, whereas 86 % mapped from CC7, the clone of the individual used to generate the reference genome. Two of the sequenced individuals, BM1 and HI1, were derived from the same clonal line as BM2 and HI2 respectively. Unlike BM1 and HI1, BM2 and HI2 were aposymbiotic: they did not contain observable populations of *Symbiodinium* within host tissues. However, the proportions of mapped reads from BM1 and HI1 were within the range of values for the symbiotic samples, suggesting a relatively low contribution of *Symbiodinium* sequences to the genomic libraries.

Evolutionary relationships in Aiptasia

Analyses of evolutionary relationships among strains were based on high confidence SNPs identified with GATK (Fig. 2.1) (McKenna *et al.* 2010). Over three million high-quality SNPs were initially identified with a minimum coverage of 8x and a maximum genotype error of 0.4 %, using data from all 10 anemones. After excluding BM1 and HI1, the two aposymbiotic clones, 671,546 SNPs were called with high confidence in at least six of the eight genetically unique samples. The majority of these polymorphisms (58 %) represented transition mutations and were divided evenly between C/T and A/G mutation types. C/G, C/A, T/G and A/T transversion mutations represented 7 %, 11 %, 11 %, and 13 % of all SNPs, respectively. Most SNPs were heterozygous in at least one of the anemone genomes seqenced. However, 14,310 (~2 %) of these polymorphic sites had only homozygous calls in all samples.

Because of the large proportion of heterozygous polymorphisms observed for these samples, evolutionary history was inferred using two complimentary approaches: 1) a phylogenetic network based on 14,310 homozygous polymorphisms (Fig. 2.2a), and 2) a clustering analysis that included information from heterozygous sites (Fig. 2.2b). In the phylogenetic network, anemones from Hawaii (HI1, HI2, and HI3) clustered with UN1 and UN3 at one end of the network with relatively short branches, suggesting these anemones are more genetically similar to each other than to the other strains included in the analysis. Long branch lengths were observed for samples from Bermuda and Florida and for CC7. Evolutionary relationships inferred from phylogenetic networks were broadly consistent with results from a clustering analysis that included heterozygous sites

(Fig. 2.2). Clustering analysis also suggested that UN2, CC7, and FL1 may be part of a larger genetically related group distinct from the Hawaii and Bermuda samples.

Consistent with the notoriously slow substitution rates of sea anemone mitochondrial DNA (mtDNA) (Shearer *et al.* 2002), only three mitochondrial polymorphisms were observed. Each of these was identified in a separate sample, characterized by relatively long branch lengths in the phylogenetic network (Fig. 2.2a). CC7 had one synonymous SNP at position 19,207, in ATP synthase subunit 6 (*ATP6;* A→T). UN2 had one synonymous SNP at position 3,245, in NADH dehydrogenase subunit 5 (*ND5*; C→A). One heteroplasmic site, or a mixture of mtDNA sequence types, was observed in BM1 and BM2 anemones at position 15,357 (C/T) in the 77 bp intergenic region between cytochrome oxidase subunits I and III (*COIII* and *COI*). mtDNA coverage normalized to average coverage of nuclear exome contigs for each sample ranged from 10x to 42x, with an average of 19x (Table 2.2).

Genome-wide heterozygosity

The proportion of heterozygous sites in an individual genome (H_I), was estimated based on the SNPs identified with GATK (Fig. 2.1). H_I ranged between 0.37 and 0.58 %, with an average of 0.49 % (Table 2.2). This estimate corresponds to one heterozygous site every 206 bp. H_I in exonic regions of the genome was significantly lower than H_I in non-exon regions ($p < 0.01$, $n = 8$ strains, Wilcoxon signed-rank test). Within coding regions, heterozygosity at nonsynonymous sites (H_A) was significantly lower than heterozygosity at synonymous sites (H_S) ($p < 0.01$, $n = 8$ strains, Wilcoxon signed-rank test). The average H_S, 0.85 % was unexpectedly high relative to H_I estimates, but the former was calculated using an approach that corrected for multiple substitutions whereas the approach for the latter did not (see Methods).

Though BM1 and HI1, aposymbiotic clones of BM2 and HI2 respectively, were not included for statistical comparisons described above, H_I was analyzed in these samples to enable comparisons of genotype calls between clone pairs. Out of 568,129 SNPs with high-quality genotype calls in both HI1 and HI2, 1.3 % were called as a homozygote in one sample but a heterozygote in the other. Out of 1,086,096 SNPs with

high-quality genotype calls in both BM1 and BM2, 1.2 % were called as a homozygote in one but a heterozygote in the other. The vast majority of these discrepancies were likely to be artifacts of low coverage and the genotype calling process based on close examination of 10 randomly chosen polymorphisms called as a homozygote in one clone but a heterozygote in the other. In all 10 of these cases, reads covering the alternate allele were present in the alignments for the homozygous sample but had low mapping quality and were therefore not considered by the genotype calling program.

To evaluate heterozygosity at the population level, window heterozygosity (H_W) was calculated as the number of heterozygous individuals relative to homozygous individuals at all SNP sites in a given window of the genome (Fig. 2.3, upper panel). On average, 307 SNPs were evaluated with a standard deviation (SD) of 145 in each 100 kilobase (kb) window for calculations of H_W. Across all 100 kb windows, the average proportion of heterozygous calls relative to all called genotypes at SNP sites in a window was 0.37 (SD = 0.052). There were 72 windows with extremely high values (>3 SD from the mean) of H_W; 67 % of these windows were from seven different scaffolds that had extreme values of H_W over at least four consecutive windows (Appendix Table A2). In contrast, only 17 windows had extremely low values of H_W, and 70 % of these were from two different scaffolds with extreme values of H_W over a minimum of four consecutive windows (Appendix Table A2).

Nucleotide diversity and Tajima's D

Pairwise nucleotide diversity (π) and Tajima's D were also calculated in sliding windows across the genomes of the eight genetically unique symbiotic anemones, but these analyses were implemented using a more sophisticated approach based on genotype likelihoods rather than directly on genotype calls for each sample (Korneliussen *et al.* 2013). Using this approach, the mean π in a 100 kb window was estimated as 0.00403 (SD = 0.00134), corresponding to a pairwise difference of one nucleotide every 248 bp (Fig. 2.3, middle panel). While no regions were identified with statistically extremely low nucleotide diversity (<3 SD from the mean), 78 windows had extremely high values of nucleotide diversity (>3 SD from the mean). Over 92 % of these were consecutive

windows from four different scaffolds (Appendix Table A2). For Tajima's D, 24 consecutive windows from four different scaffolds had extremely high values (>3 SD) compared to the mean Tajima's D of −0.55 (SD = 0.34); 107 windows had extremely low values of Tajima's D, and 74 % of these were consecutive windows from nine different scaffolds (Appendix Table A2).

We further investigated genes present in the 26 regions described above that had at least four consecutive windows with extreme values of H_W, π, and Tajima's D (>3 SD from the mean, Appendix Table A2). Gene Ontology (GO) enrichment analysis of gene models present in regions with extremely high values of H_W, π, or Tajima's D revealed eight significantly ($p < 0.01$) enriched GO categories after adjustment for multiple comparisons (Appendix Table A3). The molecular function GO term with the largest number of gene models was associated with 16 genes related to carbohydrate binding ([GO:0030246]; $p < 0.001$). GO enrichment analysis of gene lists with low values of Tajima's D or H_W revealed 156 GO terms with significant ($p < 0.01$) enrichment after adjustment for multiple comparisons (Appendix Table A3). Of these 156 GO terms, 141 were associated with genes in the list of regions with extremely low values of Tajima's D. The significant enrichment of the 141 GO terms was driven by a suite of 68 gene models with high homology to Rho guanine nucleotide exchange factors (GEFs) that exhibited significant physical overlap: all were alternatively spliced variants corresponding to three tandemly arranged genes.

Evolution of protein-coding genes

To investigate genome-wide patterns of selection on protein-coding genes, H_A / H_S was calculated for 17,211 of the 29,269 gene models in the *Aiptasia* genome that had more than five heterozygous SNPs in the coding region of at least one anemone (Fig. 2.4). Of these gene models, 55 were present in a region identified with extremely high H_W, 145 were in a region with extremely low Tajima's D, 42 were in a region with extremely high Tajima's D, and 114 were present in a list of 165 genes previously identified as having elevated rates of amino acid substitution compared to other cnidarians (Baumgarten *et al.* 2015). Median H_A / H_S values were 0.22 (all genes), 0.64

(high H_W genes), 0.07 (low Tajima's D genes), 0.25 (high Tajima's D genes), and 0.07 (fast-evolving genes). Compared to the genome-wide values, H_A / H_S was significantly elevated for highly heterozygous genes ($p < 0.001$; Fig. 2.4 a and d) but not for genes with high Tajima's D ($p = 0.28$; Fig. 2.4b and e). H_A / H_S was significantly decreased for fast-evolving genes (Fig.3.4c and f) and genes with low Tajima's D (both $p < 0.001$; Fig. 2.4b and e). However, significance for the low Tajima's D group was driven by low H_A / H_S values of 33 gene models homologous to RhoGEFs; there was no evidence to suggest that median H_A / H_S of the low Tajima's D group with RhoGEFs removed was significantly decreased compared to the genome-wide median ($p = 0.9$). Most gene models with $H_A / H_S > 1$ did not have a known function (Appendix Table A4).

Characterization of Symbiodinium *communities*

Coverage of algal marker sequences varied considerably among samples, likely due to differences in algal density within hosts and/or gene copy number. Relatively few (0–7 %) of the *Symbiodinium* specific reads mapped to the internal transcribed spacer region 2 (*ITS2*) rRNA gene, suggesting *ITS2* may be present at lower copy number than mitochondrial and chloroplast sequences or that *ITS2* from some samples may have greater than 10 % nucleotide divergence compared to the reference sequence. Correspondingly, only mitochondrial and chloroplast markers were used to characterize genotypes of associated *Symbiodinium*.

Anemones in our study hosted algae with over 99 % similarity to chloroplast and mitochondrial sequences from *Symbiodinium* clades A, B1 (*S. minutum)*, and B2 (*S. psygmophilum)* (Table 2.1, Appendix Table A1) (Lajeunesse *et al.* 2012). Mixed infections were evident in two samples: UN2 and UN3. Reads from UN2 mapped to sequences from clades A and B, and there was evidence that both species of clade B were present within UN2 based on sequences from chloroplast 23S rRNA (*cp23s)* and mitochondrial cytochrome *b* (*cyt b;* Appendix Table A1; Lajeunesse *et al.* 2012). For UN3, all reads were most similar to the clade B1 *Symbiodinium* marker sequences, but we observed evidence for two different clade B1 multilocus genotypes (MLGs) within this sample (Appendix Table A1). In total, we observed evidence for at least five

distinguishable MLGs in clade B based on three nonsynonymous SNPs in *cyt b*, two synonymous SNPs in the chloroplast D1 protein of photosystem II (*psbA)*, and one insertion-deletion polymorphism (indel) in *cp23s*: two MLGs of *S. psygmophilum* (clade B2) were observed, while the other three MLGs corresponded to *S. minutum* (clade B1) (Appendix Table A1). All clade A *Symbiodinium* in our samples differed at four positions from reference sequences, with one substitution in *cp23s*, one synonymous substitution in *cyt b*, and two synonymous substitutions in *psbA*.

DISCUSSION

Evolutionary relationships in Aiptasia

Decades of laboratory research using the *Aiptasia* model system have advanced our fundamental knowledge of cnidarian-dinoflagellate symbioses, but focused investigations of evolutionary relationships among *Aiptasia* spp. and their symbiotic partners have only recently been undertaken (Thornhill *et al.* 2013; Grajales & Rodríguez 2014, 2016; Grajales *et al.* 2016). Our high-resolution genomic data were generally consistent with the observation of Thornhill et al. which revealed relatively large genetic distances between anemones naturally harboring only *Symbiodinium* clade B and a 'Florida' group that forms diverse assemblages with *Symbiodinium* of multiple clades (Fig. 2.2) (Thornhill *et al.* 2013). However, we observed substantial heterozygosity in *Aiptasia* genomes, an important consideration for marker-based analyses of genetic differentiation (Table 2.2). We estimated that an average of 37% of samples genotyped were heterozygous at any given polymorphic site (Fig. 2.3, upper panel). Nevertheless, phylogenomic networks constructed from a concatenated set of homozygous polymorphisms were supported by a clustering analysis that included heterozygous sites (Fig. 2.2). In both analyses, anemones known to originate from Hawaii, including samples originating from the same location 33 years apart, formed a distinct genetic cluster (Fig. 2.2). Anemones known or presumed to originate from the US South Atlantic formed a separate genetic cluster, to the exclusion of the Hawaii and Bermuda samples (Fig. 2.2).

Importantly, we observed few shared derived polymorphisms among samples in

the US South Atlantic cluster (Fig. 2.2). The relatively long branch lengths and large genetic distances were further supported by patterns of mtDNA polymorphism (Fig. 2.2). Only two fixed SNPs were observed in mtDNA in the ten samples sequenced for our study, consistent with the low nucleotide substitution rates characteristic of cnidarian mtDNA reported elsewhere (Shearer *et al.* 2002). However, both fixed SNPs were identified in strains harboring clade A *Symbiodinium,* though the SNPs were not shared by the two strains (Table 2.1). Correspondingly, the two anemones associated with *Symbiodinium* clade A in our study may have descended from lineages that diverged from each other a relatively long time ago. Long branch lengths and a lack of shared derived polymorphism were also observed for the Bermuda lineage, and were similarly supported by the presence of the only heteroplasmic site in mtDNA detected (Fig. 2.2). This was slightly fewer heteroplasmic sites than the 3–7 sites reported for other sea anemone species sequenced at higher depth (Emblem *et al.* 2014). Alternatively, this polymorphism could derive from a nuclear copy of mtDNA (NUMT), though NUMTs may be relatively scarce in cnidarians with circular genomes (Song *et al.* 2013), and the putatively heteroplasmic site was discovered in only one strain. Taken together, our findings imply relatively high genetic diversity within the group of *Aiptasia* that naturally forms associations with *Symbiodinium* clade A, though the small sample size and unknown origin of some samples limit the conclusions that can be drawn.

We detected multiple *Symbiodinium* genotypes in some of the symbiotic anemone samples examined, as is commonly observed in studies of coral-*Symbiodinium* symbioses (Appendix Table A1) (Silverstein *et al.* 2012; Thomas *et al.* 2014; Shinzato *et al.* 2014). Three distinct MLGs were detected among the *Symbiodinium* clade B1 associated with the Bermuda and Hawaii samples and one sample of unknown origin that clustered with the Florida group (Appendix Table A1). However, there was no clear pattern of association between host genotype and *Symbiodinium* clade B1 MLG, and one anemone, originally selected from a large stock tank of mixed host origin, hosted two MLGs of *Symbiodinium* clade B1 (Appendix Table A1). The *Aiptasia* laboratory strains genetically characterized for this study, which host *Symbiodinium* assemblages differing within and between clades, could be a useful resource for further evaluating the tradeoffs associated

with hosting genetically variable but closely related algal communities.

Genome-wide polymorphism and selection in Aiptasia

Our approach identified more than 670,000 well-supported SNPs, enabling us to investigate rates and patterns of polymorphism in *Aiptasia* at genome-scale resolution. Transition/transversion ratios were consistent with estimates from transcriptome-based analyses in *Aiptasia* (Lehnert *et al.* 2012). However, our individual heterozygosity estimate of 0.49 % was four-fold greater than the transcriptome-based estimate of 1 heterozygous site per 808 bp or 0.12 % (Lehnert *et al.* 2012), though our exonic heterozygosity estimate of 0.28 % was lowest for CC7, the strain used to generate the transcriptome reference (Table 2.2). Several additional factors may contribute to lower transcriptome-based heterozygosity estimates, such as reduced counts of heterozygotes resulting from allele expression bias, reduced ability to call SNPs at intron-exon boundaries, and reduced power for SNP discovery with a single sample compared to several. While our estimated rate of individual heterozygosity was much higher than that reported previously for *Aiptasia,* it was similar to or lower than values reported for other cnidarian genomes (*Porites australiensis*, 1.0 % (Shinzato *et al.* 2014); *Acropora digitifera,* 0.4 % (Shinzato *et al.* 2014); and *Hydra magnipapillata,* 0.69 % (Chapman *et al.* 2010). Our findings further suggest that genome-wide levels of heterozygosity may vary significantly within species (e.g., 0.37–0.58 %, Table 2.2), to an extent comparable with between-species comparisons. Notably, we did not correct for multiple substitutions or take into account heterozygous indel polymorphisms, and the values we report have therefore likely underestimated heterozygosity.

Our genome-wide estimate of nucleotide diversity (0.004 SNPs/bp surveyed) was similar to the estimated rate of individual heterozygosity (0.49 % or 0.0049 heterozygous sites/bp surveyed) (Fig. 2.3, middle panel; Table 2.2). While the values are not directly comparable due to the different analytical methodologies used to generate them, the similarity between these values is in agreement with the observation that a majority of SNP sites were heterozygous in one or more of the samples genotyped. Average pairwise nucleotide diversity was lower than the genome-wide SNP rate estimated for the sea

anemone *Nematostella* (0.0065 SNPs/bp, Putnam *et al.* 2007), but higher than estimates of average pairwise nucleotide diversity for well-studied metazoans such as *Caenorhabditis elegans* (~0.001 SNPs/bp, Swan *et al.* 2002), *Drosophila pseudoobscura* (~0.002 SNPs/bp, Kulathinal *et al.* 2009), and *Homo sapiens* (7.51 × 10−4 SNPs/bp, Sachidanandam *et al.* 2001).

The genome-wide average value of Tajima's D, −0.55, was slightly negative, indicating an excess of low frequency, unique polymorphisms compared to high-frequency, shared polymorphisms among the anemones studied in this analysis (Fig. 2.3, lower panel) (Tajima 1989). This skew towards an excess of rare alleles was corroborated by the roughly star-shaped topology of the phylogenetic network, indicating relatively few shared derived polymorphisms among the anemone lineages in this study (Fig. 2.3). Such a signature is consistent with the interpretation that most of these lineages diverged separately from a common ancestral group (e.g., population expansion after bottleneck). However, the haphazard sampling scheme used in our analysis could also account for these results. Discovery of more rare alleles is to be expected in a pooled sample of individuals from multiple subpopulations, and even very low levels of population subdivision can negatively bias the allele-frequency spectrum (Ptak & Przeworski 2002; Stadler *et al.* 2009). Though an allele-frequency based population genetic study has yet to be carried out for *Aiptasia*, further study of populations from Bermuda, Hawaii, and Florida may reveal more genetic differentiation than previously reported (Thornhill *et al.* 2013; Grajales & Rodríguez 2014, 2016).

Functional analysis of genome-wide H_A / H_S values suggested an excess of individual heterozygosity at synonymous sites compared to nonsynonymous sites, consistent with widespread purifying selection acting across *Aiptasia* protein-coding loci (Fig. 2.4). H_A / H_S values for the most highly heterozygous genes in our data set were elevated compared to the genome-wide median, indicating relaxation of purifying selection in highly heterozygous regions (Fig. 2.4a and d). We also observed significantly reduced H_A / H_S values (compared to the genome-wide median) in a set of genes previously reported to have elevated amino acid substitution rates in *Aiptasia* compared to the other cnidarians *N. vectensis, A. digitifera,* and *H. magnipapillata* (Fig. 2.4c and f)

(Baumgarten *et al.* 2015). Our analysis suggested that these 'fast-evolving' genes are subject to strong purifying selection within *Aiptasia* (Fig. 2.4). With elevated amino acid substitution rates in between-species comparisons but reduced substitution rates within-species at non-synonymous sites, these genes may have important adaptive functions unique to the *Aiptasia* lineage.

Genes in outlier regions

Genome-wide polymorphism data allowed us to scan the *Aiptasia* genome for putative candidate loci under selection. On average ~120 million sites met coverage specifications for analysis in each genome, compared to 213 Mb of sequence in the *Aiptasia* draft genome (excluding N's). Therefore, because our analysis was not fully comprehensive, we chose to focus only on the most extreme outlier regions. Regions greater than 3 SD from genome-wide means, or the 0.3 % of data that deviated most drastically, were selected for subsequent consideration. To further limit false positives, we selected regions with the strongest outlier signals that had multiple consecutive windows with extreme values.

The first set of identified genes displayed signatures of evolution under balancing selection, or selection to maintain genetic diversity. Classic targets of balancing selection include genes involved in host-microbe interaction and immunity, which is known to play an important role in cnidarian symbiosis (Meyer & Weis 2012). Genetic hallmarks of balancing selection include an excess of high-frequency polymorphisms, indicated by positive values of Tajima's D, a large number of heterozygotes (H_W), and/or high π, which is predicted to increase under long-term balancing selection (Charlesworth 2006). A history of population admixture or bottleneck may also elevate Tajima's D values, when combination of separate populations results in intermediate allele frequencies or rare alleles are eliminated. Since population demographic changes are expected to have a relatively homogeneous effect across the genome, we focused on regions that deviated most strongly from the genome-wide signal and were therefore the most likely targets of balancing selection. Loci that displayed signatures of balancing selection in our study with possible functions in cnidarian symbioses included an intelectin, several galactoside-

specific lectins, and techylectin (Appendix Table A2) (Wood-Charlson *et al.* 2006; Weis *et al.* 2008). Rab GTPase, TNF Receptor-Associated Factors (TRAFs), peroxiredoxins, ficolin, and E3 ubiquitin-protein ligases have previously been implicated in heat stress, heat acclimation and/or symbiosis in cnidarians and were also identified in our study as candidates under balancing selection (Ganot *et al.* 2011; Davy *et al.* 2012; Meyer & Weis 2012; Rosic *et al.* 2014; Palumbi *et al.* 2014).

The second set of identified genes represent candidates for positive or purifying selection based on an excess of low frequency polymorphism (Tajima's D) or a deficiency of heterozygotes (H_W). These signatures are expected when genetic variation is selected against (purifying selection) or following recovery from a selective sweep, when an advantageous allele rapidly rises to fixation and reduces genetic diversity in flanking regions (positive selection). However, negative Tajima's D values may also be expected under scenarios of population expansion or subdivision. One large candidate region with very low values of Tajima's D contained a large cluster of 68 gene models, all with homology to Rho guanine nucleotide exchange factors (Rho GEFs) and corresponding to alternatively spliced variants of 3 tandemly arranged genes. By stimulating exchange of GDP for GTP, Rho GEFs activate intracellular membrane-anchored Rho GTPases, can be targeted by invading bacterial pathogens (Boquet & Lemichez 2003), and are involved in regulation of many actin-dependent cellular processes including cell adhesion, phagocytosis, and morphogenesis (Rossman *et al.* 2005). Allene oxide synthase lipoxygenase, NF-κB repressing factor, and E3 ubiquitin-protein ligase represent additional genes with putative roles in heat stress response or cnidarian symbiosis that were identified in lists of candidate loci under positive or purifying selection (Appendix Table A2) (Davy *et al.* 2012; Rosic *et al.* 2014; Lehnert *et al.* 2014).

Finally, we discovered a suite of functionally related gene models on a scaffold with elevated signatures (>2 SD from the genome-wide mean) of Tajima's D, H_W, and nucleotide diversity (Appendix Table A5). These gene models displayed homology to fibroblast growth factors (FGFs; 3 gene models), FGF inhibitors (3 gene models), and FGF receptors (FGFRs; 7 gene models). FGFRs are characterized by an extracellular ligand region containing three immunoglobulin-like domains as well as an intracellular

tyrosine kinase domain and activate multiple signalling pathways involved in innate immunity (e.g., Ras/ERK/MAPK, PI3K/AKT, PLCγ) (Newton & Dixit 2012; Oulion *et al.* 2012). In the *Aiptasia* genome, 30 gene models are annotated as FGFRs compared to only three FGFR homologs in the *Nematostella* genome, suggesting that FGFRs may have expanded and diversified during the evolution of *Aiptasia* (Matus *et al.* 2007). Despite not meeting the 3 SD outlier requirement for any one of these statistics, genes identified in this region may be potentially interesting targets of balancing selection given their fundamental role in cell proliferation and differentiation in metazoans.

Importantly, we cannot exclude the possibility that the striking patterns of polymorphism observed for these candidate targets of selection arose as a consequence of undetected paralogy in the reference genome. Mapping reads to a duplicated gene present as a single locus in the reference could lead to the elevated values of Tajima's D, nucleotide diversity, and heterozygosity we interpreted as evidence of balancing selection. Conversely, mapping of reads from alleles that were split into distinct loci in the reference genome could lead to genetic signatures that we interpreted as evidence of positive/purifying selection. We attempted to minimize such issues by using conservative mapping quality and coverage filters and by only focusing on relatively large regions that displayed consistent signatures across multiple windows. However, additional study will be needed to clarify whether candidate genes identified in this study are indeed targets of selection and the extent to which they play an important role in the biology of early-diverging symbiotic metazoans.

CONCLUSIONS

An improved basic understanding of evolutionary processes and population-genomic structuring is crucial to predicting responses of symbiotic cnidarians, including reef-building corals, to rapid climate change (Santos 2014; Logan *et al.* 2014). Yet, few studies in cnidarian systems have investigated standing patterns of genome-wide variation, the raw material acted on by natural selection. This study provided a first look into patterns of genome-wide polymorphism in *Aiptasia,* an important laboratory model system for investigating cnidarian-dinoflagellate symbioses. We discovered relatively

large genetic distances within a group of *Aiptasia* naturally harboring diverse *Symbiodinium* clades and between *Aiptasia* from Bermuda, Florida, and Hawaii. Functional analysis of heterozygosity in coding regions suggested that highly heterozygous regions are evolving under relaxed purifying selection. In contrast, genes evolving faster in *Aiptasia* compared to other cnidarians may be subject to much stronger purifying selection than the rest of the genome. Finally, our study identified regions exhibiting striking patterns of polymorphism compared to the genome-wide landscape. Further experimental study focused on candidate loci reported here could provide additional insight into fundamental cellular processes in early-diverging symbiotic metazoans.

METHODS

Anemone strains and maintenance

We analyzed the genomes of single *Aiptasia* anemones from ten different genetic lineages, including individuals originating from Florida, Hawaii, and Bermuda (Table 2.1). Anemone strains were kindly provided by D. Kemp (FL1), J. Pringle (CC7), and V. Weis (HI1-3, UN3, and BM1-2). Animals from each lineage were maintained and propagated in individual culture dishes under ambient temperature and lighting conditions in our laboratory at Oregon State University, with the exception of BM1 and HI1, which were kept in darkness to maintain their aposymbiotic state. Water changes were performed weekly with artificial seawater (Instant Ocean, Blacksburg, VA, USA), and animals were fed freshly hatched *Artemia salina* nauplii twice weekly.

Genome sequencing

DNA for genomic library preparation was extracted from entire individual anemones (~1 cm oral disc diameter) using a DNeasy Blood and Tissue Kit (Qiagen, Valencia, CA, USA), according to the manufacturer's instructions. Libraries were prepared from 2 to 3 μg of total genomic DNA according to standard Illumina protocols, using either the Illumina TruSeq DNA sample prep kit (San Diego, CA, USA) for samples CC7, FL1, and UN2 (~200 bp fragment size) or custom adaptors for the

remaining samples (~350 bp fragment size). Paired-end, 100 bp sequencing of barcoded DNA libraries was performed over three separate runs on the Illumina HiSeq 2000 at the Center for Genome Research and Biocomputing at Oregon State University (Corvallis, OR). Raw reads are available from NCBI's Sequence Read Archive (SRA) under BioProject number PRJNA304763.

After sequencing, reads for which more than 20% of called bases had Phred quality scores <20 were excluded from the dataset. Filtered reads were then mapped to the *Aiptasia* reference genome for strain CC7 (Baumgarten *et al.* 2015) using *BWA* (aln algorithm, version 0.5.7) under default settings (Li & Durbin 2009), and PCR duplicates were removed with *Picard* version 1.114 (MarkDuplicates, http://broadinstitute.github.io/picard/). Targeted realignment around indels was performed with GATK version 2.6, first for each individual, and then for the merged dataset, requiring a minimum of 4 reads and a LOD score of 2.0 at a locus to perform realignment (DePristo *et al.* 2011).

Genome-wide diversity in Aiptasia

Evolutionary relationships among samples were assessed based on high-quality variants identified using the GATK HaplotypeCaller version 3.2 (DePristo *et al.* 2011). Genotype likelihoods were computed in gVCF mode at all loci for the 10 samples individually before joint genotyping across all samples. SNPs were extracted and filtered based on parameters recommended by GATK developers (QD < 2.0, FS > 40.0, MQ < 40, HaplotypeScore >13.0, MappingQualityRankSum < −12.5, ReadPosRankSum < −8.0) (van der Auwera *et al.* 2013). In addition, we excluded all sites with variant quality less than 50 and sites with overall coverage less than 50x or greater than 1.5 times the mean across all 10 samples (>185x), so as to minimize inclusion of paralogous genes or sites not represented in a majority of samples. Individual genotypes were called only if there was at least 8x coverage and the genotype call had less than 0.4 % chance of error (GQ ≥ 24).

Evolutionary relationships among samples were based on the filtered SNP callset with high quality genotype calls in at least six of eight genetically unique samples. After

excluding all sites with heterozygous calls in any sample, basecalls for the 14310 remaining SNP sites were concatenated into a single alignment and imported into *SplitsTree4* version 4.13.1 to construct NeighborNet phylogenetic networks based on uncorrected p-distances (Huson & Bryant 2006). For hierarchical clustering analyses, the Hamming distance for pairwise comparisons between samples was calculated including heterozygous sites. Sites for which one sample was heterozygous but the other was homozygous increased the total distance score by 0.5 whereas homozygous differences between samples increased the distance score by 1. The total distance was then normalized to the number of sites considered for each sample pair. Clustering analyses based on the resulting distance matrix were performed in *R* with the heatmap.2 function from the *gplots* package (Warnes *et al.* 2015).

To calculate H_I , genotype-level filters (GQ ≥ 24, coverage ≥ 8x) were applied to the 3 million SNP call-set for each sample separately to identify all high-quality genotype calls for that sample. Even with a minimum read coverage of 8x, the probability of sampling only one allele at a heterozygous site is $(1/2)^8$ or 0.4 %, slightly lower than the 1.3 % of sites called as homozygous in one anemone but heterozygous in another for two clone pairs. However, the number of SNPs meeting minimum thresholds for genotype calling represented a fraction of the total sites considered in each sample (~1 million SNPs vs. 120 million sites with adequate coverage) and genotyping errors of 1–2 % were thus assumed to minimally influence heterozygosity estimates. Individual heterozygosity was calculated as follows:

$$H_I = \frac{S_{HET}}{S_{TOT} - S_{N/A}}$$

where S_{HET} is the total number of high-quality heterozygous SNP sites in a sample with a minimum coverage of 8x and genotype quality of 24, S_{TOT} is the total number of sites considered that met the overall coverage requirements for both genotype calling in the sample (≥8x) and variant calling across all samples (≥50x and ≤185x), and $S_{N/A}$ is the number of variants in the call set that were unable to be called in the sample with high confidence despite passing coverage filters. SNPs were classified as exonic if annotated as in a coding region or 5'/3' untranslated region in the *Aiptasia* genome (Baumgarten *et*

al. 2015). All other positions were considered non-exonic. Heterozygosity at synonymous and non-synonymous positions was estimated for each sample separately using *KaKs_Calculator* version 2.0 with the standard genetic code and the model averaging method (Zhang *et al.* 2006). Genome-wide H_A and H_S estimates were based on average values calculated using concatenated coding regions from 100 randomly selected genes over 1,000 replicates.

Heterozygosity in sliding windows (H_W) was calculated excluding BM1 and HI1 (genetic clones of BM2 and HI2, respectively). This value was based on the set of 671,546 SNPs with high-confidence genotype calls in six of eight samples (Fig. 2.1). H_W was calculated using a custom perl script, as the number of called heterozygotes divided by the total number of called genotypes at all SNP positions within 100 kb sliding windows with a step size of 10 kb.

Nucleotide diversity and Tajima's D for the eight genetically unique samples were calculated using the software ANGSD, which estimates test statistics directly based on genotype likelihoods rather than from called genotypes (Korneliussen *et al.* 2013). Genotype likelihoods were estimated using the GATK model (−GL 2), excluding reads with mapping quality less than 30 and bases with Phred scores less than 20. We applied similar filtering criteria as for genotype calling, removing sites with overall read coverage less than 50x or greater than 1.5 times the mean, as well as sites not represented in at least six of the eight individuals. Nucleotide diversity and Tajima's D values were calculated in sliding windows of 100 kb with a step size of 10 kb.

For analysis of mitochondrial polymorphism, reads from each sample were aligned to the complete *Aiptasia* mitochondrial genome [GenBank: HG423148] using *BWA* with default settings. After removing PCR duplicates, mitochondrial SNPs were called with *SAMtool*s version 0.1.18 and manually inspected with IGV to verify SNPs and heteroplasmic sites (Li *et al.* 2009). mtDNA copy number in each sample was estimated as the ratio of average per-site coverage of the mitochondrial genome to average per-site coverage of nuclear loci.

Locus-specific patterns of polymorphism

Regions were identified as outliers if they had at least four consecutive windows with extreme (>3 SD from the mean) values of Tajima's D, H_W, or π. Analyses of Gene Ontology (GO) term enrichment for genes present in outlier regions were performed with GOEAST, using the hypergeometric test and the Yekutieli method to adjust for multiple comparisons (Zheng & Wang 2008). H_A / H_S was calculated for individual genes with *KaKs_Calculator* as described above, except only for gene models with a minimum of five heterozygous sites (Zhang *et al.* 2006). Median H_A / H_S for gene sets with high H_W, high or low Tajima's D, or a set of fast-evolving genes (Baumgarten *et al.* 2015) was compared to the median value obtained from 10,000 permutations of the same number of genes selected at random from 17,211 genes with a minimum of five heterozygous sites in at least one sample. The p-value was calculated as the number of times that the H_A / H_S of the permuted data set equaled or exceeded the observed H_A / H_S, divided by the total number of permutations (Good 2013).

Characterization of Symbiodinium *communities*

To assess genetic diversity of associated *Symbiodinium* communities, reads that did not map to the *Aiptasia* reference genome were mapped to 12 *Symbiodinium* reference sequences. Two chloroplast markers, *psbA* [GenBank: JN557866 and JN557856] and *cp23s* [GenBank: JN557995 and AY035404], were used from *Symbiodinium* clades A and B. Three mitochondrial markers from clades A and B were used, including *COI* [GenBank: JN557910 and JN557902], *COIII* [GenBank: JN557929 and JN557936], and *cyt b* [GenBank: JN557962 and JN557955]. Sequences were also included for regions spanning *ITS2* in *Symbiodinium* clades A and B isolated from *Aiptasia* [GenBank: AF427465 and AF36056].

To allow for detection of intra-clade diversity, flexible mapping parameters were used to align filtered reads from each sample to *Symbiodinium* reference sequences with *BWA* as described above (10 % divergence between a read and reference, −n 10, and 5 mismatches allowed within initial seeds, −k 5) (Li & Durbin 2009). Alignments from each sample were manually inspected using IGV version 2.3 to check for mapping errors

and evidence of intra-clade polymorphism before calculating average read coverage for each marker (Thorvaldsdóttir *et al.* 2013). Specific designation as *Symbiodinium* clade B1 or B2, which represent formally described species *S. minutum* and *S. psygmophilum* respectively, was determined based on similarity to *cp23s* and *cyt b* from *S. minutum* [GenBank: JX213587 and JX213580] or *S. psygmophilum* [GenBank: JX213590 and JX213583] (Lajeunesse *et al.* 2012).

ACKNOWLEDGMENTS

This study was funded by a National Science Foundation Graduate Research Fellowship to ESB under Grant No. 0946928. We thank V. Weis, L. Hambleton, J. Pringle, and D. Kemp for providing anemone strains, M. Dasenko for sequencing assistance, and C. Voolstra and colleagues for graciously sharing the *Aiptasia* genome and annotations ahead of publication. We also thank V. Weis, E. Meyer, members of the Denver lab, and two anonymous reviewers for invaluable comments and discussion.

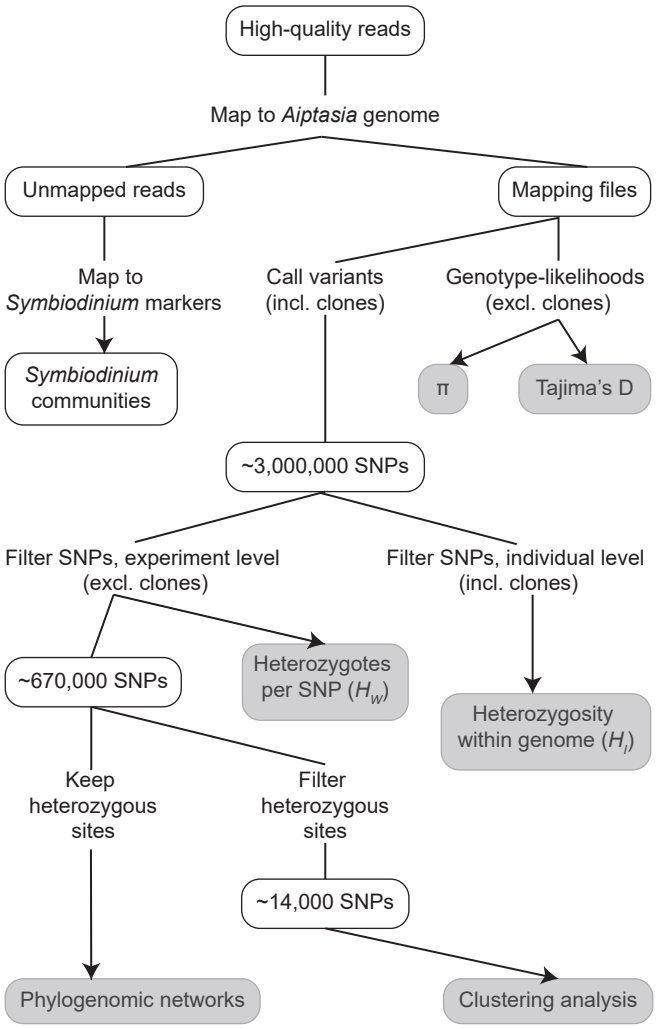

Fig. 2.1. Outline of data analysis workflow. An abbreviated workflow is shown, beginning with trimmed reads from sequencing libraries. Grey boxes represent final outputs used for tables and/or figures presented in the manuscript.

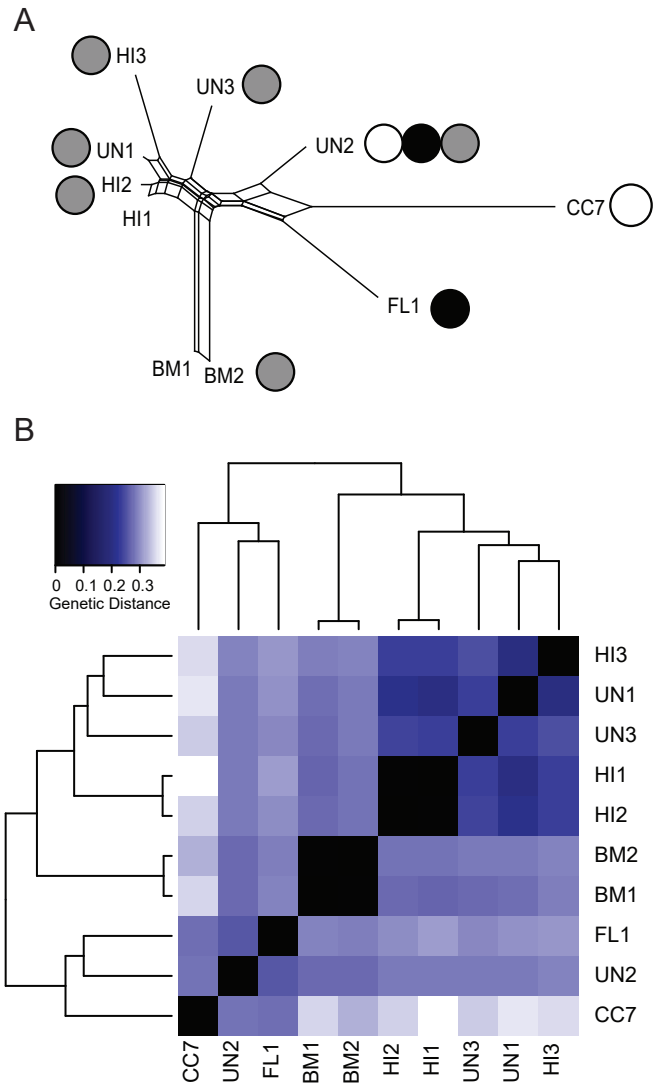

Fig. 2.2. Evolutionary relationships among *Aiptasia* lab strains. A NeighborNet phylogenetic network based on a concatenated set of 14,310 homozygous polymorphisms, ignoring heterozygous sites. Filled circles indicate genotypes of associated *Symbiodinium* algae (white: clade A, grey: clade B1, black: clade B2). The scale bar represents the number of differences per fixed polymorphic site. b Clustering analysis based on full 671,546 SNP callset, including heterozygous sites. Polymorphisms that were heterozygous in one sample received half the distance score of homozygous polymorphisms.

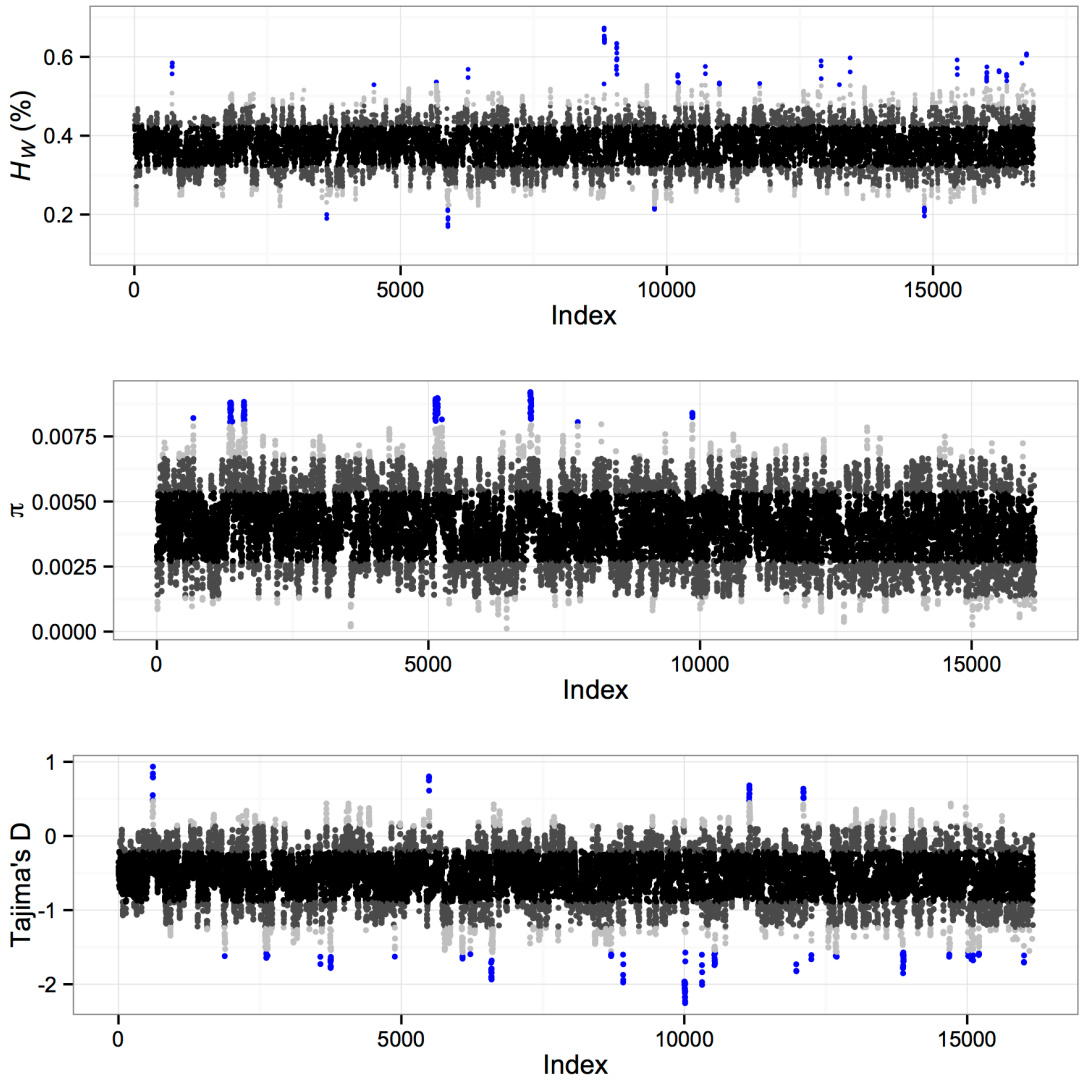

Fig. 2.3. Patterns of genome-wide polymorphism in *Aiptasia*. Genome-wide statistics were calculated in 100 kb sliding windows across the genome with a step size of 10 kb, with contigs sorted along the x-axis from longest to shortest. Each point represents a single 100 kb window and is colored according to standard deviation from the mean (black: within 1 SD, dark grey: 1–2 SD, light grey: 2–3 SD, blue: >3 SD). Proportion of heterozygous genotypes at SNP sites in a window (H_W, upper panel), average pairwise nucleotide diversity (π, middle panel), and Tajima's D (lower panel) are shown.

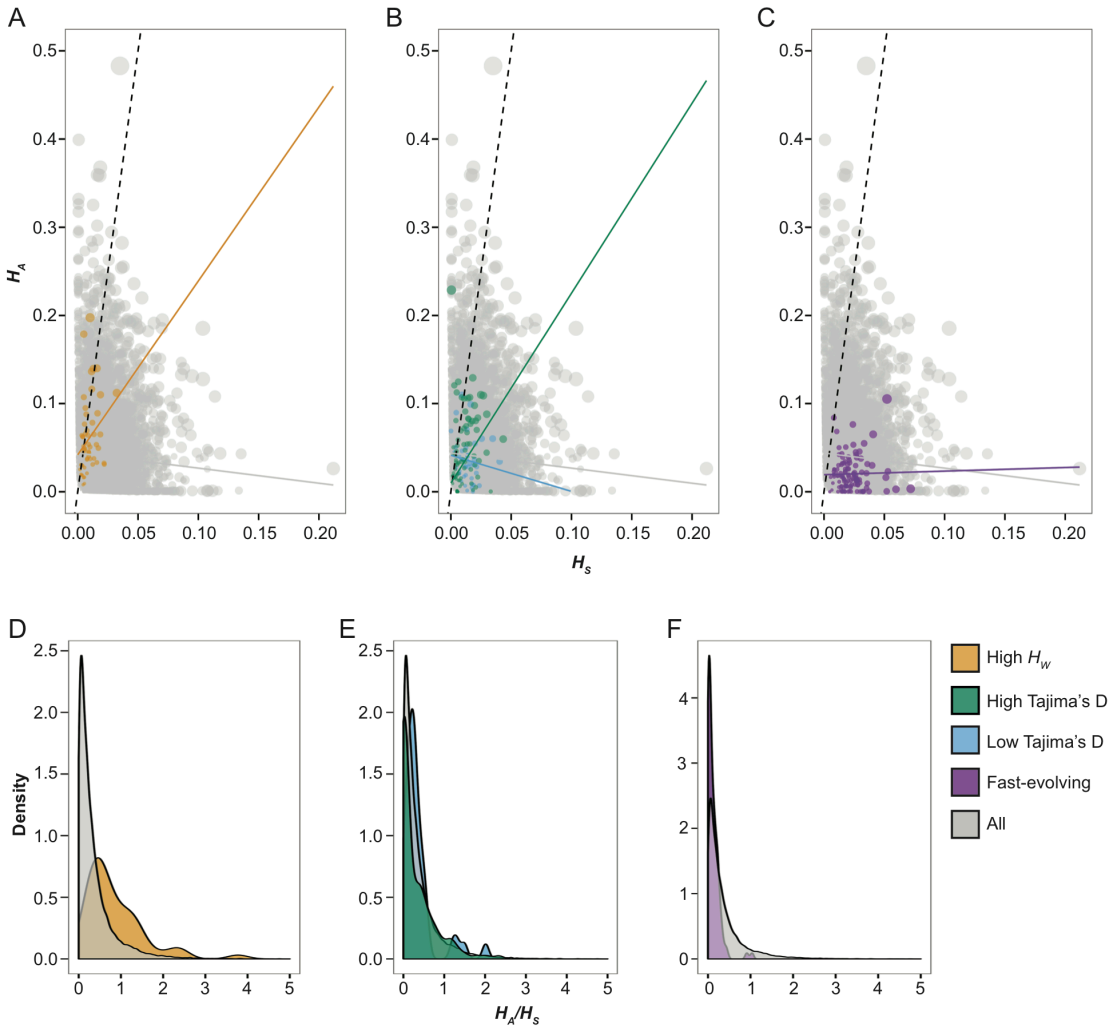

Fig. 2.4. H_A/H_S in outlier gene sets. In a–c, each point represents the heterozygosity at nonsynonymous sites (H_A) relative to synonymous sites (H_S) for a single gene, averaged across all samples with at least 5 heterozygous sites in the coding sequence. The size of the point is proportional to the average number of heterozygous sites relative to the length of the coding region. Best fit lines are shown for each gene set. Kernel density curves in d–f reflect the distribution of H_A/H_S values in each gene set.

Table 2.1. Sequencing yield of 10 *Aiptasia* strains. Anemones without algal symbionts are marked with superscripted letter a.

Sample ID	Strain Origin	Algal Genotype	Reads Sequenced (Millions)	% High Quality	% Mapped	Average Genome Coverage
BM1[a]	Walsingham Pond, Bermuda, 1980s	NA	52.76	63.8	77.0	9x
BM2	Walsingham Pond, Bermuda, 1980s	B1	66.81	60.3	74.7	11x
HI1[a]	Kaneohe Bay, Hawaii, 1979	NA	58.85	51.9	63.7	7x
HI2	Kaneohe Bay, Hawaii, 1979	B1	48.51	66.5	73.1	8x
HI3	Kaneohe Bay, Hawaii, 2012	B1	48.11	63.6	78.9	9x
FL1	Key Largo, FL, 2012	B2	52.89	84.3	77.3	13x
CC7	Wilmington, NC (Carolina Biological Supply)	A	52.34	82.4	85.5	14x
UN1	Pet Store, Corvallis, OR	B1	50.63	53.2	70.7	7x
UN2	Pet Store, Albany, OR	A, B1, B2	72.00	68.4	50.9	9x
UN3	Unknown	B1	45.66	67.9	78.4	9x

Table 2.2. Summary of genome-wide polymorphism among 10 *Aiptasia* strains. Aposymbiotic samples are marked with superscripted letter a. Individual heterozygosity, or the proportion of heterozygous sites in an individual genome, is shown for the complete genome and for non-exon, exon, non-synonymous (H_A), and synonymous positions (H_S) separately.

Sample ID	H_I (% Genome-wide)	H_I (% Non-exonic)	H_I (% Exonic)	H_A (%)	H_S (%)	mtDNA/ nDNA coverage
BM1[a]	0.520	0.544	0.475	0.193	0.979	10
BM2	0.528	0.554	0.478	0.190	0.978	11
HI1[a]	0.554	0.580	0.502	0.183	0.934	21
HI2	0.576	0.604	0.522	0.202	1.013	19
HI3	0.416	0.433	0.383	0.145	0.771	12
FL1	0.473	0.480	0.427	0.170	0.876	14
CC7	0.367	0.410	0.280	0.091	0.459	10
UN1	0.482	0.503	0.441	0.160	0.850	24
UN2	0.513	0.534	0.473	0.181	0.931	42
UN3	0.528	0.553	0.480	0.182	0.937	21
Average	0.485	0.509	0.436	0.165	0.852	19

CHAPTER 3 – Natural variation in responses to acute heat- and cold-stress in a sea anemone model system for coral bleaching

Emily S. Bellis and Dee R. Denver

Accepted, *in revision*:
Biological Bulletin
The University of Chicago Press
Chicago, IL

ABSTRACT

Rising ocean temperatures disrupt the symbiosis between corals and their microalgae, accelerating global decline of coral reef ecosystems. Due to the difficulty of performing laboratory experiments with corals, the sea anemone *Aiptasia* has emerged as an important model system for molecular studies of coral bleaching and symbiosis. Here, we investigate natural variation in bleaching responses among different genetic lineages of *Aiptasia*. Both heat- and cold-induced paths to symbiosis breakdown were analyzed. Significant genetic variation in response to acute heat stress was observed, with severe bleaching of two *Aiptasia* strains from Hawaii but minimal bleaching of four strains from the US South Atlantic, including the strain used to generate the *Aiptasia* reference genome. Both strains from Hawaii hosted *Symbiodinium* clade B1, whereas strains from the US South Atlantic hosted clades A4 or B2. In contrast to the results from exposures to acute heat-stress, negligible variation was observed in response to a pulsed cold shock, despite moderate bleaching across all strains. These results support our hypothesis that bleaching responses to distinct stressors are independent. Our findings emphasize the role of stress regime when predicting adaptive responses of symbiotic cnidarians to changing climates, as genetic variation may exist for some forms of stress-induced bleaching but not others.

INTRODUCTION

In the absence of a significant adaptive response, most of the world's coral reef cover is projected to vanish within the century (Frieler *et al.* 2012; Logan *et al.* 2014). Yet the complex nature of coral stress responses challenges our ability to accurately predict evolutionary potential. In addition to abiotic factors, coral stress responses depend on interactions among multiple organisms including the coral animal, its endosymbiotic microalgae, and numerous other mucus- or skeleton-associated microbes, all together termed the coral holobiont (Vega Thurber *et al.* 2009). In particular, the health of coral reef ecosystems hinges on mutualistic symbioses between corals and dinoflagellate microalgae of the genus *Symbiodinium*. *Symbiodinium*, a hyperdiverse taxon comprising 9 subgeneric clades (A-I), also forms nutritional symbioses with giant

clams, foraminaferans, and other cnidarians (e.g. sea anemones and jellyfish) (Pochon *et al.* 2006; Pochon & Gates 2010). Living inside cnidarian gastrodermal cells, *Symbiodinium* accesses inorganic nutrients in return for compounds produced through photosynthesis. Exogenous stressors induce expulsion of *Symbiodinium* cells or photosynthetic pigments from host tissues, or "bleaching", causing coral mortality in severe cases (Venn *et al.* 2006).

The primary trigger of coral bleaching in natural environments is elevated temperature, though exceedingly low temperatures, high solar radiation, nutrients, disease, and pollutants can also induce or exacerbate bleaching (Weis 2008). Severe bleaching and mortality associated with cold temperatures have been described for tropical coral populations from the Great Barrier Reef (GBR), the Caribbean, and the Arabian Gulf (Coles & Fadlallah 1991; Hoegh-Guldberg *et al.* 2005; Lirman *et al.* 2011). These natural bleaching events were associated with exposure to temperatures less than 16°C for up to 140 hours in the Florida Reef Tract, surface temperatures down to 9°C during predawn low tides for two days for the GBR, and 4 days where temperatures dropped below 12°C in the Arabian Gulf (Coles & Fadlallah 1991; Hoegh-Guldberg *et al.* 2005; Lirman *et al.* 2011). Far fewer studies have investigated coral cold tolerance compared to heat tolerance, but an experimental study of the coral *Acropora yongei* exposed to 26 ± 5°C suggests that short-term exposure to cold-stress (<5 days) may be more detrimental to photosynthesis and growth rate compared to heat stress (Roth *et al.* 2012).

Evidence exists supporting several mechanisms of coral temperature stress tolerance. For example, association with different *Symbiodinium* species or genotypes has a substantial influence on holobiont thermal tolerance (Rowan *et al.* 1997; Rowan 2004; Howells *et al.* 2012). Intraspecific genetic diversity in hosts, a major determinant of adaptive potential, also contributes to the considerable variation in bleaching observed for natural coral populations. Comparisons of reciprocally transplanted corals in American Samoa suggest that 38% of the difference in heat tolerance between populations of *Acropora hyacinthus* is attributable to fixed effects including holobiont genotype, whereas 62% can be attributed to acclimatization achievable over two years

(Palumbi *et al.* 2014). Additional studies highlight the importance of host genotype in shaping heat tolerance of *Porites astreoides* and altering photochemistry of *Symbiodinium* in *Acropora palmata* subjected to cold stress (Kenkel *et al.* 2013; Parkinson *et al.* 2015). These studies have gone far towards characterizing genetic variation in responses to single stressors in corals. However, the extent to which bleaching resistance may vary in the same population under different or combined stressors remains unclear.

A major obstacle to investigating functional variation with genotype-level resolution is the difficulty of performing laboratory experiments with corals. Corals are slow-growing and challenging to maintain, making long-term study by different investigators on the same genetic background practically impossible. For this reason and others, the tropical sea anemone *Aiptasia* sp. has emerged as a laboratory model for studies of cnidarian-dinoflagellate symbiosis (Weis *et al.* 2008; Goldstein & King 2016). *Aiptasia* grows rapidly and reproduces asexually through pedal laceration, enabling clonal strains to be maintained in large laboratory populations over long periods of time. Furthermore, extensive genomic resources are available, including a reference genome for *Aiptasia* strain CC7 and transcriptomes for both *Aiptasia* and its *Symbiodinium* (Lehnert *et al.* 2014; Baumgarten *et al.* 2015; Xiang *et al.* 2015). Like many corals, *Aiptasia* associates with a diversity of *Symbiodinium* genotypes across its geographic range: global populations most often harbor *Symbiodinium minutum* (ITS2-type clade B1), though populations in the Western Atlantic have been observed in association with other *Symbiodinium* species corresponding to clades B2, A4, and rarely, C1 (Thornhill *et al.* 2013; Grajales *et al.* 2016).

In addition to genomic resources, numerous cellular and laboratory protocols for *Aiptasia* are also available. Recently, Kirk and colleagues (*in preparation*) developed a non-destructive sampling method to measure *Symbiodinium* density in *Aiptasia.* This method uses *Symbiodinium* chlorophyll autofluorescence as a measure of chlorophyll *a* concentration and a proxy of *Symbiodinium* density. A similar approach based on chlorophyll autofluorescence in tentacles was recently used to investigate temperature dependency of *Symbiodinium* infection during symbiosis onset in *Aiptasia* (Hawkins *et*

al. 2016b). In both studies, measurements of chlorophyll autofluorescence were highly consistent with *Symbiodinium* cell counts (Hawkins *et al.* 2016b). Correlation between anemone color and chlorophyll *a* concentration or *Symbiodinium* cell density was also demonstrated for *Aiptasia* (Johnson & Goulet 2007).

In this study, we applied the *Aiptasia* model system to investigate natural variation in bleaching response. First, we used statistical analyses of anemone color and chlorophyll autofluorescence to independently verify the method of Kirk *et al.* across a broader range of anemone strains. Then, we evaluated the hypothesis (*H1*) that *Aiptasia* exhibits genetic variation in bleaching response by exposing six genetically distinct anemone strains to two different temperature stress regimes. On discovery of significant variation in bleaching, we further hypothesized that ($H1_A$) some holobiont genotypes are most resistant to breakdown, regardless of stressor type; ($H1_B$) trade-offs are associated with resistance to dissimilar stressors, such that holobionts most resistant to one bleaching stress are least resistant to another; or ($H1_C$) bleaching responses to different stressors are independent. In addition to bleaching, we tracked mortality and changes in anemone behavior over time to investigate alternate responses to thermal stress.

MATERIALS AND METHODS

Anemone strains

We analyzed bleaching responses of six genetically distinct laboratory strains of *Aiptasia* sea anemones in response to two different stressors (Table 3.1). *Aiptasia* strains were initially provided by the laboratories of J. Pringle (CC7 and H2), D. Kemp (FL1), V. Weis (FL2 and HI1), and E. Meyer (UN1). To confirm that each strain represented a unique genotype, we sequenced two *Symbiodinium* specific loci and six *Aiptasia* specific loci from three clonal representatives of each strain. DNA was extracted from whole frozen anemones using a DNeasy Blood and Tissue Kit (Qiagen, Valencia, CA, USA). *Symbiodinium* were genotyped as clade A or B based on sequencing of chloroplast photosystem II protein D1 (*psbA*) using PCR primers 5'-GGATGGGTAGAGAATGGGAATTCAG-3' and 5'-CGAGAGTTATTGAAGGAAGCATATTG-3' modified from Barbrook et al. (2006).

Further designation as clade B1 or B2 was based on sequence from chloroplast 23S ribosomal DNA (*cp23s)* (Lajeunesse *et al.* 2012). For *Aiptasia* genotyping, primers amplified DNA from six genes chosen from a random subset of *Aiptasia* gene models (Appendix Table B1) (Baumgarten *et al.* 2015). All PCR reactions were performed with EconoTaq DNA Polymerase (Lucigen, Middleton, WI, USA) according to the manufacturer's instructions with an annealing temperature of 56°C. Amplicons were sequenced using BigDye Terminators (Applied Biosystems, Waltham, MA, USA). Phylogenetic networks for *Aiptasia* were constructed in *SplitsTree4* version 4.13.1 based on sequences from six genes concatenated into a single 3.4 kb alignment with uncorrected p-distances and averaging across heterozygous sites (Huson & Bryant 2006). Sequences are available in GenBank under accessions KU847812-KU847847.

Laboratory bleaching experiment

Bleaching experiments were conducted in May - June 2015, using anemones maintained and propagated in laboratory aquaria for a minimum of one year. Seven weeks before temperature stress, 30 small polyps per strain with average oral disc diameter (ODD) 2.24 ± 0.65 (SD) mm were transferred to individual 60 x 15 mm polystyrene petri dishes and assigned to two experimental blocks. Anemones of each strain were placed in stacks of three, matched based on ODD to control for effects of size on bleaching response (Muscatine *et al.* 1991). Anemones were maintained at 25°C in an I36LL incubator (Percival Scientific, Perry, IA, USA) under a blue fluorescent light (Marine-GLO T8 15W aquarium bulb, Hagen Corp., Mansfield, MA, USA) providing a maximum 15 μmol photon m^{-2} s^{-1} at the top of stacks on a 12:12 hour light:dark cycle. Stacks in a block and dishes within a stack were rearranged daily to randomize effects of light variation. Once weekly, anemones were fed freshly hatched *Artemia salina* (Carolina Biological Supply, Burlington, NC, USA), and water changes were performed within 24 h of feeding.

After seven weeks of acclimation to incubator conditions, anemones were exposed to one of two distinct bleaching treatments. One anemone from each stack was randomly assigned to heat shock, cold shock or control treatments. Treatments were not

designed to be environmentally relevant but to facilitate comparisons with published studies that use cold-shock temperatures of 4°C and heat-stress temperatures of 34°C to elicit a marked bleaching response in *Aiptasia* (Steen & Muscatine 1987; Muscatine *et al.* 1991; Dunn *et al.* 2004, 2007b; Goulet *et al.* 2005; Tolleter *et al.* 2013; Bieri *et al.* 2016). For heat treatment, anemones were moved to an identical Percival incubator as for controls, except temperature was increased to 34°C over 10 h and maintained at 34°C for 48 h before returning anemones to the control incubator, following an experimental stress regime similar to Tolleter *et al.* (2013). For cold treatments, longer exposure times proved lethal, so anemones were exposed to two consecutive pulses of temperature stress: a 5-h exposure to 4°C, 48 h of recovery in the control incubator, and a second 2.5-h exposure to 4°C, with cold shocks initiated at the beginning of the dark phase of the light:dark cycle. Stress treatments for the second experimental block were initiated four days following stress treatments for the first block.

Measurement of bleaching response

We quantified anemone bleaching across four time points to compare natural variation in bleaching response and to evaluate the chlorophyll autofluorescence method of Kirk *et al.* (*in preparation)* across a broader range of anemone genotypes. Briefly, fluorescence measurements were obtained by collecting images of each anemone using a Zeiss Stemi 2000-C stereomicroscope (Thornwood, NY, USA) equipped with a CooLED pE-100 excitation light source (Andover, Hampshire, UK) and red filter. An excitation wavelength of 470 nm and an exposure time of 1.3 s were used for all images. Images of all anemones in a block were obtained in the mornings at four timepoints: 10 days before temperature stress (day 0), the morning before temperature stress initiation (day 10), three days following initiation of heat-shock (day 13), and five days post-exposure (day 18). Images were randomly assigned a numerical identifier before analysis with ImageJ version 1.48. The mean gray value of 20 measurements from the brightest areas of each image was used to calculate average fluorescence. Region-specific measurements were also taken for the tentacles (base), oral disc (central and peripheral), and body column, based on the average of 5 separate measurements per region per image. Region-specific

measurements were not taken if the region was not visible in the image due to the orientation of the anemone in the petri dish. Bleaching response (ΔF) was calculated as the difference in fluorescence of a treated anemone compared to the size-matched control anemone assigned to the same stack.

Our independent verification of the method served three purposes: 1) to confirm the predictive relationship between fluorescence and *Symbiodinium* density, 2) to assess stability in fluorescence values from control individuals over time during our experiment, and 3) to examine natural variation in fluorescence of different anatomical regions across anemone strains. To test whether raw fluorescence values were a significant predictor of visual bleaching score, anemone color at the end of the experiment was scored through comparison to a color reference card (CoralWatch Coral Health Chart, St. Lucia, Queensland, Australia). Color scores were based on a 6-point brightness/saturation scale (1=lightest; 6=darkest) within 4 color hues (Siebeck *et al.* 2006). Anemone color was analyzed using ordered logistic regression, with color score as the dependent variable and fluorescence at day 18 as the predictor using the 'polr' function of the MASS package version 7.3-45 (Venables & Ripley 2002).

Stability of measurements in controls was compared over four time points. Fluorescence values were negatively skewed even after data transformation, and so statistical analyses were performed using generalized linear mixed models (GLMMs). To minimize missing data, this analysis was restricted to measurements taken for tentacles and over the brightest areas of anemones (n = 10 per strain). Analyses were implemented with the 'glmer' function of the *lme4* package version 1.1.12, specifying a Gamma distribution and the identity link function (Bates *et al.* 2015). Model selection was performed through stepwise regression, with the likelihood ratio test as the search criterion and a significance level of α=0.01. Strain, anatomical region measured, day, size, block, and interaction terms between previously included predictors were investigated as possible explanatory variables for inclusion at each step of the model selection process, with individual anemone as a random effect to account for repeated measures over time. *Post hoc* tests were conducted with the 'glht' function of the *multcomp* package version 1.4-6 (Hothorn *et al.* 2008).

We also investigated natural variation in fluorescence values across different anemone strains and anatomical regions before temperature stress (n = 30 per strain). The difference between measurements on the same individual and region from days 0 and 10 was not significantly different from zero, and so fluorescence values from the two time points were averaged before further analysis (t = -1.76, d.f. = 583, P = 0.08, pairwise t-test). Average fluorescence was analyzed using generalized linear models (GLMs), implemented with the 'glm' function of the *stats* package (version 3.3.0) and specifying a Gamma distribution with the identity link function (R Core Team 2014). Model selection was performed as described for GLMMs, except region, strain, assigned treatment group, experimental block, and size were the possible explanatory variables tested.

Statistical analyses of ΔF were performed as described for GLMs except that results for each day and region were analyzed separately, and strain, experimental block, anemone size and strain by region interaction were the explanatory variables of interest for the full models. All statistical analyses were implemented in R version 3.3.0 (R Core Team 2014). R code and raw data files are available online (Bellis 2016).

Behavior and mortality

For each timepoint, we also investigated the effects of temperature stress on behavior and mortality. Based on photos taken for each timepoint, anemones were scored as 'expanded' (tentacles and oral disc fully visible), 'retracted' (tentacles and oral disc withdrawn), 'detached' (not attached to petri dish with healthy tissue appearance), or 'not alive' (tissue heavily degraded such that anatomical features were not distinguishable). In addition, several expanded anemones appeared to be missing significant proportions of tentacles on day 13. Correspondingly, we scored images from all timepoints for short tentacles, characterized as having all tentacles less than ¼ of the ODD. Measurements of tentacle length and ODD were performed in ImageJ.

RESULTS

We measured bleaching of six *Aiptasia* strains over time in response to two thermal stress regimes (Fig. 3.1, Table 3.1). The six strains included members of two

major genetic networks previously described for *Aiptasia*: the 'global' network (HI1 and H2) and the US South Atlantic network (CC7, FL1, and FL2) (Thornhill *et al.* 2013; Grawunder *et al.* 2015). Anemone strains were genetically distinct, but a strong phylogenetic signal was not observed based on 3.4 kb of aligned DNA sequence including 85 polymorphic sites (Fig. 3.1, Appendix Table B1). Anemones hosted *Symbiodinium* clades B1, B2, or A4. Only a single *Symbiodinium* genotype was detected within each anemone strain. Though our approach lacked resolution to detect genotypes present at low frequency, only a single *Symbiodinium* genotype was observed in three strains (CC7, HI1, and FL1) that were included in a previous whole genome sequencing-based analysis (Bellis *et al.* 2016).

Method verification across genotypes

Fluorescence was a highly significant predictor of visual bleaching status when measured in tentacles ($P < 0.001$, $t = 9.01$, ordered logistic regression) and over the brightest image areas ($P < 0.001$, $t = 9.46$, ordered logistic regression). The effect size was the same for both regions: for every unit increase in measured fluorescence value, anemones were 1.2 times more likely to be assigned a darker color score (Fig. 3.2). Correspondingly, we used the change in chlorophyll autofluorescence (ΔF) between size-matched pairs of control and treated anemones to measure bleaching response.

Stability of measurements over time in our experiment was investigated by comparing fluorescence in controls across four timepoints. Day was a significant predictor of raw fluorescence in controls ($P < 0.001$, LRT, Appendix Table B2). The effect of day was driven by day 18, and measurements taken on day 18 were 7.5 ± 0.6 (SE) fluorescence units lower on average than measurements taken at timepoints during the first two weeks of the experiment. It is likely that this difference resulted from changes in microscope software or hardware associated with a maintenance visit that occurred between day 13 and 18, of which we were unaware until after the experiment. Because the lower fluorescence detected on day 18 likely pertained to all anemones, it was not expected to influence our analyses of bleaching response (ΔF), which measures the difference in fluorescence values between size-matched pairs of control and treated

anemones on the same day. In addition, variation among measurements was similar on day 18 compared to the previous days (Appendix Table B2). However, for severely bleached anemones with measured fluorescence values close to the lower detection limit, it is possible that our estimates of ΔF on day 18 may underestimate the true bleaching response. After accounting for effects of day, region, and strain, block and size were not significant predictors of fluorescence in controls (P=0.55 and P=0.17, LRT).

Chlorophyll autofluorescence was also compared across anatomical regions at two time points prior to temperature stress (n = 30 per strain). Chlorophyll autofluorescence at 25°C varied significantly across strains and regions measured (Fig. 3.3, Table 3.2). In general, fluorescence values measured over the brightest areas of each image were similar to measurements from the periphery of the oral disc, but higher than measurements taken at the base of tentacles, the center of the oral disc, or the body column (Table 3.2, Fig. 3.3). With the exception of FL2, which exhibited lower fluorescence, most strains exhibited slightly higher fluorescence compared to CC7 when measured over the brightest areas of an image, but these differences were not statistically significant (P >0.01, Table 3.2). The effect of anatomical region on chlorophyll autofluorescence also depended on strain, with the most notable strain x region interaction effects for tentacles. FL1, UN1, and H2 had lower fluorescence than CC7 and HI1 when measured at the base of tentacles, while HI1 had significantly higher fluorescence than all other strains (all P < 0.001, Tukey HSD). Sample sizes for measurements of body column and oral disc were sometimes less than 30 due to the orientation of anemones in an image (e.g. side vs. bottom of petri dish), which may have reduced power to detect significant differences among strains for regions other than tentacles (Fig. 3.3). There was also some evidence for a relationship between anemone size and chlorophyll autofluorescence (P=0.05, LRT for comparison of full and reduced GLM). However, the predicted increase of 0.59 fluorescence units for every millimeter increase in oral disc diameter was minimal compared to the range of ODD sizes investigated in the study, and the effect was not significant at the chosen threshold of 0.01. No significant differences between treatment groups or experimental blocks were observed prior to temperature stress after accounting for strain and region measured.

Natural variation in bleaching response

We measured bleaching responses of anemone strains the morning after completion of temperature treatments (day 13) and five days post-recovery (day 18). Bleaching responses were analyzed as the magnitude of the difference in chlorophyll autofluorescence between a treated anemone and a size-matched control anemone of the same strain (ΔF). In the corresponding analyses (Tables 3.3-3.5), intercepts not significantly different from zero suggest similar *Symbiodinium* density in control and treated anemones. Larger, more positive values indicate a stronger bleaching response.

All strains bleached moderately in response to cold-stress, but little evidence was observed to support significant strain-specific differences (Fig. 3.4). Responses to cold-shock were analyzed using GLMs, with separate analyses for each day (13 or 18) and region (tentacle or brightest area). Raw fluorescence values in the brightest areas were typically higher than for tentacles, with less resolution to distinguish darker anemones (Fig. 3.2). This difference could contribute to the greater ΔF and larger range of values observed for tentacles on day 13 (Table 3.3). However, similar results for model selection were obtained for both regions, with strain as the only significant predictor of ΔF at day 13 and the intercept-only model exhibiting the best fit at day 18 (Table 3.3). *Post hoc* tests did not reveal significant differences in pairwise comparisons between strains based on brightest image areas ($P > 0.01$, Tukey HSD). Conversely, *post hoc* comparisons revealed decreased ΔF in tentacles of FL1 compared to UN1 or HI1 on day 13 ($P = 0.006$ and 0.005, Tukey HSD).

In contrast to the overall lack of strain-specific bleaching responses to cold-shock, significant differences were identified among strains in response to heat-stress (Fig. 3.5-3.6). Two strains originally collected from Hawaii, both associated with *Symbiodinium* clade B1, bleached severely in response to heat-stress whereas other strains exhibited resistance to heat-induced bleaching. Results were generally similar for measurements from the brightest areas of images compared to tentacles, though trends were stronger for the former. For measurements from the brightest areas of images, significant effects of strain, experimental block and anemone size were detected for both days (Table 3.4). On day 13, significant differences between strains were only observed for block B, with

strains H2 and HI2 exhibiting significantly greater bleaching compared to CC7 and FL1 and HI1 more bleached than FL2 ($P < 0.01$, Tukey HSD). Block effects were less prominent for day 18, on which both HI1 and H2 had significantly greater bleaching responses compared to all other strains in both blocks ($P < 0.01$, Tukey HSD, Table 3.4). The overall effect of block differed across strains: HI1 and H2 anemones in block B bleached more severely than anemones in block A on both days according to the brightest areas, whereas other strains in block B bleached less severely compared to block A on both days (CC7, FL1, FL2) or differed between days (UN1) (Table 3.4). No recorded differences in experimental conditions could be found to explain the origin of these block effects. After accounting for strain and block, larger anemones responded more severely to heat-stress, with an average decrease of 5.96 ± 2.01 (SE, day 13) or 3.43 ± 1.27 (SE, day 18) fluorescence units for every one mm increase in ODD $P = 0.005$, day 13; $P = 0.010$, day 18; Table 3.4). A similar effect of anemone size on bleaching responses to cold shock was previously demonstrated (Muscatine *et al.* 1991).

Change in chlorophyll autofluorescence in response to heat stress was also measured for tentacles (Fig. 3.5B). Block effects were detected on day 13, on which bleaching in block B was less severe than block A. However, block effects were less apparent for tentacle measurements than for the brightest areas as evidenced by absence of strain x block interaction effects on day 13 or a main effect of block on day 18 (Table 3.5). H2 was significantly more bleached than CC7, UN1, or FL2 on day 13 and more bleached than FL1 or FL2 on day 18 ($P < 0.01$, Tukey HSD). HI1 was excluded from comparisons of tentacle fluorescence on day 13 due to the large number of retracted individuals on this day but exhibited greater changes in fluorescence in response to heat-stress than all other strains besides H2 on day 18 ($P < 0.01$, Tukey HSD). Smaller ΔF values for FL1 and FL2 compared to UN1 and CC7 suggested that Florida strains might exhibit higher resistance to heat-induced bleaching when measured with respect to tentacles ($0.005 \leq P \leq 0.009$, Tukey HSD).

Behavior and mortality

In addition to bleaching, we tracked behavior and mortality in response to temperature stress. Behavioral responses included detachment from petri dishes and retraction of the oral disc and tentacles. Behavioral responses were most apparent on day 13 for three strains in particular: the heat-susceptible anemone strain HI1 and two heat-resistant strains that hosted *Symbiodinium* clade A4 (CC7 and FL2). On day 13, four anemones were detached from their petri dish and 11 anemones were retracted whereas on days prior to temperature stress, no unattached anemones and up to three retracted anemones were observed on either day. All 11 retracted anemones from day 13 had been subjected to heat stress and comprised four FL2 individuals, one FL1 individual, one CC7 individual (which later died), and five HI1 individuals. The four unattached anemones included two anemones exposed to heat stress (one CC7 individual and an HI1 individual that later died) and two HI1 individuals exposed to cold-shock. One cold-shocked HI1 individual was still unattached at day 18, along with one FL2 individual that had been exposed to heat stress.

Throughout the experiment, anemones were also observed for shortening of tentacles that was characterized by having all tentacles shorter than ~1/4 of the ODD. Detached tentacles were not observed during the experiment or in acquired images; shorter, stubby tentacles may therefore have resulted from either substantial degradation or contraction of the tentacle tissue. Short tentacles were most apparent at day 13; no individuals were recorded with short tentacles prior to day 13 and only three individuals were recorded on day 18, suggesting that tentacles had either significantly expanded or regenerated by this time. Twenty individuals exhibited short tentacles on day 13, including four cold-stressed individuals and 16 heat-stressed individuals (five CC7 anemones, five HI1 anemones, and six FL2 anemones). Mortality was minimal during the experiment, involving one HI2 individual exposed to heat-shock and three CC7 individuals (one from each of the three treatments).

DISCUSSION

In this study, we identified strain-specific variation in bleaching in response to acute heat-stress but not in responses to cold-shock in the sea anemone *Aiptasia.* This finding has important implications for understanding cellular mechanisms of bleaching and thermal tolerance in cnidarian-dinoflagellate symbiosis. In addition, our analyses served to independently verify a previously developed non-destructive algal quantification method across a broader range of genetic backgrounds in an important laboratory model symbiosis system.

Chlorophyll autofluorescence generally proved to be a reliable indicator of bleaching response across diverse *Aiptasia* genotypes (Fig. 3.2), but several factors warrant further discussion. First, reductions in chlorophyll fluorescence can also occur as a result of photochemical and non-photochemical quenching (NPQ), and NPQ increases under conditions associated with bleaching stress (Müller *et al.* 2001; Hill *et al.* 2005). However, relaxation of most NPQ processes occurs on timescales of seconds to hours and thus would be expected to have a greater effect during and immediately following bleaching stress rather than after 5 days of recovery under control conditions (Maxwell & Johnson 2000). Furthermore, microscopic observations of the two severely bleached strains revealed large numbers of *Symbiodinium* cells being expelled from the coelenteron after heat-stressed anemones were returned to room temperature and only small numbers of *Symbiodinium* cells remaining in host tissues at day 18, suggesting that low fluorescence values were due to loss of *Symbiodinium* rather than reductions in chlorophyll fluorescence associated with quenching or decreases in the amount of chlorophyll per symbiont cell. However, for moderately bleached anemones, potential for chlorophyll autofluorescence to change over time due to recovery of algal symbionts that were damaged but not expelled cannot be excluded.

Another factor that may influence results reported here is vertical stratification of *Symbiodinium* within host tissues. Correspondingly, measurements of tentacles may be more robust than measurements of other regions, since variation associated with differential layering of body column and oral disc tissues due to anemone position in images is avoided. In keeping with this assertion, tentacle fluorescence was found to be

more sensitive for distinguishing between darker anemones than measurements over the brightest areas of images (Fig. 3.5), which were generally higher than tentacle measurements and became saturated at lower color scores (Fig. 3.2). Future studies should exercise caution when basing interpretations on raw tentacle fluorescence, however, since our study also revealed significant variation in tentacle chlorophyll fluorescence among strains under control conditions (Fig. 3.3). Importantly, if the shorter tentacles for some strains on day 13 resulted from tissue contraction, higher fluorescence measurements in contracted tentacles could also cause underestimation of bleaching response.

Our results revealed significant genetic variation associated with response to acute heat stress in *Aiptasia* holobionts, with severe bleaching of two strains from Hawaii but minimal bleaching of four strains from the US South Atlantic (Fig. 3.5). Because strains were acclimated to laboratory culture conditions for more than one year, and no differences were observed between strains collected from the same location more than 30 years apart (HI1 vs. H2), we attribute the majority of the observed variation in bleaching to genetic differences among holobionts. Because both susceptible strains harbored *Symbiodinium* clade B1, it is unclear how much of the observed variation between susceptible and tolerant strains was attributable to host genotype, symbiont genotype, or genotype-genotype interaction. With evidence for impaired photosynthetic performance at elevated temperatures in *Aiptasia* hosting clade B compared to clade A *Symbiodinium*, it is not surprising that in our study anemones hosting *Symbiodinium* clade B1 bleached more severely under heat stress than anemones hosting *Symbiodinium* clade A (Perez *et al.* 2001; Goulet *et al.* 2005). However, to our knowledge, ours is the first study to demonstrate resistance to heat-induced bleaching in *Aiptasia* lineages naturally harboring *S. psygmophilum* (clade B2). This may be particularly interesting given that *S. psygmophilum* is considered a cold-tolerant lineage, and rapidly recovers photosynthetic efficiency after weeks of exposure to 10°C whereas *S. minutum* (clade B1) does not (Thornhill *et al.* 2008; Lajeunesse *et al.* 2012). Despite lack of a strong bleaching response, we observed some indication that elevated temperature influenced the behavior or physiology of CC7 and FL2, two heat-resistant anemone strains that hosted clade A4

Symbiodinium, indicated by shortened tentacles in both strains and retraction of FL2 anemones. The observed variability in holobiont heat stress responses may therefore result from distinctive photobiological characteristics of A4, B1, and B2 lineages in combination with host factors (Goulet *et al.* 2005; Suggett *et al.* 2015).

In response to a pulsed cold-shock, we observed moderate reductions in chlorophyll autofluorescence across all strains, but negligible strain-specific differences, even for strains hosting *Symbiodinium* lineages that exhibit cold-tolerance in culture (Thornhill *et al.* 2008; Lajeunesse *et al.* 2012). In genetically distinct colonies of the coral *Acropora palmata* associated with a single *Symbiodinium 'fitti'* strain, Parkinson *et al.* (2015) observed significant variation in photosynthetic performance under extreme cold stress correlated with differences in host gene expression. It is possible that significant variation in other traits related to symbiosis physiology may exist in *Aiptasia* under extreme cold stress but that negligible variation in outward bleaching response masks dynamic molecular interactions between host and symbiont.

With no evidence to suggest heat-susceptible strains were either more or less tolerant to cold-shock (Fig. 3.6), our findings support $H1_C$, the hypothesis of independence in bleaching responses between the two thermal stress regimes tested. A similar pattern was observed at the species level for Florida corals, with resistance to warm-water anomalies a poor predictor of responses to a severe cold-water event in 2010 (Lirman *et al.* 2011). Though inclusion of additional strains or use of different bleaching treatments might alter our conclusions, our results could suggest different cellular mechanisms of bleaching under disparate thermal stress regimes (i.e. *in situ* degradation, exocytosis, host cell detachment, host cell apoptosis, and/or host cell necrosis) (Weis 2008). Support for each of these mechanisms has been observed in *Aiptasia* subjected to various hypothermic and/or hyperthermic stress regimes, but much remains unknown regarding the relative importance of and potential interactions among these mechanisms under different environmental contexts (Steen & Muscatine 1987; Gates *et al.* 1992; Dunn *et al.* 2004, 2007b; Weis 2008). A recent study utilizing *Aiptasia* strain CC7 suggested that expulsion of intact *Symbiodinium* was the predominant bleaching mechanism under short-term heat and light stress, whereas *in situ* degradation and host

cell detachment occurred at a high frequency only during acute cold-shock (Bieri *et al.* 2016). However, important roles of host cell detachment and apoptosis under hyperthermic stress have been supported in other investigations utilizing the *Aiptasia* model system (Gates *et al.* 1992; Dunn *et al.* 2004, 2007b; Paxton *et al.* 2013). One distinction between these studies is that the latter focused on Hawaiian *Aiptasia*, found in our study to be relatively heat-susceptible compared to strain CC7 when harboring their endogenous *Symbiodinium*.

Rather than the nature of the stressor, it is possible that variation in bleaching mechanisms under different stressors is driven by the severity of stress ultimately perceived by the holobiont. One interpretation of our results is that severe photoinhibition of *S. minutum* under acute heat stress markedly increased production of harmful reactive oxygen species (ROS) compared to anemones hosting *S. linucheae* and *S. psygmophilum* (Goulet *et al.* 2005), whereas photoinhibition of all three species was similar under pulsed cold-shock. Much remains unknown regarding the cellular signaling cascades that eventually lead to loss of *Symbiodinium* (Weis 2008). However, ROS concentrations that overwhelm antioxidant responses of the holobiont are thought to play a central role in triggering early stages of the bleaching response (Lesser 2006; Weis 2008). In the most widely accepted model, temperature and/or light stress generate ROS in *Symbiodinium* chloroplasts through back-up of excitation energy at photosystem II; this may occur through damage to the water-splitting D1 protein of photosystem II, reduced photosystem repair, or inhibition of the dark reactions of photosynthesis (Douglas 2003; Takahashi *et al.* 2004; Weis 2008). Heat-induced bleaching in the absence of light has also been demonstrated in *Aiptasia*, suggesting that non-photosynthetically derived ROS or other molecular signals such as nitric oxide could also contribute to the observed variation in bleaching responses (Nii & Muscatine 1997; Dunn *et al.* 2012; Hawkins *et al.* 2013; Tolleter *et al.* 2013). Future studies comparing diverse *Aiptasia* strains and their associated *Symbiodinium* under different stress regimes could hold the key for linking holobiont production of ROS, antioxidants, and other molecules to the diverse cellular pathways mediating breakdown of the symbiosis.

ACKNOWLEDGMENTS

The authors wish to thank N. Kirk, K. Corey and V. Weis for sharing details of the algal quantification method ahead of publication. We thank R. Edlund for assistance with maintenance of anemone cultures and *Symbiodinium* genotyping, E. Meyer for use of the stereomicroscope, J. Nixon at the Center for Genome Research and Biocomputing at Oregon State University for sequencing assistance, and V. Weis and three reviewers for their instructive comments on early versions of the manuscript. C. Crowder, S. Guermond, E. Hambleton, D. Kemp, J. Pringle, and V. Weis provided anemone strains. This material is based upon work supported by a National Science Foundation Graduate Research Fellowship [0946928 to ESB].

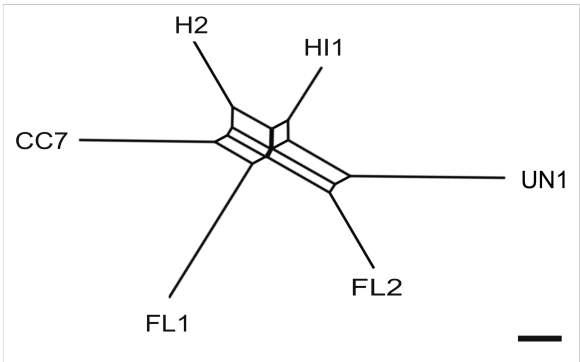

Fig. 3.1. Phylogenetic network of the six *Aiptasia* strains studied. Network was based on 3.4 kb of sequence from six nuclear genes, with genetic distance averaged across heterozygous sites. Scale bar represents 0.001 substitutions/site.

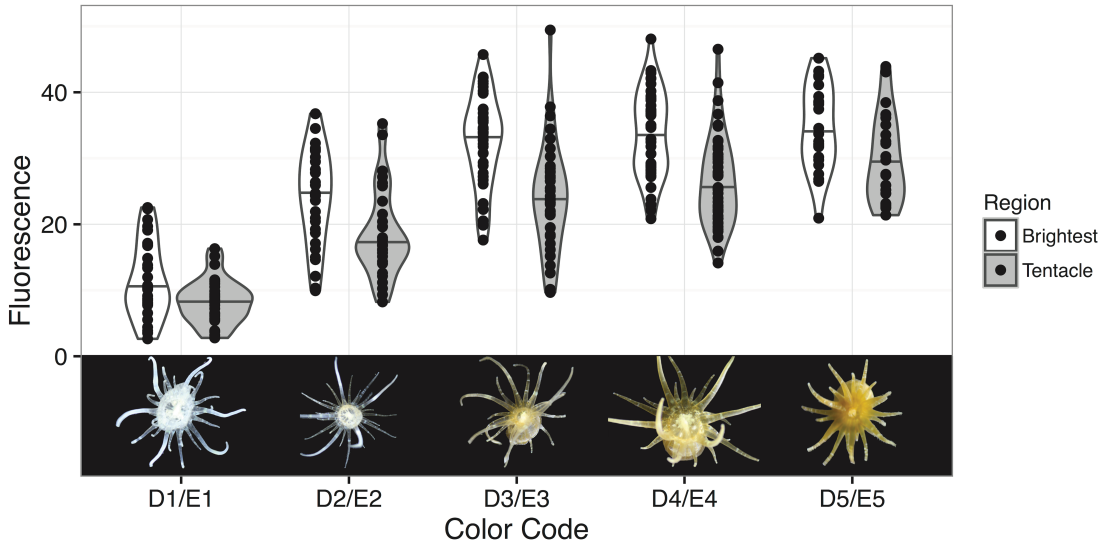

Fig. 3.2. Correspondence between chlorophyll autofluorescence and bleaching score. Analysis was based on combined data from day 18 for individuals subject to heat-shock, cold-shock, and control treatments. Horizontal bars indicate the median fluorescence for each color score. D and E refer to color hue and numeric scores (1-5) reflect brightness/saturation (Siebeck *et al.* 2006) .

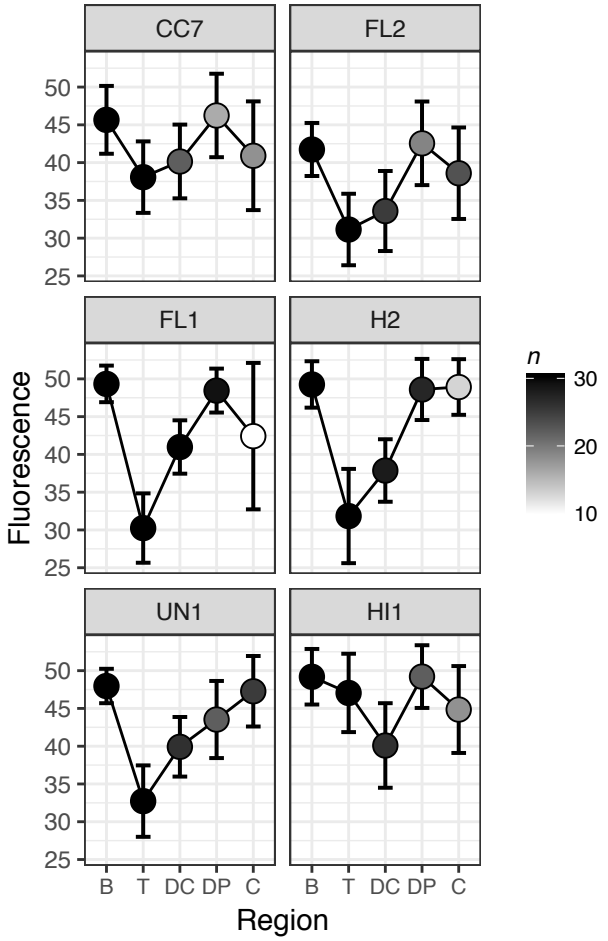

Fig. 3.3. Natural variation in chlorophyll autofluorescence at 25°C. Fluorescence was measured for each anemone for five regions: over the brightest areas of each image (B), at the base of tentacles (T), the center of the oral disc (DC), the periphery of the oral disc (DP), or the body column (C). Shown are means ± SD ($n \leq 30$ measurements per strain, indicated by point color).

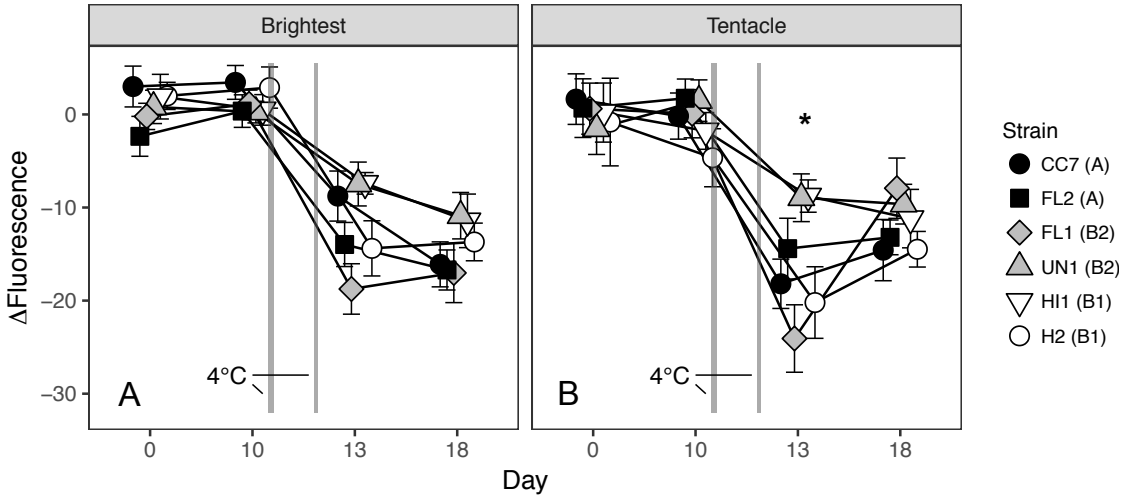

Fig. 3.4. Bleaching response to pulsed cold-shock. Asterisks indicate that strain was a significant predictor in the best-fit model and in *post hoc* pairwise comparisons ($P <$ 0.01). The *Symbiodinium* clade harbored by each strain (A, B1, or B2) is given in parentheses in the legend. Grey rectangles indicate duration and timing of the temperature treatments. Bleaching response (ΔF) was measured as difference in *Symbiodinium* chlorophyll autofluorescence between size-matched pairs of treated relative to control anemones measured over the brightest areas of each image (A) or at the base of tentacles (B). Mean ΔF ± SE is shown (n=10).

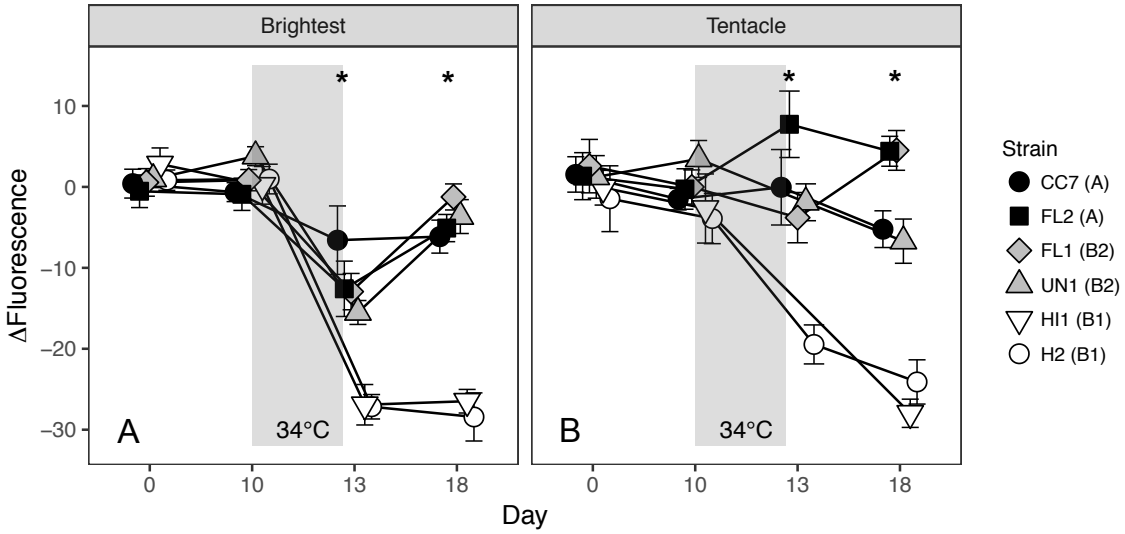

Fig. 3.5. Bleaching response to acute heat-stress. Asterisks indicate that strain was a significant predictor in the best-fit model and in *post hoc* pairwise comparisons ($P <$ 0.01). The *Symbiodinium* clade harbored by each strain (A, B1, or B2) is given in parentheses in the legend. Grey rectangles indicate duration and timing of the temperature treatments. Bleaching response (ΔF) was measured as difference in *Symbiodinium* chlorophyll autofluorescence between size-matched pairs of treated relative to control anemones measured over the brightest areas of each image (A) or at the base of tentacles (B). Mean ΔF ± SE is shown (n=10). Tentacle measurements were not obtained for HI1 at day 13 since 5 of 10 anemones were retracted and tentacles were missing or considerably contracted for the remaining anemones.

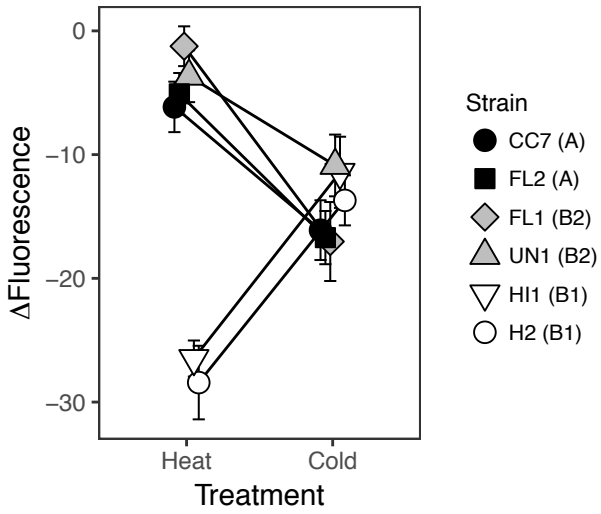

Fig. 3.6. Bleaching response reaction norm for day 18. Anemones were exposed to 48 h at 34°C or a pulsed 4°C treatment. Bleaching response (ΔF) was measured as difference in *Symbiodinium* chlorophyll autofluorescence in size-matched pairs of treated relative to control anemones measured over the brightest areas of images (mean ± SE, $n = 10$).

Table 3.1. *Aiptasia* strains studied.

Strain Name	Origin	*Symbiodinium ITS2* clade	Alternative strain names
CC7	Wilmington, North Carolina	A4	-
FL1	Key Largo, Florida, 2012	B2	DD3
FL2	St. Augustine, Florida, 2014	A4	MB1
HI1	Coconut Island, Hawaii, 1979	B1	GM10; *A. pulchella* "A"
H2	Coconut Island, Hawaii	B1	-
UN1	Aquarium, possibly from Texas Gulf, 2013	B2	EM5

Table 3.2. Fluorescence across strains and anatomical regions at 25°C. Shown are results from a GLM with strain CC7 measured over the brightest areas of each image as the reference category. Measurements for days 0 and 10 from the same individual and region were averaged before analysis. *P*-values lower than the significance threshold of 0.01 are bolded and italicized.

	Estimate	**Std. Error**	**t-value**	***P*-value**
Intercept	45.66	0.98	46.73	***<0.001***
Region				
Tentacle	-7.58	1.27	-5.96	***<0.001***
Disc_Central	-5.51	1.40	-3.93	***<0.001***
Disc_Peripheral	0.58	1.67	0.35	0.729
Column	-4.75	1.49	-3.18	***0.002***
Strain				
FL1	3.67	1.44	2.55	0.011
UN1	2.31	1.42	1.63	0.104
HI1	3.53	1.44	2.46	0.014
H2	3.60	1.44	2.50	0.013
FL2	-3.92	1.32	-2.96	***0.003***
Region:Strain				
Tentacle:FL1	-11.50	1.78	-6.48	***<0.001***
Disc_Central:FL1	-2.84	1.96	-1.45	0.147
Disc_Peripheral:FL1	-1.46	2.24	-0.65	0.513
Column:FL1	-2.16	3.40	-0.64	0.526
Tentacle:UN1	-7.65	1.78	-4.30	***<0.001***
Disc_Central UN1	-2.54	1.96	-1.29	0.197
Disc_Peripheral UN1	-5.02	2.24	-2.24	0.026
Column:UN1	4.06	2.12	1.91	0.056
Tentacle:HI1	5.44	1.93	2.82	***0.005***
Disc_Central:HI1	-3.59	1.98	-1.81	0.070
Disc_Peripheral:HI1	-0.56	2.33	-0.24	0.811
Column:HI1	0.42	2.21	0.19	0.850
Tentacle:H2	-9.84	1.79	-5.50	***<0.001***
Disc_Central:H2	-5.88	1.94	-3.03	***0.003***
Disc_Peripheral: H2	-1.24	2.26	-0.55	0.583
Column:H2	4.42	2.42	1.82	0.069
Tentacle:FL2	-3.01	1.69	-1.78	0.076
Disc_Central:FL2	-2.64	1.84	-1.43	0.152
Disc_Peripheral:FL2	0.24	2.21	0.11	0.915
Column:FL2	1.61	1.98	0.82	0.415

Table 3.3. Parameter estimates for GLMs of bleaching response to cold-shock. Measurements were taken immediate following treatment (day 13) and 5 days post-recovery (day18). *P*-values lower than the significance threshold of 0.01 are bolded and italicized.

	Estimate	**Std. Error**	***t*-value**	***P*-value**
Cold-shock (Brightest, Day 13)				
Intercept	8.77	2.17	11.40	***<0.001***
Strain				
FL1	9.98	3.74	2.67	***0.010***
UN1	-1.30	2.99	-0.43	0.667
HI1	-1.37	2.99	-0.46	0.649
H2	5.62	3.44	1.63	0.108
FL2	5.20	3.41	1.53	0.133
Cold-shock (Brightest, Day 18)				
Intercept	14.28	1.05	28.77	***<0.001***
Cold-shock (Tentacles, Day 13)				
Intercept	18.19	3.11	12.93	***<0.001***
Strain				
FL1	5.88	4.73	1.24	0.219
UN1	-9.24	3.92	-2.36	0.022
HI1	-9.42	3.92	-2.41	0.020
H2	2.02	4.64	0.44	0.666
FL2	-3.78	4.20	-0.90	0.372
Cold-shock (Tentacles, Day 18)				
Intercept	11.74	1.08	31.30	***<0.001***

Table 3.4. Parameter estimates for GLMs of bleaching response to heat-stress, measured in brightest image areas. *P*-values lower than the significance threshold of 0.01 are bolded and italicized.

	Estimate	Std. Error	*t*-value	*P*-value
Heat-shock (Brightest, Day 13)				
Intercept	3.84	5.15	3.85	***<0.001***
Strain				
FL1	-2.40	5.10	-0.47	0.640
UN1	-0.98	5.43	-0.18	0.857
HI1	6.47	5.84	1.11	0.273
H2	9.23	6.02	1.53	0.132
FL2	-2.72	5.30	-0.51	0.610
Block				
B	-17.31	4.02	-4.31	***<0.001***
Size	5.96	2.01	2.97	***0.005***
Strain:Block				
FL1:B	11.92	6.19	1.92	0.060
UN1:B	12.98	6.60	1.97	0.055
HI1:B	28.63	8.34	3.43	***0.001***
H2:B	21.00	8.21	2.56	0.014
FL2:B	7.19	6.05	1.19	0.241
Heat-shock (Brightest, Day 18)				
Intercept	2.53	4.21	4.41	***<0.001***
Strain				
FL1	-5.81	3.95	-1.47	0.149
UN1	-12.21	3.80	-3.21	***0.002***
HI1	15.98	5.12	3.12	***0.003***
H2	13.16	4.91	2.68	***0.010***
FL2	-5.23	4.07	-1.29	0.205
Block				
B	-4.73	3.98	-1.19	0.242
Size	3.43	1.27	2.71	***0.010***
Strain:Block				
FL1:B	-2.16	4.54	-0.48	0.636
UN1:B	14.28	4.73	3.02	***0.004***
HI1:B	7.81	7.00	1.12	0.271
H2:B	15.61	6.89	2.27	0.029
FL2:B	2.38	4.77	0.50	0.620

Table 3.5. Parameter estimates for GLMs of bleaching response to heat-stress, measured in tentacles. Tentacle measurements were not obtained for HI1 at day 13 since 4 of 5 anemones were retracted and tentacles were missing from the remaining anemone in block A. *P*-values lower than the significance threshold of 0.01 are bolded and italicized.

	Estimate	**Std. Error**	***t*-value**	***P*-value**
Heat-shock (Tentacles, Day 13)				
Intercept	3.69	3.17	8.11	***<0.001***
Strain				
FL1	5.24	3.68	1.43	0.163
UN1	2.66	3.40	0.78	0.439
H2	19.95	4.92	4.05	***<0.001***
FL2	-7.53	3.76	-2.01	0.053
Block				
B	-7.93	2.78	-2.86	***0.007***
Heat-shock (Tentacles, Day 18)				
Intercept	5.22	3.08	8.84	***<0.001***
Strain				
FL1	-9.73	3.50	-2.78	***0.008***
UN1	1.48	4.11	0.36	0.720
HI1	22.75	6.44	3.53	***0.001***
H2	18.88	5.77	3.27	***0.002***
FL2	-9.62	3.50	-2.75	***0.009***

CHAPTER 4 – Population genomics of cryptic species from Caribbean Panama supports habitat specialization of sea anemone-*Symbiodinium* holobionts

Emily S. Bellis, Reid Edlund, Hazel K. Berrios, Harilaos A. Lessios, and Dee R. Denver

In preparation for:
Molecular Ecology
John Wiley & Sons
111 River Street, 8-02
Hoboken, New Jersey

ABSTRACT

Coral reef ecosystems are declining globally due in large part due to rising ocean temperatures. However, the influence of warmer, more variable temperatures on evolutionary dynamics of the mutualism between corals and their intracellular photosymbionts (genus *Symbiodinium*) remains unknown. Symbiosis breakdown has the potential to elicit colonization by opportunistic or antagonistic symbionts, for example, or to facilitate switching to more environmentally tolerant partners. We investigated the possible impacts of long-term exposure to elevated, variable temperature by studying four natural populations of *Aiptasia,* a sea anemone laboratory model system for coral bleaching and symbiosis, from thermally stable and dynamic environments in Caribbean Panama. Population genomic sequencing revealed two closely related cryptic species within our dataset (*Exaiptasia brasiliensis* and the *Aiptasia* sp. laboratory model) and two distinct *Aiptasia* populations: one specific to the Bocas del Toro archipelago and the other closely related to globally widespread *Aiptasia*. Representatives of both species were found in both locations, but *Aiptasia* was more abundant attached to mangrove roots in thermally stable, intermediate light environments of the Bocas del Toro archipelago, whereas *E. brasiliensis* was common on a shoaling reef flat in Galeta characterized by high light and warmer, more variable temperatures. Patterns of *Symbiodinium* community structure also reflected environmental conditions: *S. minutum* (clade B1) dominated anemones of both species in the Bocas del Toro archipelago whereas *S. linucheae* (clade A4) dominated *E. brasiliensis* in Galeta. High-resolution genotyping suggested relatively limited spatial extent of colonization by clones. Our findings support specialization of anemone holobionts to distinct abiotic environments and emphasize the importance of characterizing both host and symbiont genetic diversity in field studies of cnidarians, for which morphological plasticity can be considerable and cryptic species are pervasive.

INTRODUCTION

Climate warming alters symbiotic interactions, disrupting mutualisms and changing parasite dynamics in terrestrial and marine ecosystems (Harvell *et al.* 2002; Six

2009; Kiers *et al.* 2010; Altizer *et al.* 2013). The far-reaching consequences of changing climates on symbioses are typified by unprecedented severity of contemporary coral bleaching events (Hughes *et al.* 2017). In most cases, bleaching is primarily attributed to elevated temperature that induces breakdown of nutritional symbiosis and loss of microalgal photosymbionts (genus *Symbiodinium*) from tissues of the coral host (Brown 1997). Bleaching is associated with decreased coral growth, fecundity, calcification, and in severe cases, mortality (Hoegh-Guldberg 1999). Mass bleaching events have become more widespread in recent years and the frequency of bleaching-level thermal stress is predicted to increase rapidly in the future (Heron *et al.* 2016).

While the ecological impacts of bleaching are well-documented, the evolutionary consequences of increased bleaching in corals are poorly understood (Hoegh-Guldberg 1999; Kiers *et al.* 2010). In the 1990s, the 'Adaptive Bleaching Hypothesis' proposed that bleaching might improve coral resilience by facilitating shifts to more thermally tolerant partners (Buddemeier & Fautin 1993; Kinzie *et al.* 2001). However, later studies revealed trade-offs associated with bleaching resistance and the tendency for natural populations to revert to their original symbiont types (Little *et al.* 2004; Sampayo *et al.* 2008; Coffroth *et al.* 2010; Jones & Berkelmans 2010, 2011; but see Cunning *et al.* 2015). Despite potential benefits of short-term ecological flexibility, theory predicts increased bleaching might promote evolutionary conflict given 1) horizontal symbiont acquisition modes typical of most coral host species, 2) significant *Symbiodinium* diversity often observed even within the same host colony, and 3) strong potential for rapid evolution in *Symbiodinium* due to shorter generation times, large effective population sizes, and probable absence of strict asexual reproduction (Herre *et al.* 1999; Sachs & Wilcox 2006; Sachs *et al.* 2011; Chi *et al.* 2014; Chakravarti *et al.* 2017; Thornhill *et al.* 2017). In contrast to predictions associated with the Adaptive Bleaching Hypothesis, the potential for colonization of bleached hosts by opportunistic symbionts to influence eco-evolutionary dynamics of cnidarian symbioses has received little attention.

Symbiodinium is a hyperdiverse genus of dinoflagellates comprising free-living, relatively opportunistic/parasitic, and mutualistic lineages that engage in symbioses with marine organisms including cnidarians (e.g. corals, sea anemones, jellyfish), sponges, and

molluscs and foraminaferans (Pochon *et al.* 2006; Takabayashi *et al.* 2011; Jeong *et al.* 2014; LaJeunesse *et al.* 2015). *Symbiodinium* taxa are organized at the subgeneric level into nine distinct clades designated A-I, though recent studies point to striking functional diversity even below the subclade level (Pochon *et al.* 2006; Pochon & Gates 2010; Parkinson *et al.* 2016). Many host species engage in stable mutualistic symbioses with representatives of multiple clades, with clades A and B particularly common in the Caribbean and among sea anemone and soft coral hosts and clade C prevalent in Indo-Pacific corals (Baker 2003; Pochon *et al.* 2006). Free-living representatives of most described clades have been found in reef habitats including the water column, sediment, coral rubble, and sea-grass beds (Takabayashi *et al.* 2011; Granados-Cifuentes *et al.* 2015). More parasitic lineages likely also exist, and several studies suggest that some members of the earliest diverging *Symbiodinium* clade (clade A) provide less benefit to hosts and exhibit opportunistic characteristics compared to more derived lineages (Stat *et al.* 2008; Lesser *et al.* 2013; LaJeunesse *et al.* 2015; Rouzé *et al.* 2016).

The sea anemone *Aiptasia* sp. is an emerging model system for studying the ecological and evolutionary dynamics of symbioses with diverse *Symbiodinium*. *Aiptasia* sp. has a rich history as a laboratory model symbiosis system, particularly at the cellular level (Weis *et al.* 2008). *Aiptasia* reproduce both sexually through broadcast spawning and asexually through pedal laceration, and large populations of genetically identical individuals can be easily propagated in the laboratory (Clayton 1985). Larvae acquire *Symbiodinium* horizontally, and bleached adults can be experimentally reinfected with cultured symbionts (Hambleton *et al.* 2014; Wolfowicz *et al.* 2016). Until recently, however, evolutionary perspectives on phylogenetic relationships and genetic diversity of the anemone host have been few (Thornhill *et al.* 2013; Grajales & Rodríguez 2014, 2016). Morphological evidence supported by molecular data suggest unification of all previously described tropical and subtropical *Aiptasia* spp. as a single species (a.k.a. *Exaiptasia pallida*; Grajales & Rodríguez 2014, 2016). Investigations by Grajales & Rodríguez (2014, 2016) also revealed a morphologically indistinguishable sister species, *E. brasiliensis*. In the first population genetic study of *Aiptasia,* Thornhill *et al.* (2013) identified a 'global' population that naturally harbors *Symbiodinium* clade B1 (*S.*

minutum) and a genetically differentiated population from Florida that hosts diverse genotypes including clade B1, clade A4, and rarely, clade C1 (Thornhill *et al.* 2013). Additional sampling efforts revealed natural associations with clades B2 (*S. psygmophilum*), C1, and A4 throughout the broader Western Atlantic (Bellis *et al.* 2016; Grajales *et al.* 2016). The diversity of *Aiptasia*-*Symbiodinium* assemblages in the Western Atlantic provides an exceptional opportunity to investigate ecological and evolutionary dynamics of the symbiosis in natural populations.

In this study, we examine natural *Aiptasia* populations in Caribbean Panama to determine if exposure to warmer, more variable temperatures could destabilize cnidarian-dinoflagellate interactions and promote antagonistic evolutionary dynamics. As a measure of host population health, anemone abundance and population genetic diversity are compared among four sites where 25 years of meteorological and oceanographic data are available. Clade-level diversity of *Symbiodinium* within anemone populations is also determined, as well as cell division rate and algal density within host tissues. Sampled sites include three locations characterized by relatively stable temperatures in the Bocas del Toro archipelago, though the inshore site, Cayo Roldán (CR), exhibits greater seasonal variation and summer maxima approximately 1°C warmer than the two other sites (Fig. 1, Kaufmann & Thompson 2005). The fourth site, Galeta, is a relatively exposed location near the Caribbean entrance to the Panama Canal characterized by the warmest temperatures with daily variation up to 3°C (Fig. 1B-C, Cubit *et al.* 1989). We evaluated three hypotheses to explain the distribution of *Aiptasia*-*Symbiodinium* diversity across these environments: (H_1) population structure of anemone holobionts is consistent with isolation by distance; (H_2) host and symbiont populations are specialized for particular habitats, with genetic differentiation between thermally stressful and stable sites but little difference in anemone abundance or population genetic diversity; and (H_3) stressful environments promote antagonistic co-evolutionary dynamics, with reduced host abundance linked to higher diversity of associated *Symbiodinium* communities. For H_3, we predicted that host genetic diversity might be either lower, resulting from loss of genetic variation due to population decline, or higher, if colonization by opportunistic symbionts drives parasitic arms race dynamics and increased rates of sexual reproduction

by hosts (King *et al.* 2009; Sachs *et al.* 2011).

MATERIALS AND METHODS

Sample collection and preparation

Aiptasia sp. sea anemones were surveyed in Summer 2015 from four sites in Caribbean Panama: Isla Colón, Cayo Roldán, Cayo de Agua, and Galeta (Figure 4.1). Sites were chosen based on proximity to long-term water temperature monitoring sites operated by the Smithsonian Tropical Research Institute's Physical Monitoring Program. At each site, anemones were collected from 30 m x 1 m belted transects established parallel to shore. Abundance was estimated at each site by counting all anemones per transect, with a maximum of 100 anemones counted per mangrove root. Surveys were conducted continuously along the shoreline perimeter. Transects were initiated upon observation of at least one anemone and are considered as distinct population patches throughout the manuscript. In Galeta, anemones were only found attached to rocks in shallow intertidal areas, and so surveys were conducted parallel to shore at <0.5 m depth, with a maximum of 100 anemones counted per 30 m x 1 m belted transect. After collection, samples were homogenized in 200 uL Buffer EB (Qiagen, Valencia, CA, USA), and a 100-uL aliquot of the tissue homogenate was used for DNA extraction with the DNeasy Blood and Tissue Kit (Qiagen, Valencia, CA, USA). The remainder of the homogenate was centrifuged, the pellet suspended in 500 uL filtered seawater (FSW), and the re-suspension centrifuged again. The combined supernatants and the resulting algal pellet were frozen for determination of *Symbiodinium* cell density (Muller-Parker 1984, see supplementary methods in Appendix C).

Population genomic analysis

Genomic libraries were prepared and analyzed following the 2b-RAD method (Wang *et al.* 2012). We sequenced 2b-RAD libraries generated from 150 samples in total from Caribbean Panama. In addition, we sequenced 2b-RAD libraries prepared from 4 laboratory strains of *Aiptasia* including CC7, the strain used to create the reference genome (Baumgarten *et al.* 2015), and created *in silico* digested libraries from 100-bp

reads previously generated to sequence the genomes of 10 laboratory *Aiptasia* strains at ~10x coverage (Bellis *et al.* 2016). *In vitro* 2b-RAD libraries were prepared by digesting genomic DNA with the enzyme *BcgI* (New England BioLabs, Ipswich, MA, USA) and dual-indexed during PCR amplification. Gel-purified amplification products were pooled and sequenced on the NextSeq 500 at the University of Oregon Genomics and Cell Characterization Core Facility (Eugene, OR). After sequencing, reads were quality-filtered reads and aligned to the set of all 44,428 *BcgI* recognition sites present in the *Aiptasia* genome using SHRiMP v2.2.2 (Rumble *et al.* 2009; Baumgarten *et al.* 2015). Genotypes with minor allele frequencies (MAF) below 5% were called as homozygous and above 30% were called as heterozygous; genotypes were not called if MAF was between these thresholds or if coverage was less than 5x, 10x, or 15x (Appendix C).

To investigate population structure, we used two complementary methods: a Bayesian clustering approach implemented in the program *STRUCTURE* and an analysis of principal components with the R program *adegenet* version 2.0.1 (Jombart 2008). Analyses were first performed in *STRUCTURE* version 2.3.4 (Pritchard *et al.* 2000; Falush *et al.* 2003). All *STRUCTURE* analyses used the admixture model with correlated allele frequencies, which provides greater power to distinguish closely related populations compared with the independent allele frequency model (Falush *et al.* 2003). Five replicates were run for values of *K* ranging between 1 and 6, and each simulation was run for 500,000 MCMC repetitions after a burn-in period of 100,000. The optimum number of population clusters, *K*, was determined using the Evanno method implemented in *STRUCTURE HARVESTER* (Evanno *et al.* 2005; Earl & vonHoldt 2012). Output from replicate *STRUCTURE* runs was combined with *CLUMPP* version 1.1.2 and visualized using *DISTRUCT* version 1.1 (Rosenberg 2004; Jakobsson & Rosenberg 2007).

Clones were identified using 5x, 10x, and 15x SNP callsets. Clone detection was implemented in R with 'poppr' version 2.3.0, with genotypes contracted based on Prevosti's absolute genetic distance and clusters merged based on the maximum distance in each cluster (Kamvar *et al.* 2014). Thresholds for MLG clustering were chosen based on genetic distances observed for known clones in the dataset (HI1/HI2 and BM1/BM2 *in silico* digested libraries from Bellis *et al.* [2016]; CC7 *in silico* and *in vitro* digested

libraries). Chosen thresholds were 0.006 for the 5x callset for each species and 0.001 for the 10x and 15x callsets.

After removing clones, genetic diversity and differentiation summary statistics were calculated for each population. Pairwise differentiation statistics F_{ST} and G''_{ST} and observed and expected heterozygosity (H_O and H_S) were calculated for each population in GenoDive v2.0b27, randomizing populations over the two species groups with 999 permutations to test significance (Meirmans & Van Tienderen 2004). Individual heterozygosity (H_I), or the proportion of heterozygous sites relative to all sites genotyped in a sample, was calculated with custom scripts based on the combined species 10x SNP dataset before filtering for polymorphic sites (Appendix C). H_I was analyzed using binomial logistic regression and the logit link function, with the chosen model (HI ~ Species + Species:Population + Species:Site) selected based on the Akaike information criterion.

Outlier analysis

Candidate SNPs under selection in *Aiptasia* from warmer, more variable environments were identified using an F_{ST}-outlier approach. We used two complementary methods: one based on simulation of neutral F_{ST} values implemented in *LOSITAN* (Antao *et al.* 2008) and a Bayesian approach for detecting F_{ST}-outliers in *BayeScan* v2.0 (Foll & Gaggiotti 2008). For analyses in *LOSITAN*, 50000 simulations were run on clone-corrected 10x SNP datasets with the infinite alleles mutation model, a subsample size of 50, FDR < 0.10, and the neutral mean F_{ST} and force mean F_{ST} options. Analyses in *BayeScan* were run with 5000 iterations after a burn-in length of 50000, a thinning interval of 10, 20 pilot runs, and prior odds for the neutral model of 10.

To perform GO-term enrichment analysis, 130 gene models with SNPs in the top 5% of highly differentiated loci from the 5x callset were compared to the set of 2524 *Aiptasia* gene models containing at least one SNP in intronic, exonic, 5' untranslated, or 3' untranslated regions. GO-term enrichment was performed with GOEAST and the hypergeometric method (Zheng & Wang 2008).

Symbiodinium *genotyping*

The dominant *Symbiodinium* clade in each sample was genotyped as clade A, B1, or B2 using a two-stage PCR banding assay. The first PCR reaction was specific for the chloroplast 23S ribosomal RNA (*cp23s*) from *Symbiodinium* clade B1 or B2. Primers 5'-TGC TGC TGA CAC TAA AGG ACA-3' and 5'-ATC GCC CCA ATT AAA CAG TG-3' were designed to flank an insertion/deletion polymorphism between voucher specimens of *Symbiodinium* clade B1 [GenBank accession: JN557991] and clade B2 [GenBank accession: JN557995], yielding a 165 bp band for clade B1 or a 205 bp band for clade B2. The second PCR reaction was specific for the chloroplast photosystem II subunit D1 (*psbA*) from *Symbiodinium* clade A and did not amplify DNA from clade B1 or B2 (primers 5'-CTT TCT CAG CTC CAG TAG TT-3' and 5'-AGA TTG AGT GAA ATG TCT CCT G-3'). All PCRs were performed with EconoTaq DNA Polymerase (Lucigen, Middleton, WI, USA) in 25 µL reaction volumes with an annealing temperature of 56°C.

RESULTS

Anemone abundance and algal density in hospite

To determine if long-term exposure to variable temperatures might influence anemone-*Symbiodinium* population dynamics, we measured anemone abundance and *Symbiodinium* density and mitotic indices for all four sites. Evidence was not observed to support lower anemone abundance at the warmer, more variable sites (Fig. 4.1). Anemones were abundant on the roots of island-fringing mangroves at all three sites within the Bocas del Toro archipelago (~0.5 m to 3 m depth). However, in Galeta, anemones were only found attached to rocks and coral rubble in shallow intertidal areas (≤0.5 m depth) or on dock pilings near the Galeta Point Marine Laboratory; no anemones were found attached to mangrove roots in surrounding areas or during additional surveys in Portobelo National Park. Anemone abundance was highest at Cayo Roldán, the warmest site within the Bocas del Toro archipelago (Fig. 4.2; Table 4.1). The median number of anemones observed per mangrove root for 30-m transects in Cayo Roldán was 18, which was significantly higher compared to other sites ($p < 0.01$, GLM; Figure 4.2A).

A greater number of mangrove roots were colonized within anemone patches in Cayo Roldán compared to other sites, with an estimated 12 colonized roots in Cayo Roldán compared to 3.4 or 3.5 roots for Cayo de Agua and Isla Colón, respectively ($p < 0.001$, GLM; Figure 4.2B). Anemone patches were also closer together at Cayo Roldán than at the other sites, with an estimated 30 m between patches compared to 66 m or 67 m for Cayo de Agua and Isla Colón, respectively ($p < 0.01$, GLM; Figure 4.2C). Because no anemones were observed colonizing mangrove roots in Galeta, the median abundance of 22 anemones per 30-m transect (~0.5 m depth) was not directly compared to abundances estimated for sites in the Bocas del Toro archipelago, where anemones were primarily observed colonizing mangrove roots. The distance between colonized patches in Galeta, however, was not significantly different than in Cayo de Agua or Isla Colón (Figure 4.2C, Table 4.1).

Within-anemone *Symbiodinium* density was also determined by normalizing cell counts from homogenized tissue to total protein (Appendix C). *Symbiodinium* density was similar among the four sites studied (P=0.08, GLM), with a median density of 3.69 cells x 10^6 per mg protein (95% CI: 3.41-4.0, Appendix Figure C1). Average mitotic index for *Symbiodinium in hospite* was 1.9%, with evidence for lower division rates in *Symbiodinium* harbored by anemones from Galeta compared to Cayo Roldán (P<0.001, Tukey HSD) and Cayo de Agua (P=0.014, Tukey HSD).

Anemone population structure

We performed type IIb restriction-site associated DNA sequencing (2bRAD-Seq) of individual anemones to determine population genetic structure of anemones sampled from the Caribbean coast of Panama. To facilitate comparison with commonly studied laboratory strains, sequences from 15 anemones sampled from geographically widespread locations were also included. Analyses of population genetic data revealed the presence of two closely related, co-occurring species of sea anemones: *Exaiptasia brasiliensis* and the *Aiptasia* sp. commonly studied as a laboratory model system (Fig. 4.3, top panel). On average, 1.2 million reads were generated for each of the 150 samples sequenced (range: 12,116 – 2,632,344 reads). Significantly fewer reads mapped uniquely to the reference

genome from *E. brasiliensis* (32.8%) compared to *Aiptasia* (43.2%, $p < 0.001$, Welch Two Sample t-test). The vast majority of SNPs (97%) were bi-allelic. Across SNP datasets with different coverage thresholds, between 30% and 43% of identified SNPs were present in coding regions of the genome (Appendix Table C1).

The first stage of our hierarchical population structure analysis in *STRUCTURE* suggested two major genetic clusters, corresponding to the *Aiptasia* sp. usually studied as a laboratory model and the recently described *Exaiptasia brasiliensis* (Grajales & Rodríguez 2016). Principle component analysis of 5x and 10x SNP datasets further supported the presence of two closely related but differentiated species (Fig. 4.4). The first PC, which explained 43.5% of the total variation, clearly separated the two identified species into distinct clusters; the second and third PCs explained 3.3% or 1.7% of the total variance and primarily characterized genetic variation within *Aiptasia* sp. or *E. brasiliensis*, respectively (Fig. 4.4). Pairwise F_{ST} and G''_{ST} comparisons exceeding 0.79 indicated high genetic differentiation between *E. brasiliensis* and *Aiptasia* sp. populations (Table 4.2). Sanger sequencing of a 3.2 kb region of the mitochondrial genome spanning the 16S rRNA and COIII genes revealed 10 polymorphisms between putative representatives of *E. brasiliensis* and *Aiptasia* sp. individuals (Fig. 4.5, Appendix C). Two of the observed polymorphisms in COIII were previously identified as diagnostic of *E. brasiliensis*: a synonymous C/T at position 14899 [GenBank accession: HG423148] and a G/A at position 14987 resulting in an amino acid replacement from glutamic acid to lysine (Grajales & Rodríguez 2016). We observed two additional synonymous substitutions in COIII (a C/T at positions 14566 and 14620), four substitutions in 16s (A/G at 13282, G/A at position 13628, T/C at position 13844, and A/T at position 14383), and 2 polymorphisms in the intergenic region between COIII and COI (a 2 bp deletion at position 15336 and a G/A at position 15371). Sequences for all identified *Aiptasia* sp. individuals were identical to previously reported mitochondrial sequence for *Aiptasia* [GenBank accession: HG423148].

Within-species population differentiation was observed for both *E. brasiliensis* and *Aiptasia* sp., with two genetically distinct population clusters identified for each species (Fig. 4.3, lower panel). The majority of *E. brasiliensis* individuals were found in

Galeta (n = 31), though four *E. brasiliensis* were identified in the Bocas del Toro archipelago. These four individuals clustered together as a genetically distinct group from the Galeta individuals (Fig. 4.3-4). In contrast, most anemones collected within the Bocas del Toro archipelago were classified as *Aiptasia* (n=108), along with four Galeta anemones collected from two adjacent dock pilings. Two distinct population clusters of *Aiptasia* sp. were identified that exhibited moderate differentiation unrelated to collection site (median locus-specific F_{ST} = 0.06; Fig. 4.3-4). The first population cluster included four individuals from Galeta, 12 anemones from different sampling sites in the Bocas del Toro archipelago, and laboratory strains derived from the previously described global and Western Atlantic *Aiptasia* populations (Thornhill *et al.* 2013). The remaining 96 *Aiptasia* sp. individuals formed a separate genetically distinct cluster specific to the Bocas del Toro Archipelago, and significant genetic structuring was not observed among these individuals when analyzed as a separate group (results not shown). Results were qualitatively indistinguishable among the 5x, 10x or 15x datasets including 5391, 2991, and 1474 SNPs, respectively. Throughout the remainder of this manuscript, we refer to these two identified *Aiptasia* sp. clusters as the 'global ancestral population' and the 'Bocas ancestral population'.

Anemone genetic diversity

We observed some evidence for higher genetic diversity in *E. brasiliensis* relative to *A. pallida* based on patterns of observed and expected heterozygosity within subpopulations and the degree of heterozygosity within individual genomes. Subpopulation heterozygosity in *E. brasiliensis* from Galeta was more than twice that of *Aiptasia* sp. populations from the Bocas del Toro Archipelago though differences in H_O and H_S between the two species were not statistically significant, likely due to the small number of populations studied (Table 4.3, p = 0.1, permutation test). However, the proportion of heterozygous sites within individual genomes (H_I) was significantly higher in *E. brasiliensis* (Table 4.4). Species, collection site, and ancestral population (global vs. Bocas) were significant predictors of H_I (AIC=3542 for full model vs. AIC=3795 for reduced model). H_I was lowest in *A. pallida* populations from Cayo de Agua (Table 4.4).

H_I was 1.34x higher in *E. brasiliensis* from Galeta, 1.06x higher in Cayo Roldán, 1.08x higher in Isla Colón, and 1.11x higher in *A. pallida* genotypes more representative of the global ancestral population (Table 4.4).

Locus-specific patterns of genetic differentiation

We used two complementary F_{ST}-outlier methods to identify candidate loci associated with local adaptation of *Aiptasia* to warm, variable environments. Within the Bocas del Toro archipelago, the inshore site experiences maximum summer temperatures ~1°C warmer than the other sites within the Bocas del Toro archipelago, and loci involved in local adaptation to higher temperature might be expected to exhibit strong differentiation in Cayo Roldán (CR) compared to other sampled populations. *LOSITAN* detected 19 outlier regions in the 10x SNP dataset, including three loci present in introns and nine loci in exons (Table 4.5). Of 19 outliers among the three populations, five exhibited allele frequencies differentiated by at least 0.10 in CR compared to the other populations (Table 4.5). Notably, two of these loci were also highly differentiated between the ancestral global and Bocas populations. *BayeScan* detected three outliers (FDR < 1.0), two of which were also detected by *LOSITAN*. Two of the outliers were located in intergenic regions and the third was a synonymous polymorphism in phosphotidylinositide phosphatase SAC2 (Table 4.5).

We further investigated the set of loci that were most highly differentiated between the ancestral global and Bocas *Aiptasia* populations. After removing loci in intergenic regions, 80 of 2524 loci were present in the top 3% of most highly differentiated genes in the 5x SNP dataset compared to 33 of 1205 in the 10x SNP dataset. Two GO-terms were found that were significantly enriched in both the 5x and 10x datasets (P <0.01, Table 4.6). The first, involved in SH3-domain binding, was associated with polymorphisms in predicted mRNA sequence for Dedicator of cytokinesis protein 1 (both datasets; involved in cytoskeletal rearrangements required for phagocytosis), Contactin-associated protein 1 (both datasets; a cell adhesion molecule), and Disintegrin and metalloprotease domain-containing protein 9 (5x dataset only; mediates cell-cell and cell-matrix interactions). The second GO term was associated with

two distinct SNPs in Titin, a large muscle protein which is downregulated in *Aiptasia* larvae during symbiosis establishment (Wolfowicz *et al.* 2016). The set of highly differentiated genes also included signaling genes that may play an important role in host responses to microbial symbionts (e.g. complement C3, hemicentin, and lactadherin), though these genes were not involved in pathways with significant GO-term enrichment (Appendix Table C2).

Contribution of clonal reproduction to population structure

Of particular note was the seemingly minor contribution of clonal reproduction to genetic structure of natural *Aiptasia* sp. and *E. brasiliensis* populations at the spatial scales studied. Among the 112 *A. pallida* individuals genotyped, 97 unique multilocus genotypes (MLGs) were detected, with seven MLGs shared by two anemones, one MLG shared by three anemones, and two MLGs shared by four anemones. Shared MLGs for which anemones were collected more than 30 m apart were not observed, except for two clone pairs collected from neighboring transects in Cayo Roldán a maximum estimated distance of 50 m apart. For individuals genotyped from different mangrove roots within the same 30-m transect, 0 to 29% of genotyped pairs were clones, including 0/11 transects in Isla Colón, 1/13 transects in Cayo Roldán, and 2/7 transects in Cayo de Agua. Six anemone pairs were genotyped that were sampled from the same mangrove root (or dock piling, for *A. pallida* from Galeta); in all six cases, anemones shared a clonal genotype with the other individual collected from the same root. For *E. brasiliensis* from Galeta, six pairs of anemones shared an MLG for a total of 29 unique MLGs among 35 individuals. Four clone pairs were collected less than 30 m apart, whereas two pairs of clones were collected approximately 100 m apart.

Symbiodinium *diversity*

Presence of three *Symbiodinium* species that commonly associate with *Aiptasia* was scored using a PCR approach that targeted *cp23s* and *psbA*, two chloroplast genes encoded by separate minicircles (Wisecaver & Hackett 2011). For all samples, a single dominant *Symbiodinium* type was assigned, and PCR with alternative primer pairs failed

to amplify a discernable band. However, our PCR analysis does not preclude the presence of additional genotypes present at low abundance. Most anemones from Galeta (*n*=63) were dominated by *Symbiodinium* clade A, whereas anemone individuals from the Bocas del Toro archipelago (Isla Colón: *n*=55; Cayo Roldan: *n*=56; Cayo de Agua: *n*=37) were dominated by *S. minutum* (clade B1). The four *Aiptasia* from Galeta, all collected from a dock piling, also hosted *S. minutum* as the dominant symbiont type. A single individual assigned to the global ancestral *Aiptasia* population and collected from Isla Colón hosted *S. psygmophilum* (clade B2), a cold-tolerant lineage that may be relatively rare in natural *Aiptasia* populations compared to clades A and B1 (Thornhill *et al.* 2013; Grajales *et al.* 2016). Two genotypes of *Symbiodinium* clade A were identified among six individuals for which the *psbA* region was sequenced using Sanger sequencing. Four individuals had a *psbA* sequence identical to a *Symbiodinium* clade A isolated from the jellyfish *Cassiopeia xamachana* [GenBank: AJ884905]. Sequences for the remaining two anemones exhibited a synonymous substitution (C→G) at position 431 shared by *Symbiodinium* clade A associated with *Aiptasia* CC7, the laboratory strain used to sequence the reference genome (Baumgarten *et al.* 2015).

DISCUSSION

Among the studied populations in Caribbean Panama, striking differences were observed in distribution of anemone holobionts across environments. *Aiptasia* hosting *Symbiodinium* clade B1 was most common in stable thermal environments shaded by mangrove canopy in Bocas del Toro, whereas *E. brasiliensis* hosting *Symbiodinium* clade A was prevalent in thermally variable, high light environments in Galeta. Overall, observed patterns of distribution and genetic diversity in host species and their *Symbiodinium* communities were most consistent with hypothesis H_2, specialization of holobiont assemblages for different habitats. Unexpectedly, results from our study also suggested relatively limited spatial extent of clonal reproduction in the populations studied.

Are clade A Symbiodinium *less beneficial?*

Our observations are consistent with the interpretation that under stable temperature and/or intermediate irradiance, clade B1 *Symbiodinium* (*S. minutum*) may provide more benefit to hosts than clade A4 *Symbiodinium*. Clade B1 dominated both *A. pallida* and *E. brasiliensis* individuals throughout the Bocas del Toro archipelago, consistent with the high prevalence of *S. minutum* in most populations sampled outside of the Western Atlantic (Thornhill *et al.* 2013; Grajales *et al.* 2016). The most successful *A. pallida* population in our study, as indicated by host abundance and the proximity of colonized patches, was associated with *S. minutum* (Fig. 4.2). In contrast to our original prediction, this population was present at the warmest site within the Bocas del Toro archipelago.

In contrast to patterns observed within the relatively stable Bocas del Toro archipelago, clade A4 *Symbiodinium* may be favored in thermally stressful and/or high light environments. Recent comparison of photobiological characteristics among a suite of *Symbiodinium* lineages suggest specialization of a related clade A4 *Symbiodinium* (isolated from a Caribbean octocoral) for high light/variability environments whereas *S. minutum* from *Aiptasia* belonged to a group of intermediate light/variability specialists (Suggett *et al.* 2015). Clade A4 lineages from *Aiptasia* exhibit increased photosynthetic performance compared to *S. minutum* in culture and *in hospite* at elevated temperatures of 32-34°C (Perez *et al.* 2001; Goulet *et al.* 2005). Expulsion rates are also higher for clade B1 *Symbiodinium* compared to A4 in *Aiptasia* exposed to 34°C (Perez *et al.* 2001; Bellis *et al., accepted*), though similar expulsion rates are observed at 32°C (Perez *et al.* 2001). These laboratory bleaching experiments used temperature stresses that are relatively extreme compared to those experienced by anemone populations in Caribbean Panama, with irradiances more similar to habitats shaded by mangrove canopy than in shallow, sunlit intertidal areas (Muller-Parker 1987). Specifically, 3-m temperatures recorded at CR, the warmest of the studied sites within the Bocas del Toro archipelago, never exceeded 33°C between 1999 and 2015. Recorded temperatures in Galeta were warmer, exceeding 34°C for at least an hour on 27 separate days between 2002 and 2015 at a depth of 0.5 m (though 3-m temperatures also did not exceed 33°C). Interestingly, the

few identified *Aiptasia* individuals collected from a dock piling in Galeta all hosted *S. minutum.* This pattern may be explained by differences in symbiont specificity between *Aiptasia* and *E. brasiliensis* or by recent establishment of host populations that have not yet experienced sufficient thermal-stress to induce bleaching. However, given that some *Aiptasia* strains in the laboratory can stably host clade A4 *Symbiodinium,* differences in light environment for anemones in the sunlit reef flats of Galeta compared to areas shaded by mangrove canopy (or an overhead dock) may be the best explanation for the observed patterns of *Symbiodinium* community structure (Muller-Parker 1987).

Overall, patterns of anemone holobiont diversity, distribution, and abundance in thermally variable sites in Caribbean Panama suggest *S. minutum* is favored in thermally stable, intermediate light environments but that *S. linucheae* predominates if exposure to high light and/or temperature is likely. Data regarding amounts of photosynthate transferred by diverse symbiont lineages are currently lacking for *Aiptasia* under different temperature and light regimes, though more labeled glucose may be transferred to *Aiptasia* associated with *S. minutum* compared to *S. linucheae* under stable laboratory conditions at 24°C (see Fig. 5a in Burriesci *et al.* 2012). Infection rates in laboratory studies are also higher for *S. minutum,* likely influenced by differences in molecules on *Symbiodinium* and host cell surfaces as well as symbiont cell size (Davy *et al.* 2012; Wolfowicz *et al.* 2016; Biquand *et al.* 2017). In addition to providing greater amounts of photosynthate, association with *S. minutum* might benefit anemone hosts by decreasing oxidative stress in host tissues through higher respiration relative to *S. linucheae* (Goulet *et al.* 2005; Hawkins *et al.* 2016a). Previous transcriptome and proteome studies have discovered upregulation of oxidative-stress response pathways in aposymbiotic anemones (lacking *Symbiodinium*) compared to symbiotic sea anemones (Rodriguez-Lanetty *et al.* 2006; Ganot *et al.* 2011; Lehnert *et al.* 2014; Oakley *et al.* 2016). These findings directly contrast with the prediction that an intracellular photosymbiont imposes greater oxidative stress on the host (Venn *et al.* 2008). However, upregulation of oxidative stress response pathways is consistent with increased superoxide production observed in aposymbiotic compared to symbiotic *Aiptasia* at 26°C and 32°C and heat-induced bleaching in the absence of light (Nii & Muscatine 1997; Tolleter *et al.* 2013). These studies highlight

host mitochondria as an important source of ROS-production at elevated and ambient temperature (Nii & Muscatine 1997; Weis 2008; Dunn *et al.* 2012; Dixon *et al.* 2015). In addition to algal expression of antioxidant enzymes (Rodriguez-Lanetty *et al.* 2006), higher O_2 consumption in *S. minutum* compared to *S. linucheae* might reduce oxidative stress in anemones under stable conditions (Perez *et al.* 2001; Goulet *et al.* 2005; Hawkins *et al.* 2016a).

Potential for habitat specialization by anemone hosts

In addition to differences in *Symbiodinium* community structure, distinct patterns of host species distribution were observed across environments. Habitat (i.e. mangrove or shallow intertidal) was confounded with sampling site and symbiont type, and thus we are unable to determine to what extent observed patterns of anemone distribution might result from differential host preference for particular environments, substrates, and/or symbionts. *E. brasiliensis* was commonly attached to rocks and coral rubble in sunlit, intertidal areas in Galeta, though several individuals were found attached to mangrove roots in the Bocas del Toro archipelago. In contrast, *Aiptasia* was abundant in Bocas del Toro but never found attached to rocks or coral rubble in our study. Strong genetic differentiation according to habitat type and concurrent with differences in *Symbiodinium* community structure was also found for cryptic species of the reef-building coral *Seriatopora hystrix* on the Great Barrier Reef, highlighting the importance of recognizing cryptic host diversity that might be quite prevalent among cnidarians (Ladner & Palumbi 2012; Keshavmurthy *et al.* 2013; Warner *et al.* 2015). It is possible that *E. brasiliensis* may rely less on contributions from *Symbiodinium* or exhibit increased thermal/oxidative stress tolerance compared to *Aiptasia* hosts. However, higher tolerance may come at the cost of reduced competitive ability under stable conditions, as indicated by the low abundance of *E. brasiliensis* in the Bocas del Toro archipelago compared to *Aiptasia* (both harboring *Symbiodinium* clade B1) and a more restricted geographic range (Grajales & Rodríguez 2016; Grajales *et al.* 2016). The potential variation in habitat preference is also important given the inability to induce larval settlement in the laboratory, which remains a major practical challenge for further development of *Aiptasia*

as a genetic model system (Weis *et al.* 2008). Future investigations of variation in habitat preference within and among species could provide guidance for identifying natural settlement cues that may be specific to particular marine environments (Fleck & Fitt 1999).

Local adaptation in host populations

Our high-resolution genomic data allowed us to search for candidate loci under selection in *Aiptasia* populations within the Bocas del Toro archipelago. However, compelling signatures of local adaptation at spatial scales less than 35 km were not observed with our 2bRAD data. Within the Bocas del Toro archipelago, we expected candidate loci under selection to exhibit strong differentiation in populations from CR, the most thermally stressful site, compared to CA or IC. Two candidate polymorphisms under selection were identified that resulted in nonsynonymous changes in proteins homologous to Ficolin-2 or Collagen-like Protein 2 (Table 4.5). Ficolins are secreted pattern recognition receptors that recognize glycans on the surfaces of microbial cells and activate the lectin complement pathway, thought to play a central role in the onset and maintenance of cnidarian symbiosis (Poole *et al.* 2016). Many proteins that may be involved in the complement pathway, including Cnidarian ficolin-like proteins, also include a collagen domain, and loci in relevant candidate genes (i.e. Complement C3; F_{ST} = 0.49) were found to be highly differentiated between the Bocas ancestral and global populations (Baumgarten *et al.* 2015, Appendix Table C2). Several other genes highly differentiated among sites with roles in innate immunity and symbiosis included a scavenger receptor protein, a leucine-rich repeat containing protein, a thrombospondin motif-containing protein, and a C-type mannose receptor (Table 4.5; Neubauer *et al.* 2016; Neubaeur *et al.* 2017). Despite interesting functional roles, however, differences in allele frequencies between populations from different sites were subtle, with a maximum major allele frequency of 1.0 in CA or IC versus 0.86 in CR for both loci (Table 4.5). It is possible that high gene flow among populations within the Bocas del Toro archipelago or relatively weak selection pressure at CR may result in limited genomic signatures of local adaptation. Because RAD-based approaches survey only a small proportion of the

genome, it is also likely we have missed many potential loci under selection among populations distinguished by sampling site or by genetic background (e.g. ancestral global versus Bocas-specific populations) (Lowry *et al.* 2017). For example, with perfect mapping and coverage for all predicted *BcgI* tags, we would expect to sequence only ~1% of the *Aiptasia* reference genome. Assuming linkage blocks of approximately 10 kb observed for the coral *Acropora digitifera* (Shinzato *et al.* 2015), our callset with the largest number of SNPs (4.6k) might reflect patterns of differentiation across a maximum of 18% of *Aiptasia*'s 260 Mb genome. However, our data suggest that higher resolution sequencing targeting the populations characterized here could reveal substantial genetic differentiation in components of molecular pathways important for interactions with *Symbiodinium*.

Anemone-Symbiodinium *coevolution at a broader scale*

Asexual proliferation confers a strong competitive advantage to organisms that can reproduce clonally, and clonal reproduction is expected to predominate except under conditions where environmental instability or coevolution with parasites may favor sexual reproduction (Williams 1975; Maynard Smith 1978; Highsmith 1982; King *et al.* 2009). Reproductive tradeoffs have been well-studied in sea anemones (Sebens 1980, 1982), which exhibit diverse mechanisms of asexual reproduction and independent evolution of clonality in many lineages (Chia 1976; Jackson & Hughes 1985; Geller & Walton 2001; Geller *et al.* 2005). The lack of evidence for a strong contribution of clonal reproduction to population structure in our dataset was surprising given previous studies of temperate anemones that support the "strawberry-coral model" of short-range dispersal via asexual propagules and long-range dispersal via sexual propagules, favored in stable and variable environments, respectively (Williams 1975; Sebens 1982; Ayre 1984). However, a limited contribution of asexual reproduction to population structure of the symbiotic corkscrew anemone, *Bartholomea annulata,* was suggested recently in the first study to use molecular genetics to determine clonal reproduction rates in a tropical sea anemone (Titus *et al.* 2017). It is tempting to speculate that higher rates of sexual reproduction could be more widespread among symbiotic tropical anemones compared to

temperate species (Sebens 1982; Ayre 1984). Such a pattern might suggest altered co-evolutionary dynamics in tropical seas generally characterized by high irradiance, high temperature, and low nutrient concentrations throughout the year in contrast to temperate regions that exhibit marked seasonal variation (Muller-Parker & Davy 2001). Specifically, tropical environments might represent coevolutionary 'hotspots', where the intensity of reciprocal selection is stronger and anemones benefit from hosting algal symbionts year-round compared to temperate sea 'coldspots', where anemone-*Symbiodinium* interactions may be more commensalistic or variable over time (Thompson 1999; Gomulkiewicz *et al.* 2000). As the climate changes, many marine species may undergo range shifts according to the rate and direction of temperature change over time (Precht & Aronson 2004; Greenstein & Pandolfi 2008; Pinsky *et al.* 2013). Improved understanding of how changing abiotic environments may alter ecological and evolutionary dynamics of symbiotic interactions as species ranges expand and contract is crucial to predicting the fate of marine ecosystems under global climate change.

ACKNOWLEDGMENTS

This work was funded by an NSF Graduate Research Fellowship [0946928], a Short-Term Fellowship from the Smithsonian Tropical Research Institute, and a ZoRF research award from the Department of Integrative Biology at Oregon State University to ESB. The authors thank A. Calderón, R. Collin, P. Gondola, and G. Thomas for logistical support during sample collections, E. Meyer and H. Elder for advice and equipment to prepare genomic libraries, and D. Turnbull at Genomics and Cell Characterization Core Facility at the University of Oregon for sequencing assistance. Samples were collected with permission from the Ministerio de Ambiente of the Republic of Panama under permit number SC/A-25-15.

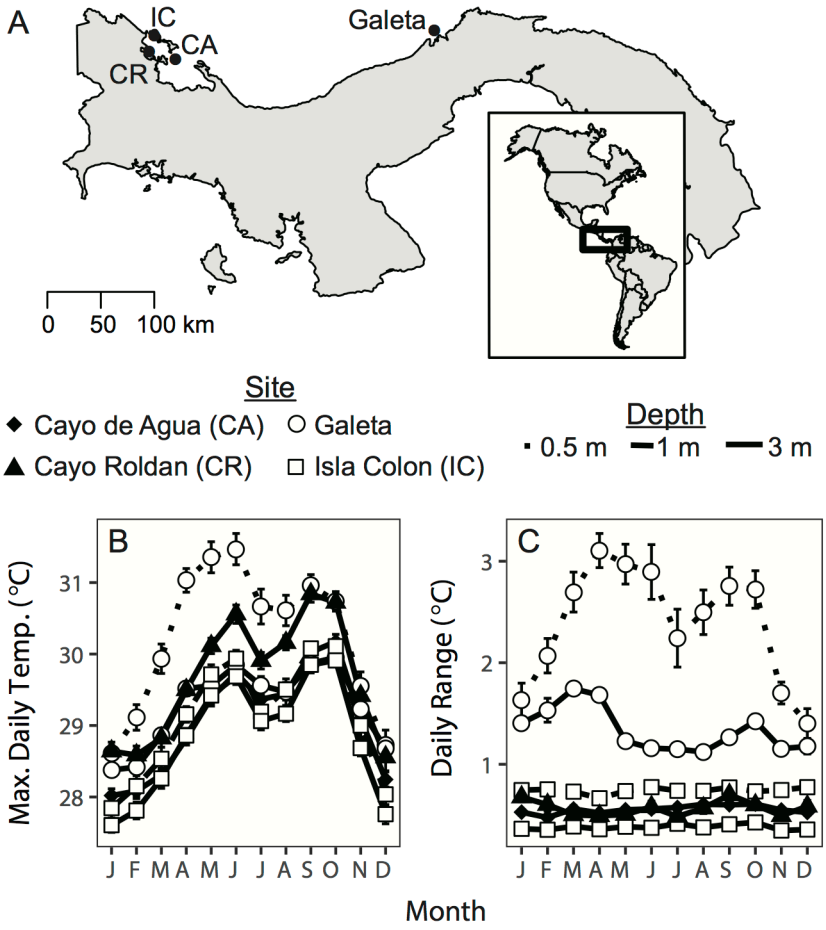

Fig. 4.1. Sampling locations in Caribbean Panama. Temperatures displayed in (B) and (C) are averages from 2000-2015 (3-m data sets) or 2002-2015 (0.5-m and 1-m data sets) and are derived from data provided by the Physical Monitoring Program of the Smithsonian Tropical Research Institute.

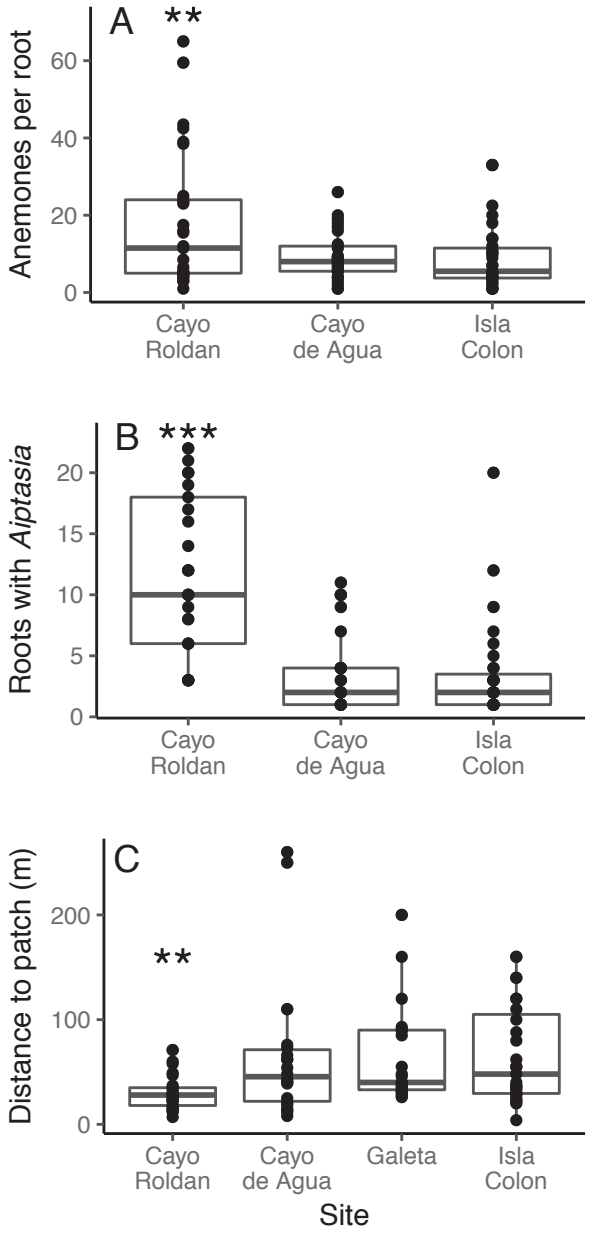

Fig. 4.2. Anemone abundance. A) Median number of anemones per mangrove root in 30-m transects with at least one anemone. Only mangrove roots inhabited by ≥1 anemone are considered, and a maximum of 100 anemones were counted per root. B) Number of roots within 30-m transects with at least one anemone. C) Distance to the next 30-m transect containing at least one anemone in continuous surveys. Galeta was not included in (A) or (B) since no anemones were observed on mangroves at this site. Asterisks indicate significant differences between Cayo Roldán and other sites ($p < 0.001$ [***] or $p < 0.01$ [**], GLM with quasi-poisson distribution).

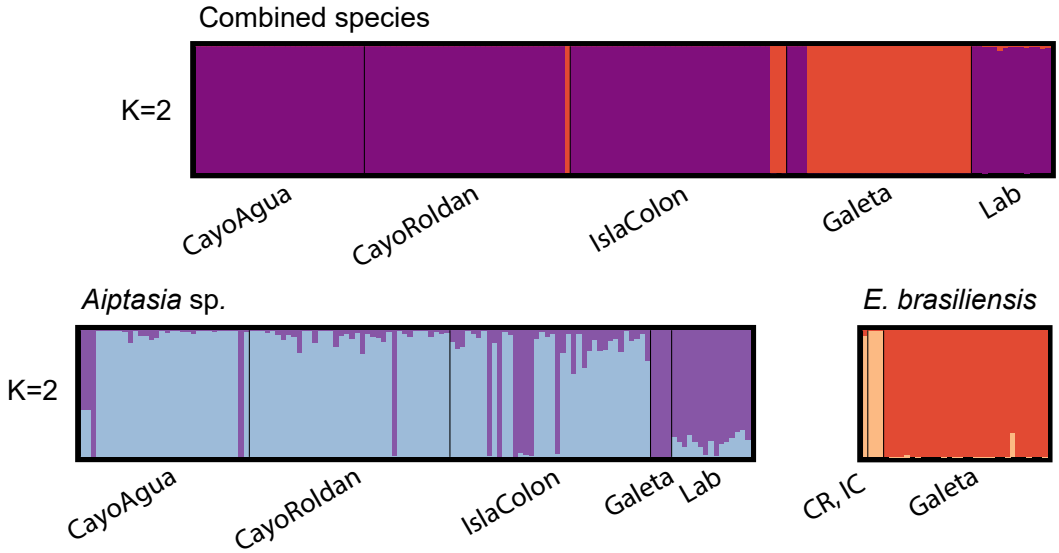

Fig. 4.3. Molecular identification of cryptic *Aiptasia* sp. and *E. brasiliensis* populations. Shown are results from STRUCTURE analyses based on 10x callsets including 2991 SNPs for comparisons between species, 2538 SNPs for comparisons within *Aiptasia* sp. (purple, n = 127), and 1257 SNPs for comparisons within *E. brasiliensis* (orange, n = 35). $K = 2$ was determined as the optimum number of population clusters for both within-species analyses and for the combined species dataset according to the Evanno method. CR and IC refer to Cayo Roldan and Isla Colón, respectively.

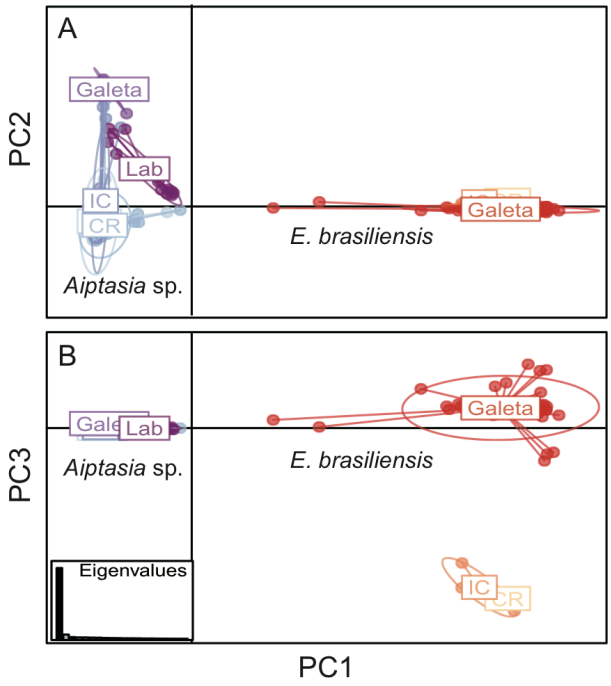

Fig. 4.4. Principal components analysis of genetic variation among populations. Results are based on the 2,991 SNPs from the 10x callset, with missing values replaced by the mean allele frequency for each population. Four populations of *Aiptasia* sp. from the Bocas del Toro archipelago and laboratory strains derived from globally widespread locations are shown in shades of blue and purple. *Exaiptasia brasiliensis* individuals from sites in the Bocas del Toro archipelago (peach) and Galeta (red) are also shown, corresponding to the colors in Fig. 4.3. CR, CA, and IC refer to Cayo Roldán, Cayo de Agua, and Isla Colón, respectively.

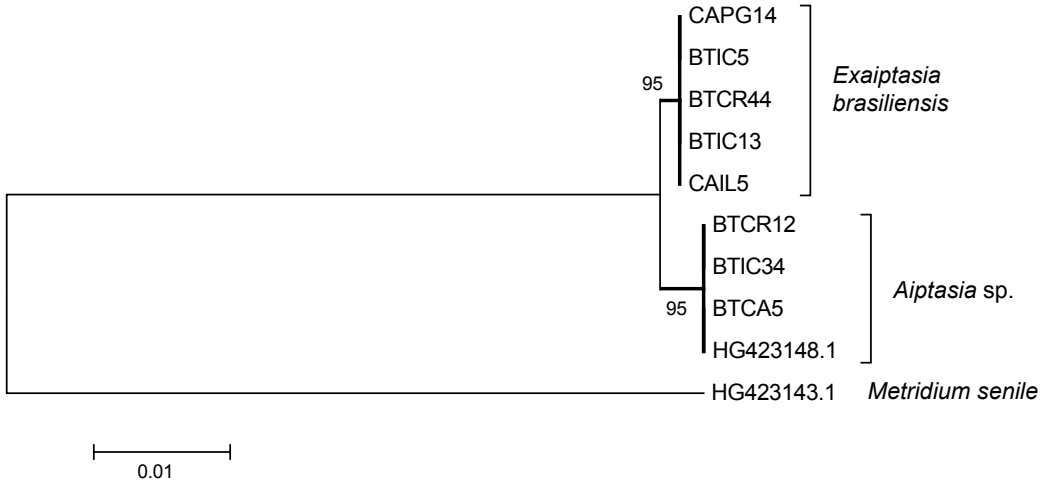

Fig. 4.5. Phylogenetic relationships among representatives of each species. Trees were based on maximum likelihood analysis of 719 bp of mtDNA. Sequenced *E. brasiliensis* included three individuals sampled from the Bocas del Toro Archipelago and two anemones from Galeta. The three sequenced *Aiptasia* sp. individuals were representatives of the Bocas-specific population. Bootstrap values (1,000 replicates) are indicated to the left of the corresponding node. Branch lengths are measured in substitutions per site.

Table 4.1. Statistical analyses of anemone abundance. Estimates of log counts are given for each response variable. Count data for all response variables were modeled using GLMs assuming a quasi-poisson distribution to account for overdispersion.

	Estimate	Std. Error	*t*-value	*P*-value
Anemones per root				
Intercept	2.89	0.14	20.85	***<0.001***
Site				
CA	-0.65	0.24	-2.68	***0.009***
IC	-0.68	0.23	-2.91	***0.005***
Roots with *Aiptasia*				
Intercept	2.47	0.10	23.76	***<0.001***
Site				
CA	-1.24	0.23	-5.51	***<0.001***
IC	-1.21	0.21	-5.73	***<0.001***
Distance between clusters (meters)				
Intercept	3.40	0.22	15.583	***<0.001***
Site				
CA	0.78	0.27	2.91	***0.005***
IC	0.80	0.26	3.06	***0.003***
Galeta	0.76	0.27	2.79	***0.006***

Table 4.2. Mean pairwise population differentiation over all loci. F_{ST} is shown above the diagonal and G''_{ST} is shown below for five populations after clone correction. Significant values (P <0.01) are italicized.

	Aiptasia sp.			*E. brasiliensis*
	CA (n=23)	CR (n=35)	IC (n=38)	Galeta (n=25)
CA	-	0.006	0.006	*0.798*
CR	0.006	-	*0.010*	*0.814*
IC	0.007	*0.011*	-	*0.803*
Galeta	*0.883*	*0.885*	*0.878*	-

Table 4.3. Genetic diversity in anemone populations. Heterozygosity values are based on the 10x combined species dataset after clone correction. H_O: observed frequency of heterozygotes within subpopulations; H_S: expected frequency of heterozygotes within subpopulations; H_I: observed frequency of heterozygous sites within individual genomes. For H_I, the median for each population is reported, with the first and third quartiles in parentheses. The number of private alleles relative to all other populations is based on the 5x (5391 SNPs) and 10x (2991 SNPs) combined species datasets.

	H_O	H_S	H_I	Private Alleles (5x)	Private Alleles (10x)
Aiptasia sp.					
CA	0.067	0.070	0.0049 (0.0047-0.0051)	17	4
CR	0.069	0.066	0.0051 (0.0048-0.0055)	12	2
IC	0.075	0.078	0.0053 (0.0050-0057)	59	29
E. brasiliensis					
Galeta	0.171	0.151	0.0065 (0.0062-0.0066)	512	362

Table 4.4. Heterozygosity within individual genomes (H_I). Results are shown for analysis based on a generalized linear regression model assuming a binomial distribution with the logit link function. The reference groups were *Aiptasia* sp. from the Bocas ancestral population collected from CA and *E. brasiliensis* from the Bocas del Toro archipelago. Lab strains genotyped via *in silico BcgI* digestion were excluded.

	Estimate	Std. Error	*t*-value	*P*-value
Intercept	-5.32	0.0038	-1406	***<0.001***
Species				
E. brasiliensis	0.39	0.0131	29.66	***<0.001***
Collection site				
Aiptasia sp.: IC	0.08	0.0050	16.30	***<0.001***
Aiptasia sp.: CR	0.06	0.0052	10.65	***<0.001***
Aiptasia sp.: Galeta	0.19	0.0115	16.53	***<0.001***
Aiptasia sp.: Lab	0.07	0.0107	6.64	***<0.001***
E. brasiliensis: Galeta	-0.10	0.0132	-7.37	***<0.001***
Ancestral population				
Aiptasia sp.: Global	0.10	0.0063	16.17	***<0.001***

Table 4.5. F_{ST} outliers according to collection site. Frequency of the major allele is provided for *Aiptasia* collected in Cayo de Agua (CA), Cayo Roldán (CR), and Isla Colón (IC). Loci with allele frequency differences ≥0.1 in CR relative to CA and IC are in bold.

Scaffold	Position	F_{ST}	*f*(CA)	*f*(CR)	*f*(IC)	Region	Annotation
753	18739	0.14	0.79	0.45	0.42	-	-
66†‡	255991	0.14	0.98	1	0.81	CDS	Phosphatidyl-inositide phosphatase SAC2
21	**609563**	**0.14**	**0.97**	**0.65**	**0.76**	**Intron**	**Putative leucine-rich repeat containing protein**
32‡	161937	0.14	0.97	0.97	0.77	CDS	A disintegrin and metalloprotease with thrombospondin motifs 6
351‡	**47434**	**0.14**	**0.82**	**0.97**	**0.66**	**-**	**-**
561†‡	**20611**	**0.13**	**0.84**	**1**	**0.73**	**-**	**-**
50‡	439485	0.12	0.8	0.81	0.5	CDS	Latrophilin-1
52	**491379**	**0.12**	**1**	**0.86**	**1**	**CDS***	**Ficolin-2**
171	269359	0.12	0.94	0.75	0.62	CDS*	Putative ferric-chelate reductase 1
39‡	727144	0.12	0.95	0.97	0.76	-	-
139	325185	0.12	0.86	1	1	CDS	Scavenger receptor cysteine-rich type 1 protein M130
35‡	747488	0.11	0.89	0.88	0.64	-	-
81	89075	0.10	0.95	0.96	0.76	CDS*	Not annotated
564	60343	0.10	0.81	0.99	0.96	Intron	E3 ubiquitin-protein ligase UBR5
173	228073	0.09	0.75	0.91	0.97	CDS	Endoribonuclease Dicer
108	400099	0.09	0.76	0.92	0.97	Intron	C-type mannose receptor 2
41	726763	0.09	0.96	1	0.84	-	-
50	445835	0.08	1	0.97	0.86	-	-
255	**204757**	**0.08**	**1**	**0.86**	**0.96**	**CDS***	**Collagen-like protein 2**

†Also identified as outlier in *BayeScan*

‡Loci above 90th percentile in F_{ST} comparisons between ancestral global and Bocas populations.

*Non-synonymous substitution

Table 4.6. GO-term enrichment analysis for genes highly differentiated in ancestral global and Bocas populations. Results based on the 5x SNP dataset. *P*-values are shown before adjustment for multiple comparisons. Asterisks indicate GO-terms also significant when analyzed with the 10x SNP dataset.

GO ID	Ontology	Term	Number in top 3%	Number in full list	*P*
GO:0017124	Molecular function	SH3 domain binding*	3	11	0.004
GO:1901077	Biological process	Regulation of relaxation of muscle*	2	4	0.006
GO:0031514	Cellular component	Motile cilium	2	4	0.006
GO:0016758	Molecular function	Transferase activity, transferring hexosyl groups	4	27	0.009
GO:0030336	Biological process	Negative regulation of cell migration	2	5	0.009
GO:2000146	Biological process	Negative regulation of cell motility	2	5	0.009
GO:0050905	Biological process	Neuromuscular process	3	14	0.009

CHAPTER 5 – Conclusion

In this dissertation, I combined bioinformatic, experimental, and field-based approaches to investigate natural variation in a model cnidarian-dinoflagellate symbiosis. These studies span levels of biological organization, from genome to organism to population, and spatial scales from global to local. The three data chapters are united through focus on a single host species, though the last study takes a slightly broader evolutionary perspective, including population-level insights into both *Aiptasia* and its cryptic sister species *E. brasiliensis*. It is not surprising that still much remains unknown regarding the interacting roles of each of the four mechanisms of resilience (acclimatization, symbiont switching, range shifts, and adaptation) outlined in Chapter 1. However, the research discussed here is a step towards more integrated understanding of the evolution of cnidarian-dinoflagellate symbioses.

The *Aiptasia* model system has provided exceptional insights into cnidarian-dinoflagellate interactions at the cellular level, but focused investigations on the evolutionary history of the host have only recently been conducted. In Chapter 2, I described results from a low-coverage genome survey of ten laboratory *Aiptasia* strains from geographically widespread locations, including representatives of the two previously described species *A. pallida* and *A. pulchella*. Our findings were consistent with the suggested unification of *A. pallida* and *A. pulchella* as a single species and the paradigm of a global population naturally harboring a single *Symbiodinium* species but a population in the Western Atlantic that harbors diverse clades (Thornhill *et al.* 2013; Grajales & Rodríguez 2014, 2016). However, we also found substantial genetic diversity and relatively few shared derived polymorphisms among strains from the Western Atlantic. Chapter 2 further demonstrated the potential benefits of genome skimming approaches for studying genetic variation in symbiotic cnidarians. Currently, reference genomes are available for only a handful of symbiotic cnidarian species (Shinzato *et al.* 2011; Baumgarten *et al.* 2015; Wang *et al.* 2017). Restriction-site associated and transcriptome-based analyses will therefore likely remain the methods of choice for surveys of genetic variation in cnidarians in the near future. As additional reference genomes become available, investigators may also consider low-coverage whole genome

sequencing approaches (Kulathinal *et al.* 2009; Straub *et al.* 2012; Weitemier *et al.* 2014). In our study, low-coverage sequencing enabled window-based scans of polymorphism across long stretches of the genome, an analysis not easily performed with alternative methods that target individual protein-coding genes or genetic sequence surrounding restriction enzyme recognition sites, albeit across more individuals. In addition to modest coverage (~10x) of approximately half the host genome, genome skimming yielded information for host mitochondrial genomes at high coverage and symbiont chloroplast and mitochondrial genomes at coverages comparable to or higher than host nuclear loci.

Evolutionary responses to selection depend on genetic variation, but natural selection acts on phenotypes. Chapter 3 focused on characterizing natural variation in mutualism breakdown among laboratory strains harboring different *Symbiodinium* genotypes. We found significant variation in anemone responses to acute heat stress, with extensive bleaching of two strains from Hawaii associated with *S. minutum* (clade B1) but minimal bleaching of four strains dominated by either *S. psygmophilum* (clade B2) or *S. linucheae* (clade A4). In contrast to the effects of exposure to acute heat stress, exposure to cold shock resulted in moderate bleaching with negligible variation across the strains studied. These findings imply that cnidarian bleaching under acute heat stress might not accurately predict bleaching responses to other stress regimes. A recent study using confocal microscopy to visualize host cells under different stress regimes supported different cellular mechanisms of bleaching under different conditions, with evidence for bleaching via host cell death and *in situ* degradation under cold-shock but not heat or light stress (Bieri *et al.* 2016). Whether different cellular mechanisms (e.g. apoptosis, host cell detachment) might play a stronger role in modulating bleaching responses of heat-susceptible *Aiptasia* strains remains to be seen (Gates *et al.* 1992; Dunn *et al.* 2004). Chapter 3 underscored the importance of a mechanistic understanding of holobiont stress responses and how bleaching could vary according to host and symbiont genetic background under different stress regimes.

Findings from Chapter 3 also suggested that *Aiptasia* could respond to elevated temperatures in the wild by harboring different *Symbiodinium* genotypes selected from

among the range of previously described symbiotic partners, depending on the amount of variation due to differences in symbiont genotypes. Correspondingly, Chapter 4 examined the relationship between environment and genetic diversity of host-symbiont assemblages at four locations in Caribbean Panama characterized by a range of temperature regimes. The RAD sequencing approach revealed two species in the dataset, including *Aiptasia* and the morphologically indistinguishable, closely related species *E. brasiliensis*. Two distinct populations of *Aiptasia* were identified, including a population with a genetic background similar to *Aiptasia* laboratory strains from globally widespread locations and a population specific to the Bocas del Toro archipelago. Symbiont and host genetic diversity were both associated with habitat at the species level. *E. brasiliensis* and *Symbiodinium linucheae* were more common in a shallow reef flat exposed to elevated temperature and irradiance, whereas *Aiptasia* and *Symbiodinium minutum* were more abundant on vertical substrate under shade. Variation in *Symbiodinium* communities according to light availability and thermal environment is a well-described phenomenon in natural populations of reef-building corals (Rowan *et al.* 1997; LaJeunesse *et al.* 2010; Cooper *et al.* 2011). Host genetic differences corresponding to environment are less well documented, though another study found differences in habitat also associated with differences in *Symbiodinium* community structure in cryptic species of the coral *Seriatopora hystrix* (Warner *et al.* 2015). The potential for cryptic host species diversity to be linked to environmental variation underscores the importance of examining *Symbiodinium* diversity in the context of host population structure (Baums *et al.* 2014; Santos 2014). In contrast to species-level genetic distinctions, intraspecific genetic structure of *Aiptasia* within the Bocas del Toro archipelago was not well correlated with recorded differences in temperature regime, substrate, or light availability.

Taken together, Chapters 2-4 provide a broad new view of the genetic landscape of *Aiptasia*-dinoflagellate interactions and important evolutionary context for future studies utilizing the *Aiptasia* model system. These results paint the picture of a widespread global population distributed throughout tropical and subtropical latitudes, from which the majority of commonly studied laboratory strains appear to be derived

(Chapters 2 and 4). However, diverged lineages also exist, with evidence for a genetically differentiated sub-population specific to a region in Caribbean Panama and a morphologically indistinguishable sister species with at least partially overlapping geographic distribution (Chapter 4). In the Western Atlantic, individuals engage in symbiosis with *Symbiodinium* of clades B1, A (*E. brasiliensis* and *Aiptasia* global population), and B2 (evidence for *Aiptasia* global population only). The Western Atlantic appears to be the center of both host genetic diversity and the diversity of holobiont assemblages. Within the tropical Western Atlantic, distribution of holobiont assemblages may depend strongly on abiotic environmental factors including substrate type, temperature regime, and/or light availability.

Chapter 4 further provided the opportunity to explore the spatial dynamics of clonal reproduction in natural *Aiptasia* and *E. brasiliensis* populations. Individuals sampled from the same mangrove root were genetic clones in all cases for which anemones were genotyped; in contrast, individuals sampled from nearby mangrove roots or from the same patch of coral rubble were infrequently identified as clones. In general, these findings supported the "strawberry-coral model" that clonal proliferation contributes to colonization of continuous substrate but sexual reproduction is more important for colonizing new environments (Williams 1975). However, the general lack of evidence to support widespread distribution of clonal genotypes on spatial scales less than ~30-m for either *Aiptasia* or *E. brasiliensis* was unexpected. The extent to which clonal reproduction may be more frequent in different anemone populations or species remains to be seen, though a recent study also suggested relatively minimal contribution of clonal reproduction to population structure of *Bartholomea annulata,* another tropical representative of the Aiptasiidae family (Titus *et al.* 2017).

The *Aiptasia* model system provides exciting future opportunities to address outstanding questions regarding the influence of abiotic environment on the evolution of cnidarian-dinoflagellate symbosis. In contrast to the case for host-parasite interactions, theoretical predictions involving the evolutionary dynamics of mutualism are unclear. For example, Sachs *et al.* proposed two contrasting frameworks for the evolution of beneficial interactions: the 'mutualistic environment' framework and the 'antagonistic

arms race' framework (Sachs *et al.* 2011). The 'mutualistic environment' framework posits that hosts and symbionts evolve to benefit the partnership. Correspondingly, hosts are expected to select for common symbiont types and against rare or novel genotypes, favoring evolutionary stasis and asexuality of microbial symbionts. Evolutionary stasis in mutualisms is further supported by evolutionary game theory models predicting that the slower-evolving species is favored in mutualistic interactions, the phenomenon termed the 'Red King' effect (Bergstrom & Lachmann 2003; but see Gokhale & Traulsen 2012). The 'antagonistic arms race framework' offers the alternative perspective: conflicts of interest in mutualisms drive co-evolutionary arms race dynamics similar to those observed for host-parasite interactions. This second framework predicts increased evolutionary rates and favors sexual over asexual reproduction in accordance with the Red Queen Hypothesis (Hamilton *et al.* 1990; King *et al.* 2009).

The Geographic Mosaic Theory of Coevolution compliments the contrasting 'mutualistic environment' and 'antagonistic arms race' frameworks by considering symbiotic interactions in a spatial context (Thompson 1999; Gomulkiewicz *et al.* 2000). The Geographic Mosaic Theory of Coevolution includes three important concepts. First, variation in interspecific interactions across environments results in geographic selection mosaics; in other words, an interaction may be antagonistic in one environment but mutualistic in another, with corresponding differences in the strength and direction of selection. Second, spatial variation in selection across environments can result in co-evolutionary hotspots, where the intensity of reciprocal selection is strong, and co-evolutionary coldspots, where selection is non-reciprocal or acts on only one of the partners. Finally, evolutionary processes such as mutation, migration, and genetic drift influence the spatial distribution of coevolving genes and traits ("trait remixing") and consequently, the evolution of interspecific interactions across environments. According to this perspective, symbiotic interactions are highly context-dependent, with Red Queen and Red King dynamics playing out in different areas of the landscape.

The observed patterns of natural variation in *Aiptasia* evoke a testable hypothesis of cnidarian-dinoflagellate evolutionary dynamics: tropical environments are co-evolutionary hotspots, whereas co-evolutionary coldspots exist in temperate or sub-

tropical locations with more pronounced seasonal variation. This hypothesis is consistent with comparisons between anemone-dinoflagellate symbioses in tropical and temperature environments characterized by considerable differences in temperature, irradiance, and nutrient availability (Muller-Parker & Davy 2001). In winter months, temperate anemones receive significantly less photosynthetically active radiation than in summer, whereas PAR is relatively high for tropical anemones year-round. Correspondingly, seasonal differences in irradiance might result in reduced reciprocal selection for anemone-dinoflagellate coevolution in temperate and sub-tropical locations especially during winter months, when symbiont productivity is lowest and anemones may rely more upon heterotrophy as a source of fixed carbon than algal photosynthesis. More tropical sea anemone species have been described that exhibit a symbiotic lifestyle, with *Symbiodinium* densities typically higher than in temperate species but far more sensitive to changes in temperature and irradiance (Muller-Parker & Davy 2001). In addition, evolution of photosynthetic 'auxiliary' structures has been described only for tropical anemones (Muller-Parker & Davy 2001; Venn *et al.* 2008). Tropical anemones with specialized auxiliary structures include species of *Lebrunia,* which extends long, slender tentacles for prey capture at night but short, densely colonized tentacles during the day (Lewis 1984), and *Bunodeopsis*, which hosts dense *Symbiodinium* concentrations in inflatable vesicles on the body column instead of in tentacles that are retracted during the day (Day 1994).

Variation in symbiosis breakdown in *Aiptasia* under heat-stress but not acute cold-shock (Chapter 3) could also support stronger reciprocal selection in tropical co-evolutionary hotspots. In contrast to the case for high temperature, variation in bleaching responses under cold-stress may not strongly influence the natural distribution of *Aiptasia* holobiont assemblages (assuming similar patterns of variation for less extreme cold-stress regimes). Instead, the availability of free-living, compatible *Symbiodinium* types may be a controlling factor in subtropical locations where lower thermal tolerance limits are more likely to constrain species distributions. If tropical environments are hotspots of co-evolution, one might predict higher specificity of the *Aiptasia* sub-population from the Bocas del Toro archipelago compared to the global *Aiptasia* population (Chapter 4),

concomitant with differences in the abundance and relative proportion of compatible free-living genotypes. Additional research comparing *Symbiodinium* infection rates between these two host populations at different temperatures and the abundance of compatible free-living genotypes across latitudes could help address the hypothesis of tropical co-evolutionary hotspots in cnidarian-dinoflagellate symbioses.

The *Aiptasia* model system promises to continue provisioning the scientific community with a wealth of insights on the cellular, ecological, and evolutionary dynamics of cnidarian symbiosis. Comparative genomic approaches could shed light on the genetic mechanisms of specialization to different symbiont types, leveraging comparisons within and among populations of *Aiptasia*, *Exaiptasia brasiliensis*, and other symbiotic anemone species. These comparisons are expected to reveal specific genomic signatures. For example, evidence of selective sweeps, reduced variation, and strong differentiation might be predicted in genomic regions important for specialization; however, generalist populations would be expected to maintain high allelic diversity in these regions, low differentiation compared to other generalist populations, and high differentiation compared to specialists. Genes involved in recognition of sugar and protein moieties on the surface of symbiont cells are promising candidates to display such patterns. In the studies presented here, both lectins and opsonins were identified among candidates of balancing selection within the global *Aiptasia* population (e.g. ficolin, intelectin, techylectin, galactoside-specific lectins; Chapter 2) and as highly differentiated between the *Aiptasia* global and Bocas-specific populations (e.g. Complement C3; Chapter 4). Great potential exists for application of systems biology approaches, which could better integrate genome-scale studies of natural variation with cell biological perspectives. Indeed, *Aiptasia* is one of the most promising candidates for such an analysis, with data available from numerous 'omics' studies comparing differences between symbiotic and aposymbiotic clones in protein expression (Oakley *et al.* 2016) as well as gene expression in adults (Lehnert *et al.* 2014) and larvae (Wolfowicz *et al.* 2016) across the same host genetic background. Finally, the ability to clear and reinfect laboratory populations with cultured symbionts facilitates powerful experimental evolution approaches not possible in the vast majority of symbiotic cnidarians (Hoang *et*

al. 2016; Chakravarti *et al.* 2017). Future studies integrating diverse approaches in the *Aiptasia* model system have incredible potential to deepen our understanding of the interplay between the abiotic environment and evolution of intimate symbiotic interactions in the sea.

BIBLIOGRAPHY

Altizer S, Ostfeld RS, Johnson PTJ, Kutz S, Harvell CD (2013) Climate Change and Infectious Diseases: From Evidence to a Predictive Framework. *Science*, **341**, 514–519.

Antao T, Lopes A, Lopes RJ, Beja-Pereira A, Luikart G (2008) LOSITAN: A workbench to detect molecular adaptation based on a *Fst*-outlier method. *BMC Bioinformatics*, **9**, 1–5.

van der Auwera GA, Carneiro MO, Hartl C *et al.* (2013) From FastQ data to high confidence variant calls: the Genome Analysis Toolkit best practices pipeline. *Current Protocols Bioinformatics*, **11**, 11.10.1-11.10.33.

Ayre DJ (1984) The effects of sexual and asexual reproduction on geographic variation in the sea anemone *Actinia tenebrosa*. *Oecologia*, **62**, 222–229.

Babcock RC (1991) Comparative demography of three species of scleractinian corals using age- and size-dependant classifications. *Ecological Monographs*, **61**, 225–244.

Baird A, Cumbo V, Leggat W, Rodriguez-Lanetty M (2007) Fidelity and flexibility in coral symbioses. *Marine Ecology Progress Series*, **347**, 307–309.

Baker AC (2001) Reef corals bleach to survive change. *Nature*, **411**, 765–6.

Baker AC (2003) Flexibility and specificity in coral-algal symbiosis: Diversity, ecology, and biogeography of *Symbiodinium*. *Annual Review of Ecology, Evolution, and Systematics*, **34**, 661–689.

Baker DM, Weigt L, Fogel M, Knowlton N (2013) Ancient DNA from Coral-Hosted *Symbiodinium* Reveal a Static Mutualism over the Last 172 Years. *PLoS ONE*, **8**, 1–6.

Barbrook AC, Visram S, Douglas AE, Howe CJ (2006) Molecular diversity of dinoflagellate symbionts of Cnidaria: the psbA minicircle of *Symbiodinium*. *Protist*, **157**, 159–71.

Barshis DJ, Ladner JT, Oliver T *et al.* (2013) Genomic basis for coral resilience to climate change. *Proceedings of the National Academy of Sciences*, **110**, 1387–92.

Barshis DJ, Ladner JT, Oliver TA, Palumbi SR (2014) Lineage-specific transcriptional profiles of *Symbiodinium* spp. unaltered by heat stress in a coral host. *Molecular Biology and Evolution*, **31**, 1343–1352.

Bates D, Mächler M, Bolker B, Walker S (2015) Fitting linear mixed-effects models using lme4. *Journal of Statistical Software*, **67**, 1–48.

Baumgarten S, Simakov O, Esherick LY *et al.* (2015) The genome of *Aiptasia*, a sea anemone model for coral biology. *Proceedings of the National Academy of Sciences*, **112**, 11893–11898.

Baums IB, Devlin-Durante MK, Lajeunesse TC (2014) New insights into the dynamics between reef corals and their associated dinoflagellate endosymbionts from population genetic studies. *Molecular Ecology*, **23**, 4203–4215.

Bay RA, Palumbi SR (2014) Multilocus adaptation associated with heat resistance in reef-building corals. *Current Biology*, **24**, 2952–2956.

Belda-Baillie C, Baillie BK, Maruyama T (2002) Specificity of a model cnidarian-dinoflagellate symbiosis. *The Biological Bulletin*, **202**, 74–85.

Bellis ES (2016) *Aiptasia* bleaching variation. *Open Science Framework*.

Bellis ES, Howe DK, Denver DR (2016) Genome-wide polymorphism and signatures of selection in the symbiotic sea anemone *Aiptasia*. *BMC Genomics*, **17**, 160.

Bergstrom CT, Lachmann M (2003) The Red King effect: when the slowest runner wins the coevolutionary race. *Proceedings of the National Academy of Sciences*, **100**, 593–598.

Berkelmans R, van Oppen MJH (2006) The role of zooxanthellae in the thermal tolerance of corals: a "nugget of hope" for coral reefs in an era of climate change. *Proceedings of the Royal Society B*, **273**, 2305–12.

Bieri T, Onishi M, Xiang T, Grossman AR, Pringle JR (2016) Relative contributions of various cellular mechanisms to loss of algae during cnidarian bleaching. *PLoS ONE*, **11**, 1–24.

Biquand E, Okubo N, Aihara Y *et al.* (2017) Acceptable symbiont cell size differs among cnidarian species and may limit symbiont diversity. *The ISME Journal*, 1–11.

Blanquet R (1968) Properties and composition of the nematocyst toxin of the sea anemone, *Aiptasia pallida. Comparative Biochemistry and Physiology*, **25**, 893–902.

Boquet P, Lemichez E (2003) Bacterial virulence factors targeting Rho GTPases: Parasitism or symbiosis? *Trends in Cell Biology*, **13**, 238–246.

Braña AF, Fiedler HP, Nava H *et al.* (2015) Two Streptomyces Species Producing Antibiotic, Antitumor, and Anti-Inflammatory Compounds Are Widespread Among Intertidal Macroalgae and Deep-Sea Coral Reef Invertebrates from the Central Cantabrian Sea. *Microbial Ecology*, **69**, 512–524.

Brown BE (1997) Coral bleaching: causes and consequences. *Coral Reefs*, **16**, 129–138.

Buddemeier RW, Fautin DG (1993) Coral bleaching as an adaptive mechanism: a testable hypothesis. *BioScience*, **43**, 320–326.

Burriesci MS, Raab TK, Pringle JR (2012) Evidence that glucose is the major transferred metabolite in dinoflagellate-cnidarian symbiosis. *The Journal of Experimental Biology*, **215**, 3467–77.

Cacciapaglia C, van Woesik R (2015) Reef-coral refugia in a rapidly changing ocean. *Global Change Biology*, **21**, 2272–2282.

Chakravarti LJ, Beltran VH, van Oppen MJH (2017) Rapid thermal adaptation in photosymbionts of reef-building corals. *Global Change Biology*.

Chapman JA, Kirkness EF, Simakov O *et al.* (2010) The dynamic genome of *Hydra*. *Nature*, **464**, 592–6.

Charlesworth D (2006) Balancing selection and its effects on sequences in nearby genome regions. *PLoS Genetics*, **2**, 379–384.

Chen M-C, Cheng Y-M, Sung P-J, Kuo C-E, Fang L-S (2003) Molecular identification of Rab7 (ApRab7) in *Aiptasia pulchella* and its exclusion from phagosomes harboring zooxanthellae. *Biochemical and Biophysical Research Communications*, **308**, 586–595.

Chia F (1976) Sea anemone reproduction: patterns and adaptive radiations. *Coelenterate Ecology and Behavior*, 261–270.

Chi J, Parrow MW, Dunthorn M (2014) Cryptic sex in *Symbiodinium* (Alveolata, Dinoflagellata) is supported by an inventory of meiotic genes. *Journal of Eukaryotic Microbiology*, **61**, 322–327.

Clayton W (1985) Pedal laceration by the anemone *Aiptasia pallida*. *Marine Ecology Progress Series*, **21**, 75–80.

Coffroth MA, Poland DM, Petrou EL, Brazeau DA, Holmberg JC (2010) Environmental symbiont acquisition may not be the solution to warming seas for reef-building corals. *PLoS ONE*, **5**, e13258.

Coles SL, Fadlallah YH (1991) Reef coral survival and mortality at low temperatures in the Arabian Gulf: new species-specific lower temperature limits. *Coral Reefs*, **9**, 231–237.

Cooper TF, Berkelmans R, Ulstrup KE *et al.* (2011) Environmental factors controlling the distribution of Symbiodinium harboured by the coral Acropora millepora on the Great Barrier Reef. *PLoS ONE*, **6**, e25536.

Costanza R, Arge R, Groot R De *et al.* (1997) The value of the world's ecosystem services and natural capital. *Nature*, **387**, 253–260.

Couce E, Ridgwell A, Hendy EJ (2013) Future habitat suitability for coral reef ecosystems under global warming and ocean acidification. *Global Change Biology*, **19**, 3592–3606.

Császár NBM, Ralph PJ, Frankham R, Berkelmans R, van Oppen MJH (2010) Estimating the potential for adaptation of corals to climate warming. *PLoS ONE*, **5**, e9751.

Cubit JD, Caffey HM, Thompson RC, Windsor DM (1989) Meteorology and hydrography of a shoaling reef flat on the Caribbean coast of Panama. *Coral Reefs*, **8**, 59–66.

Cunning R, Gillette P, Capo T, Galvez K, Baker AC (2015a) Growth tradeoffs associated with thermotolerant symbionts in the coral *Pocillopora damicornis* are lost in warmer oceans. *Coral Reefs*, **34**, 155–160.

Cunning R, Glynn PW, Baker AC (2013) Flexible associations between Pocillopora corals and Symbiodinium limit utility of symbiosis ecology in defining species. *Coral Reefs*, **32**, 795–801.

Cunning R, Silverstein RN, Baker AC (2015b) Investigating the causes and consequences of symbiont shuffling in a multi-partner reef coral symbiosis under environmental change. *Proceedings of the Royal Society B*, **282**, 20141725.

Davy SK, Allemand D, Weis VM (2012) Cell biology of cnidarian-dinoflagellate symbiosis. *Microbiology and Molecular Biology Reviews*, **76**, 229–61.

Day RJ (1994) Algal symbiosis in *Bunodeopsis*: Sea anemones with "Auxiliary" structures. *Biological Bulletin*, **186**, 182–194.

DePristo MA, Banks E, Poplin R *et al.* (2011) A framework for variation discovery and genotyping using next-generation DNA sequencing data. *Nature Genetics*, **43**, 491–498.

Dimond JL, Bingham BL, Muller-Parker G, Oakley C (2013) Symbiont physiology and population dynamics before and during symbiont shifts in a flexible algal-cnidarian symbiosis. *Journal of Phycology*, **49**, 1074–1083.

Dixon GB, Davies SW, Aglyamova G V *et al.* (2015) Genomic determinants of coral heat tolerance across latitudes. *Science*, **348**, 1460–1462.

Douglas AE (2003) Coral bleaching--how and why? *Marine Pollution Bulletin*, **46**, 385–92.

Dunn SR, Pernice M, Green K, Hoegh-Guldberg O, Dove SG (2012) Thermal stress promotes host mitochondrial degradation in symbiotic cnidarians: are the batteries of the reef going to run out? *PLoS ONE*, **7**, e39024.

Dunn SR, Phillips WS, Green DR, Weis VM (2007a) Knockdown of actin and caspase gene expression by RNA interference in the symbiotic anemone *Aiptasia pallida*. *Biological Bulletin*, **212**, 250–258.

Dunn SR, Schnitzler CE, Weis VM (2007b) Apoptosis and autophagy as mechanisms of dinoflagellate symbiont release during cnidarian bleaching: every which way you lose. *Proceedings of the Royal Society B*, **274**, 3079–3085.

Dunn SR, Thomason JC, Le Tissier MDA, Bythell JC (2004) Heat stress induces different forms of cell death in sea anemones and their endosymbiotic algae depending on temperature and duration. *Cell Death and Differentiation*, **11**, 1213–22.

Dunn SR, Weis VM (2009) Apoptosis as a post-phagocytic winnowing mechanism in a coral-dinoflagellate mutualism. *Environmental Microbiology*, **11**, 268–76.

Earl DA, vonHoldt BM (2012) STRUCTURE HARVESTER: A website and program for visualizing STRUCTURE output and implementing the Evanno method. *Conservation Genetics Resources*, **4**, 359–361.

Edmunds PJ, Gates RD (2008) Acclimatization in tropical reef corals. *Marine Ecology Progress Series*, **361**, 307–310.

Emblem Å, Okkenhaug S, Weiss ES *et al.* (2014) Sea anemones possess dynamic mitogenome structures. *Molecular Phylogenetics and Evolution*, **75**, 184–193.

Evanno G, Regnaut S, Goudet J (2005) Detecting the number of clusters of individuals using the software STRUCTURE: A simulation study. *Molecular Ecology*, **14**, 2611–2620.

Fabina NS, Putnam HM, Franklin EC, Stat M, Gates RD (2012) Transmission mode predicts specificity and interaction patterns in coral-*Symbiodinium* networks. *PLoS ONE*, **7**, e44970.

Falush D, Stephens M, Pritchard JK (2003) Inference of population structure using multilocus genotype data: Linked loci and correlated allele frequencies. *Genetics*, **164**, 1567–1587.

Ferrario F, Beck MW, Storlazzi CD *et al.* (2014) The effectiveness of coral reefs for coastal hazard risk reduction and adaptation. *Nature Communications*, **5**, 3794.

Fitt WK, Trench RK (1983) Endocytosis of the symbiotic dinoflagellate *Symbiodinium microadriaticum* Freudenthal by endodermal cells of the scyphistomae of *Cassiopeia xamachana* and resistance of the algae to host digestion. *Journal of Cell Science*, **64**, 195–212.

Fleck J, Fitt WK (1999) Degrading mangrove leaves of *Rhizophora mangle* Linne provide a natural cue for settlement and metamorphosis of the upside down jellyfish *Cassiopea xamachana* Bigelow. *Journal of Experimental Marine Biology and Ecology*, **234**, 83–94.

Foll M, Gaggiotti O (2008) A genome-scan method to identify selected loci appropriate for both dominant and codominant markers: A Bayesian perspective. *Genetics*, **180**, 977–993.

Frieler K, Meinshausen M, Golly A *et al.* (2012) Limiting global warming to 2 °C is unlikely to save most coral reefs. *Nature Climate Change*, **3**, 165–170.

Ganot P, Moya A, Magnone V *et al.* (2011) Adaptations to endosymbiosis in a cnidarian-dinoflagellate association: differential gene expression and specific gene duplications. *PLoS Genetics*, **7**, e1002187.

Gates RD, Baghdasarian G, Muscatine L (1992) Temperature stress causes host-cell detachment in symbiotic Cnidarians: implications for coral bleaching. *Biological Bulletin*, **182**, 324–332.

Gates RD, Edmunds PJ (1999) The Physiological Mechanisms of Acclimatization in Tropical Reef Corals. *American Zoologist*, **39**, 30–43.

Gattuso J, Allemand D, Frankignouelle M (1999) Photosynthesis and calcification at cellular, organismal and community levels in coral reefs: a review on interactions and control by carbonate chemistry. *American Zoologist*, **39**, 160–183.

Geller JB, Fitzgerald LJ, King CE (2005) Fission in sea anemones: integrative studies of life cycle evolution. *Integrative and Comparative Biology*, **45**, 615–22.

Geller JB, Walton ED (2001) Breaking Up and Getting Together: Evolution of Symbiosis and Cloning By Fission in Sea Anemones (Genus *Anthopleura*). *Evolution*, **55**, 1781–1794.

Gittins JR, D'Angelo C, Oswald F, Edwards RJ, Wiedenmann J (2015) Fluorescent protein-mediated colour polymorphism in reef corals: Multicopy genes extend the adaptation/acclimatization potential to variable light environments. *Molecular Ecology*, **24**, 453–465.

Glynn P (1991) Coral reef bleaching in the 1980s and possible connections with global warming. *Trends in Ecology & Evolution*, **6**, 175–179.

Gokhale CS, Traulsen A (2012) Mutualism and evolutionary multiplayer games: revisiting the Red King. *Proceedings of the Royal Society B*, **279**, 4611–6.

Goldstein B, King N (2016) The Future of Cell Biology: Emerging Model Organisms. *Trends in Cell Biology*, **26**, 818–824.

Gomulkiewicz R, Thompson J, Holt R, Nuismer S, Hochberg M (2000) Hot spots, cold spots, and the Geographic Mosaic Theory of Coevolution. *The American Naturalist*, **156**, 156–174.

Good P (2013) *Permutation Tests: A Practical Guide to Resampling Methods for Testing Hypotheses.* Springer-Verlag, New York.

Goulet TL, Cook CB, Goulet D (2005) Effect of short-term exposure to elevated temperatures and light levels on photosynthesis of different host-symbiont combinations in the *Aiptasia pallida*-*Symbiodinium* symbiosis. *Limnology and Oceanography*, **50**, 1490–1498.

Grajales A, Rodríguez E (2014) Morphological revision of the genus *Aiptasia* and the family Aiptasiidae (Cnidaria, Actiniaria, Metridioidea). *Zootaxa*, **3826**, 55–100.

Grajales A, Rodríguez E (2016) Elucidating the evolutionary relationships of the Aiptasiidae, a widespread cnidarian–dinoflagellate model system (Cnidaria: Anthozoa: Actiniaria: Metridioidea). *Molecular Phylogenetics and Evolution*, **94**, 252–263.

Grajales A, Rodríguez E, Thornhill DJ (2016) Patterns of *Symbiodinium* spp. associations

within the family Aiptasiidae, a monophyletic lineage of symbiotic of sea anemones (Cnidaria, Actiniaria). *Coral Reefs*, **35**, 345–355.
Granados-Cifuentes C, Neigel J, Leberg P, Rodriguez-Lanetty M (2015) Genetic diversity of free-living *Symbiodinium* in the Caribbean: the importance of habitats and seasons. *Coral Reefs*, **34**, 927–939.
Grawunder D, Hambleton EA, Bucher M *et al.* (2015) Induction of Gametogenesis in the Cnidarian Endosymbiosis Model *Aiptasia* sp. *Scientific Reports*, **5**, 15677.
Greenstein BJ, Pandolfi JM (2008) Escaping the heat: Range shifts of reef coral taxa in coastal Western Australia. *Global Change Biology*, **14**, 513–528.
Hambleton EA, Guse A, Pringle JR (2014) Similar specificities of symbiont uptake by adults and larvae in an anemone model system for coral biology. *The Journal of Experimental Biology*, **217**, 1613–1619.
Hamilton WD, Axelrod R, Tanese R (1990) Sexual reproduction as an adaptation to resist parasites (a review). *Proceedings of the National Academy of Sciences*, **87**, 3566–73.
Harvell CD, Mitchell CE, Ward JR *et al.* (2002) Climate warming and disease risks for terrestrial and marine biota. *Science*, **296**, 2158–2162.
Hawkins TD, Bradley BJ, Davy SK (2013) Nitric oxide mediates coral bleaching through an apoptotic-like cell death pathway: Evidence from a model sea anemone-dinoflagellate symbiosis. *FASEB Journal*, **27**, 4790–4798.
Hawkins TD, Hagemeyer JCG, Hoadley KD, Marsh AG, Warner ME (2016a) Partitioning of respiration in an animal-algal symbiosis: Implications for different aerobic capacity between *Symbiodinium* spp. *Frontiers in Physiology*, **7**, 128.
Hawkins TD, Hagemeyer JCG, Warner ME (2016b) Temperature moderates the infectiousness of two conspecific Symbiodinium strains isolated from the same host population. *Environmental Microbiology*, **18**.
Heron SF, Maynard JA, van Hooidonk R, Eakin CM (2016) Warming Trends and Bleaching Stress of the World's Coral Reefs 1985–2012. *Scientific Reports*, **6**, 38402.
Herre E, Knowlton N, Mueller U, Rehner S (1999) The evolution of mutualisms: exploring the paths between conflict and cooperation. *Trends in Ecology & Evolution*, **14**, 49–53.
Highsmith RC (1982) Reproduction by fragmentation in corals. *Marine Ecology Progress Series*, **7**, 207–226.
Hill R, Frankart C, Ralph PJ (2005) Impact of bleaching conditions on the components of non-photochemical quenching in the zooxanthellae of a coral. *Journal of Experimental Marine Biology and Ecology*, **322**, 83–92.
Hoang KL, Morran LT, Gerardo NM (2016) Experimental evolution as an underutilized tool for studying beneficial animal-microbe interactions. *Frontiers in Microbiology*, **7**, 1–16.
Hoegh-Guldberg O (1999) Climate change, coral bleaching and the future of the world's coral reefs. *Marine and Freshwater Research*, **50**, 839–866.
Hoegh-Guldberg O (2009) Climate change and coral reefs: Trojan horse or false prophecy? *Coral Reefs*, **28**, 569–575.
Hoegh-Guldberg O (2012) The adaptation of coral reefs to climate change: Is the Red

Queen being outpaced? *Scientia Marina*, **76**, 403–408.
Hoegh-Guldberg O, Fine M, Skirving W *et al.* (2005) Coral bleaching following wintry weather. *Limnology and Oceanography*, **50**, 265–271.
Hoegh-Guldberg O, Muller-Parker G, Cook CB *et al.* (2007) Len Muscatine (1932-2007) and his contributions to the understanding of algal-invertebrate endosymbiosis. *Coral Reefs*, **26**, 731–739.
Hothorn T, Bretz F, Westfall P (2008) Simultaneous inference in general parametric models. *Biometrical Journal*, **50**, 346–63.
Howells E, Beltran V, Larsen N *et al.* (2012) Coral thermal tolerance shaped by local adaptation of photosymbionts. *Nature Climate Change*, **2**, 116–120.
Hughes TP, Kerry J, Álvarez-Noriega M *et al.* (2017) Global warming and recurrent mass bleaching of corals. *Nature*, **543**, 373–378.
Huson DH, Bryant D (2006) Application of phylogenetic networks in evolutionary studies. *Molecular Biology and Evolution*, **23**, 254–267.
Jackson JBC, Hughes TP (1985) Adaptive strategies of coral-reef invertebrates. *American Scientist*, **73**, 265–274.
Jakobsson M, Rosenberg NA (2007) CLUMPP: A cluster matching and permutation program for dealing with label switching and multimodality in analysis of population structure. *Bioinformatics*, **23**, 1801–1806.
Jeong HJ, Lee SY, Kang NS *et al.* (2014) Genetics and morphology characterize the dinoflagellate *Symbiodinium voratum,* n. sp., (Dinophyceae) as the sole representative of *Symbiodinium* clade E. *Journal of Eukaryotic Microbiology*, **61**, 75–94.
Johnson CE, Goulet TL (2007) A comparison of photographic analyses used to quantify zooxanthella density and pigment concentrations in Cnidarians. *Journal of Experimental Marine Biology and Ecology*, **353**, 287–295.
Jombart T (2008) Adegenet: A R package for the multivariate analysis of genetic markers. *Bioinformatics*, **24**, 1403–1405.
Jones AM, Berkelmans R (2010) Potential costs of acclimatization to a warmer climate: growth of a reef coral with heat tolerant vs. sensitive symbiont types. *PLoS ONE*, **5**, e10437.
Jones AM, Berkelmans R (2011) Tradeoffs to thermal acclimation: energetics and reproduction of a reef coral with heat tolerant *Symbiodinium* type-D. *Journal of Marine Biology*, **2011**, 1–12.
Jones AM, Berkelmans R, van Oppen MJH, Mieog JC, Sinclair W (2008) A community change in the algal endosymbionts of a scleractinian coral following a natural bleaching event: field evidence of acclimatization. *Proceedings of the Royal Society B*, **275**, 1359–65.
Kamvar ZN, Tabima JF, Grünwald NJ (2014) Poppr: an R package for genetic analysis of populations with clonal, partially clonal, and/or sexual reproduction. *PeerJ*, **2**, e281.
Kaufmann KW, Thompson RC (2005) Water temperature variation and the meteorological and hydrographic environment of Bocas del Toro, Panama. *Caribbean Journal of Science*, **41**, 392–413.
Kenkel CD, Goodbody-Gringley G, Caillaud D *et al.* (2013) Evidence for a host role in

thermotolerance divergence between populations of the mustard hill coral (*Porites astreoides*) from different reef environments. *Molecular Ecology*, **22**, 4335–48.
Keshavmurthy S, Hsu C-M, Kuo C-Y *et al.* (2012) Symbiont communities and host genetic structure of the brain coral *Platygyra verweyi*, at the outlet of a nuclear power plant and adjacent areas. *Molecular Ecology*, **21**, 4393–407.
Keshavmurthy S, Yang S-Y, Alamaru A *et al.* (2013) DNA barcoding reveals the coral "laboratory-rat", *Stylophora pistillata* encompasses multiple identities. *Scientific Reports*, **3**, 1520.
Kiers TE, Palmer TM, Ives AR, Bruno JF, Bronstein JL (2010) Mutualisms in a changing world: an evolutionary perspective. *Ecology Letters*, **13**, 1459–74.
King KC, Delph LF, Jokela J, Lively CM (2009) The geographic mosaic of sex and the Red Queen. *Current Biology*, **19**, 1438–41.
Kinzie RA, Takayama M, Santos SR, Coffroth MA (2001) The adaptive bleaching hypothesis: experimental tests of critical assumptions. *The Biological Bulletin*, **200**, 51–8.
Korneliussen TS, Moltke I, Albrechtsen A, Nielsen R (2013) Calculation of Tajima's D and other neutrality test statistics from low depth next-generation sequencing data. *BMC Bioinformatics*, **14**, 289.
Kulathinal RJ, Stevison LS, Noor MAF (2009) The genomics of speciation in *Drosophila*: Diversity, divergence, and introgression estimated using low-coverage genome sequencing. *PLoS Genetics*, **5**, e1000550.
Ladner JT, Palumbi SR (2012) Extensive sympatry, cryptic diversity and introgression throughout the geographic distribution of two coral species complexes. *Molecular Ecology*, **21**, 2224–38.
Lajeunesse TC, Andersen RA, Galbraith DW (2005) *Symbiodinium* (Pyrrophyta) genome sizes (DNA content) are smallest among dinoflagellates. *Journal of Phycology*, **41**, 880–886.
LaJeunesse TC, Lee SY, Gil-Agudelo DL, Knowlton N, Jeong HJ (2015) *Symbiodinium necroappetens* sp. nov. (Dinophyceae): an opportunist "zooxanthella" found in bleached and diseased tissues of Caribbean reef corals. *European Journal of Phycology*, **50**, 223–238.
Lajeunesse TC, Parkinson JE, Reimer JD (2012) A genetics-based description of *Symbiodinium minutum* sp. nov. and *S. psygmophilum* sp. nov. (dinophyceae), two dinoflagellates symbiotic with Cnidaria. *Journal of Phycology*, **48**, 1380–1391.
LaJeunesse TC, Pettay DT, Sampayo EM *et al.* (2010) Long-standing environmental conditions, geographic isolation and host-symbiont specificity influence the relative ecological dominance and genetic diversification of coral endosymbionts in the genus *Symbiodinium*. *Journal of Biogeography*, **37**, 785–800.
Lehnert E, Burriesci M, Pringle J (2012) Developing the anemone *Aiptasia* as a tractable model for cnidarian-dinoflagellate symbiosis: the transcriptome of aposymbiotic *A. pallida*. *BMC Genomics*, **13**, 271.
Lehnert EM, Mouchka ME, Burriesci MS *et al.* (2014) Extensive differences in gene expression between symbiotic and aposymbiotic cnidarians. *G3*, **4**, 277–295.
Lesser MP (2006) Oxidative stress in marine environments: Biochemistry and

physiological ecology. *Annual Review of Physiology*, **68**, 253–278.
Lesser MP, Stat M, Gates RD (2013) The endosymbiotic dinoflagellates (*Symbiodinium* sp.) of corals are parasites and mutualists. *Coral Reefs*, **32**, 603–611.
Levin RA, Beltran VH, Hill R *et al.* (2016) Sex, Scavengers, and Chaperones: Transcriptome Secrets of Divergent *Symbiodinium* Thermal Tolerances. *Molecular Biology and Evolution*, **33**, 2201–2215.
Lewis JB (1984) Photosynthetic production by the coral reef anemone, *Lebrunia coralligens* Wilson, and behavioral correlates of two nutritional strategies. *Biological Bulletin*, **167**, 601–612.
Li H, Durbin R (2009) Fast and accurate short read alignment with Burrows-Wheeler transform. *Bioinformatics*, **25**, 1754–60.
Li H, Handsaker B, Wysoker A *et al.* (2009) The Sequence Alignment/Map format and SAMtools. *Bioinformatics (Oxford, England)*, **25**, 2078–9.
Lirman D, Schopmeyer S, Manzello D *et al.* (2011) Severe 2010 cold-water event caused unprecedented mortality to corals of the Florida reef tract and reversed previous survivorship patterns. *PLoS ONE*, **6**, e23047.
Little AF, van Oppen MJH, Willis BL (2004) Flexibility in algal endosymbioses shapes growth in reef corals. *Science*, **304**, 1492–4.
Logan CA, Dunne JP, Eakin CM, Donner SD (2014) Incorporating adaptive responses into future projections of coral bleaching. *Global Change Biology*, **20**, 125–139.
Lowry DB, Hoban S, Kelley JL *et al.* (2017) Breaking RAD: An evaluation of the utility of restriction site associated DNA sequencing for genome scans of adaptation. *Molecular Ecology Resources*, **17**, 142–152.
Matus DQ, Thomsen GH, Martindale MQ (2007) FGF signaling in gastrulation and neural development in *Nematostella vectensis*, an anthozoan cnidarian. *Development Genes and Evolution*, **217**, 137–148.
Matz M V, Treml EA, Aglyamova G V, Oppen MJH van, Bay LK (2017) Adaptive pathways of coral populations on the Great Barrier Reef. *bioRxiv*, 114173.
Maxwell K, Johnson GN (2000) Chlorophyll fluorescence--a practical guide. *Journal of Experimental Botany*, **51**, 659–668.
Maynard Smith J (1978) *The Evolution of Sex*. Cambridge University Press, Cambridge.
McKenna A, Hanna M, Banks E *et al.* (2010) The Genome Analysis Toolkit : A MapReduce framework for analyzing next-generation DNA sequencing data. *Genome Research*, **20**, 1297–1303.
Meirmans PG, Van Tienderen PH (2004) GENOTYPE and GENODIVE: Two programs for the analysis of genetic diversity of asexual organisms. *Molecular Ecology Notes*, **4**, 792–794.
Meyer E, Weis VM (2012) Study of cnidarian-algal symbiosis in the "omics" age. *The Biological Bulletin*, **223**, 44–65.
Moberg F, Folke C (1999) Ecological goods and services of coral reef ecosystems. *Ecological Economics*, **29**, 215–233.
Muller-Parker G (1984) Photosynthesis-irradiance responses and photosynthetic periodicity in the sea anemone *Aiptasia pulchella* and its zooxanthellae. *Marine Biology*, **82**, 225–232.

Muller-Parker G (1987) Seasonal variation in light-shade adaptation of natural populations of the symbiotic sea anemone *Aiptasia pulchella* (Carlgren, 1943) in Hawaii. *Journal of Experimental Marine Biology and Ecology*, **112**, 165–183.

Muller-Parker G, Davy SK (2001) Temperate and tropical algal-sea anemone symbioses. *Invertebrate Biology*, **120**, 104–123.

Müller P, Li XP, Niyogi KK (2001) Non-photochemical quenching. A response to excess light energy. *Plant Physiology*, **125**, 1558–1566.

Muscatine L, Falkowski P, Porter J, Dubinsky Z (1984) Fate of photosynthetic fixed carbon in light- and shade-adapted colonies of the symbiotic coral *Stylophora pistillata*. *Proceedings of the Royal Society of London. Series B, Biological Sciences*, **222**, 181–202.

Muscatine L, Grossman D, Doino J (1991) Release of symbiotic algae by tropical sea anemones and corals after cold shock. *Marine Ecology Progress Series*, **77**, 233–243.

Neubauer EF, Poole AZ, Neubauer P *et al.* (2017) A diverse host thrombospondin-type-1 repeat protein repertoire promotes symbiont colonization during establishment of cnidarian-dinoflagellate symbiosis. *eLife*, **6**, e24494.

Neubauer EF, Poole AZ, Weis VM, Davy SK (2016) The scavenger receptor repertoire in six cnidarian species and its putative role in cnidarian-dinoflagellate symbiosis. *PeerJ*, **4**, e2692.

Newton K, Dixit VM (2012) Signaling in innate immunity and inflammation. *Cold Spring Harbor Perspectives in Biology*, **4**, a006049.

Nii CM, Muscatine L (1997) Oxidative stress in the symbiotic sea anemone *Aiptasia pulchella* (Carlgren, 1943): Contribution of the animal to superoxide ion production at elevated temperature. *Biological Bulletin*, **192**, 444–456.

Oakley CA, Ameismeier MF, Peng L *et al.* (2016) Symbiosis induces widespread changes in the proteome of the model cnidarian *Aiptasia*. *Cellular Microbiology*, **18**, 1009–1023.

van Oppen MJH, Oliver JK, Putnam HM, Gates RD (2015) Building coral reef resilience through assisted evolution. *Proceedings of the National Academy of Sciences*, **112**, 1–7.

Oulion S, Bertrand S, Escriva H (2012) Evolution of the FGF gene family. *International Journal of Evolutionary Biology*, **2012**, 1–12.

Palumbi SR, Barshis DJ, Traylor-Knowles N, Bay RA (2014) Mechanisms of reef coral resistance to future climate change. *Science*, **344**, 895–897.

Pandolfi JM, Connolly SR, Marshall DJ, Cohen AL (2011) Projecting coral reef futures under global warming and ocean acidification. *Science*, **333**, 418–22.

Parkinson JE, Banaszak AT, Altman NS, LaJeunesse TC, Baums IB (2015) Intraspecific diversity among partners drives functional variation in coral symbioses. *Scientific Reports*, **5**, 15667.

Parkinson JE, Baumgarten S, Michell CT *et al.* (2016) Gene expression variation resolves species and individual strains among coral-associated dinoflagellates within the genus Symbiodinium. *Genome Biology and Evolution*, **8**, 665–680.

Parkinson JE, Baums IB (2014) The extended phenotypes of marine symbioses:

ecological and evolutionary consequences of intraspecific genetic diversity in coral-algal associations. *Frontiers in Microbiology*, **5**, 1–19.
Paxton CW, Davy SK, Weis VM (2013) Stress and death of cnidarian host cells play a role in cnidarian bleaching. *The Journal of Experimental Biology*, **216**, 2813–20.
Perez SF, Cook CB, Brooks WR (2001) The role of symbiotic dinoflagellates in the temperature-induced bleaching response of the subtropical sea anemone *Aiptasia pallida*. *Journal of Experimental Marine Biology and Ecology*, **256**, 1–14.
Pinsky ML, Worm B, Fogarty MJ, Sarmiento JL, Levin SA (2013) Marine Taxa Track Local Climate Velocities. *Science*, **341**, 1239–1242.
Pochon X, Gates RD (2010) A new *Symbiodinium* clade (Dinophyceae) from soritid foraminifera in Hawai'i. *Molecular Phylogenetics and Evolution*, **56**, 492–497.
Pochon X, Montoya-Burgos JI, Stadelmann B, Pawlowski J (2006) Molecular phylogeny, evolutionary rates, and divergence timing of the symbiotic dinoflagellate genus *Symbiodinium*. *Molecular Phylogenetics and Evolution*, **38**, 20–30.
Poole AZ, Kitchen SA, Weis VM (2016) The role of complement in cnidarian-dinoflagellate symbiosis and immune challenge in the sea anemone *Aiptasia pallida*. *Frontiers in Microbiology*, **7**, 1–18.
Prada C, Hanna B, Budd AF *et al.* (2016) Empty Niches after Extinctions Increase Population Sizes of Modern Corals. *Current Biology*, **26**, 3190–3194.
Precht WF, Aronson RB (2004) Climate flickers and range shifts of reef corals. *Frontiers in Ecology and the Environment*, **2**, 307–314.
Pritchard JK, Stephens M, Donnelly P (2000) Inference of population structure using multilocus genotype data. *Genetics*, **155**, 945–59.
Ptak SE, Przeworski M (2002) Evidence for population growth in humans is confounded by fine-scale population structure. *Trends in Genetics*, **18**, 559–563.
Putnam HM, Gates RD (2015) Preconditioning in the reef-building coral *Pocillopora damicornis* and the potential for trans-generational acclimatization in coral larvae under future climate change conditions. *Journal of Experimental Biology*, **218**, 2365–2372.
Putnam N, Srivastava M, Hellsten U (2007) Sea anemone genome reveals ancestral eumetazoan gene repertoire and genomic organization. *Science*, **317**, 86–94.
Putnam HM, Stat M, Pochon X, Gates RD (2012) Endosymbiotic flexibility associates with environmental sensitivity in scleractinian corals. *Proceedings of the Royal Society B*, **279**, 4352–61.
R Core Team (2014) R: A language and environment for statistical computing.
Reitzel AM, Herrera S, Layden MJ, Martindale MQ, Shank TM (2013) Going where traditional markers have not gone before: utility of and promise for RAD sequencing in marine invertebrate phylogeography and population genomics. *Molecular Ecology*, **22**, 2953–70.
Rodriguez-Lanetty M, Phillips WS, Weis VM (2006) Transcriptome analysis of a cnidarian-dinoflagellate mutualism reveals complex modulation of host gene expression. *BMC Genomics*, **7**, 23.
Rosenberg NA (2004) DISTRUCT: A program for the graphical display of population structure. *Molecular Ecology Notes*, **4**, 137–138.

Rosic N, Kaniewska P, Chan C-KK *et al.* (2014) Early transcriptional changes in the reef-building coral *Acropora aspera* in response to thermal and nutrient stress. *BMC Genomics*, **15**, 1052.

Rossman KL, Der CJ, Sondek J (2005) GEF means go: turning on Rho GTPases with guanine nucleotide-exchange factors. *Nature Reviews. Molecular Cell Biology*, **6**, 167–180.

Roth MS, Goericke R, Deheyn DD (2012) Cold induces acute stress but heat is ultimately more deleterious for the reef-building coral *Acropora yongei*. *Scientific reports*, **2**, 240.

Rouzé H, Lecellier G, Saulnier D, Berteaux-Lecellier V (2016) *Symbiodinium* clades A and D differentially predispose *Acropora cytherea* to disease and *Vibrio* spp. colonization. *Ecology and Evolution*, **6**, 560–572.

Rowan R (2004) Thermal adaptation in reef coral symbionts. *Nature*, **430**, 742.

Rowan R, Knowlton N, Baker AC, Jara J (1997) Landscape ecology of algal symbionts creates variation in episodes of coral bleaching. *Nature*, **388**, 265–9.

Rumble SM, Lacroute P, Dalca A V. *et al.* (2009) SHRiMP: Accurate mapping of short color-space reads. *PLoS Computational Biology*, **5**, 1–11.

Sachidanandam R, Weissman D, Schmidt SC *et al.* (2001) A map of human genome sequence variation containing 1.42 million single nucleotide polymorphisms. *Nature*, **409**, 928–933.

Sachs JL, Essenberg CJ, Turcotte MM (2011) New paradigms for the evolution of beneficial infections. *Trends in Ecology & Evolution*, **26**, 202–9.

Sachs JL, Wilcox TP (2006) A shift to parasitism in the jellyfish symbiont *Symbiodinium microadriaticum*. *Proceedings of the Royal Society B*, **273**, 425–9.

Sampayo EM, Ridgway T, Bongaerts P, Hoegh-Guldberg O (2008) Bleaching susceptibility and mortality of corals are determined by fine-scale differences in symbiont type. *Proceedings of the National Academy of Sciences*, **105**, 10444–9.

Santos SR (2014) Expanding the population genetic perspective of cnidarian-*Symbiodinium* symbioses. *Molecular Ecology*, **23**, 4185–4187.

Sebens KP (1980) The regulation of asexual reproduction and indeterminate body size in the sea anemone *Anthopleura elegantissima* (Brandt). *The Biological Bulletin*, **158**, 370–382.

Sebens KP (1982) Asexual Reproduction in *Anthopleura elegantissima* (Anthozoa: Actiniaria): Seasonality and Spatial Extent of Clones. *Ecology*, **63**, 434–444.

Shearer TL, Van Oppen MJH, Romano SL, Wörheide G (2002) Slow mitochondrial DNA sequence evolution in the Anthozoa (Cnidaria). *Molecular Ecology*, **11**, 2475–87.

Shinzato C, Inoue M, Kusakabe M (2014) A snapshot of a coral "holobiont": a transcriptome assembly of the scleractinian coral, Porites, captures a wide variety of genes from both the host and symbiotic zooxanthellae. *PLoS ONE*, **9**, e85182.

Shinzato C, Mungpakdee S, Arakaki N, Satoh N (2015) Genome-wide SNP analysis explains coral diversity and recovery in the Ryukyu Archipelago. *Scientific Reports*, **5**, 1–8.

Shinzato C, Shoguchi E, Kawashima T *et al.* (2011) Using the *Acropora digitifera*

genome to understand coral responses to environmental change. *Nature*, **476**, 320–3.
Shoguchi E, Shinzato C, Kawashima T *et al.* (2013) Draft assembly of the *Symbiodinium minutum* nuclear genome reveals dinoflagellate gene structure. *Current biology : CB*, **23**, 1399–408.
Siebeck UE, Marshall NJ, Klüter A, Hoegh-Guldberg O (2006) Monitoring coral bleaching using a colour reference card. *Coral Reefs*, **25**, 453–460.
Silverstein RN, Correa AMS, Baker AC (2012) Specificity is rarely absolute in coral-algal symbiosis: implications for coral response to climate change. *Proceedings of the Royal Society B*, **279**, 2609–18.
Silverstein RN, Cunning R, Baker AC (2015) Change in algal symbiont communities after bleaching, not prior heat exposure, increases heat tolerance of reef corals. *Global Change Biology*, **21**, 236–249.
Six DL (2009) Climate change and mutualism. *Nature Reviews Microbiology*, **7**, 686.
Smith GJ, Muscatine L (1999) Cell cycle of symbiotic dinoflagellates: variation in G1 phase-duration with anemone nutritional status and macronutrient supply in the *Aiptasia pulchella-Symbiodinium pulchrorum* symbiosis. *Marine Biology*, **134**, 405–418.
Song S, Jiang F, Yuan J, Guo W, Miao Y (2013) Exceptionally high cumulative percentage of NUMTs originating from linear mitochondrial DNA molecules in the Hydra magnipapillata genome. *BMC Genomics*, **14**, 447.
Stadler T, Haubold B, Merino C, Stephan W, Pfaffelhuber P (2009) The impact of sampling schemes on the site frequency spectrum in nonequilibrium subdivided populations. *Genetics*, **182**, 205–216.
Stat M, Morris E, Gates RD (2008) Functional diversity in coral – dinoflagellate symbiosis. *Proceedings of the National Academy of Sciences*, **105**, 9256–9261.
Steen R, Muscatine L (1987) Low temperature evokes rapid exocytosis of symbiotic algae by a sea anemone. *The Biological Bulletin*, **172**, 246–263.
Straub SCK, Parks M, Weitemier K *et al.* (2012) Navigating the tip of the genomic iceberg: Next-generation sequencing for plant systematics. *American Journal of Botany*, **99**, 349–64.
Suggett DJ, Goyen S, Evenhuis C *et al.* (2015) Functional diversity of photobiological traits within the genus *Symbiodinium* appears to be governed by the interaction of cell size with cladal designation. *New Phytologist*, **208**, 370–381.
Sunagawa S, Wilson EC, Thaler M *et al.* (2009) Generation and analysis of transcriptomic resources for a model system on the rise: the sea anemone *Aiptasia pallida* and its dinoflagellate endosymbiont. *BMC Genomics*, **10**, 258.
Swan KA, Curtis DE, Mckusick KB *et al.* (2002) High-throughput gene mapping in *Caenorhabditis elegans*. *Genome Research*, **12**, 1100–1105.
Tajima F (1989) Statistical method for testing the neutral mutation hypothesis by DNA polymorphism. *Genetics*, **123**, 585–595.
Takabayashi M, Adams LM, Pochon X, Gates RD (2011) Genetic diversity of free-living *Symbiodinium* in surface water and sediment of Hawai‘i and Florida. *Coral Reefs*, **31**, 157–167.
Takahashi S, Nakamura T, Sakamizu M, van Woesik R, Yamasaki H (2004) Repair

machinery of symbiotic photosynthesis as the primary target of heat stress for reef-building corals. *Plant & Cell Physiology*, **45**, 251–5.
Takahashi S, Yoshioka-Nishimura M, Nanba D, Badger MR (2013) Thermal acclimation of the symbiotic alga *Symbiodinium* spp. alleviates photobleaching under heat stress. *Plant Physiology*, **161**, 477–85.
Tchernov D, Gorbunov MY, de Vargas C *et al.* (2004) Membrane lipids of symbiotic algae are diagnostic of sensitivity to thermal bleaching in corals. *Proceedings of the National Academy of Sciences*, **101**, 13531–5.
Thomas L, Kendrick GA, Kennington WJ, Richards ZT, Stat M (2014) Exploring *Symbiodinium* diversity and host specificity in *Acropora* corals from geographical extremes of Western Australia with 454 amplicon pyrosequencing. *Molecular Ecology*, **23**, 3113–3126.
Thompson JN (1999) Specific hypotheses on the Geographic Mosaic of Coevolution. *The American Naturalist*, **153**, S1–S14.
Thornhill DJ, Howells EJ, Wham DC, Steury TD, Santos SR (2017) Population genetics of reef coral endosymbionts (*Symbiodinium,* Dinophyceae). *Molecular Ecology*, **1**, doi:10.1111/mec.14055.
Thornhill DJ, Kemp DW, Bruns BU, Fitt WK, Schmidt GW (2008) Correspondence between cold tolerance and temperate biogeography in a western Atlantic *Symbiodinium* (Dinophyta) lineage. *Journal of Phycology*, **44**, 1126–1135.
Thornhill DJ, LaJeunesse TC, Kemp DW, Fitt WK, Schmidt GW (2005) Multi-year, seasonal genotypic surveys of coral-algal symbioses reveal prevalent stability or post-bleaching reversion. *Marine Biology*, **148**, 711–722.
Thornhill DJ, Xiang Y, Pettay DT, Zhong M, Santos SR (2013) Population genetic data of a model symbiotic cnidarian system reveal remarkable symbiotic specificity and vectored introductions across ocean basins. *Molecular Ecology*, **22**, 4499–515.
Thorvaldsdóttir H, Robinson JT, Mesirov JP (2013) Integrative Genomics Viewer (IGV): high-performance genomics data visualization and exploration. *Briefings in Bioinformatics*, **14**, 178–92.
Titus BM, Daly M, Macrander J *et al.* (2017) Contrasting abundance and contribution of clonal proliferation to the population structure of the corkscrew sea anemone *Bartholomea annulata* in the tropical Western Atlantic. *Invertebrate Biology*, **136**, 62–74.
Tolleter D, Seneca FO, DeNofrio JC *et al.* (2013) Coral bleaching independent of photosynthetic activity. *Current Biology*, **23**, 1782–6.
Vega Thurber RL, Burkepile DE, Fuchs C *et al.* (2014) Chronic nutrient enrichment increases prevalence and severity of coral disease and bleaching. *Global Change Biology*, **20**, 544–554.
Vega Thurber R, Willner-Hall D, Rodriguez-Mueller B *et al.* (2009) Metagenomic analysis of stressed coral holobionts. *Environmental Microbiology*, **11**, 2148–2163.
Venables WN, Ripley BD (2002) *Modern Applied Statistics with S*. Springer, New York.
Venn AA, Loram JE, Douglas AE (2008) Photosynthetic symbioses in animals. *Journal of Experimental Botany*, **59**, 1069–1080.
Venn AA, Wilson MA, Trapido-Rosenthal HG, Keely BJ, Douglas AE (2006) The

impact of coral bleaching on the pigment profile of the symbiotic alga, *Symbiodinium*. *Plant Cell and Environment*, **29**, 2133–2142.
Wang X, Liew YJ, Li Y *et al.* (2017) Draft genomes of the corallimorpharians *Amplexidiscus fenestrafer* and *Discosoma sp. Molecular Ecology Resources*, doi: 10.1111/1755-0998.12680.
Wang S, Meyer E, McKay J, Matz M (2012) 2b-RAD: a simple and flexible method for genome-wide genotyping. *Nature Methods*, **9**, 808–810.
Warner PA, Van Oppen MJH, Willis BL (2015) Unexpected cryptic species diversity in the widespread coral *Seriatopora hystrix* masks spatial-genetic patterns of connectivity. *Molecular Ecology*, **24**, 2993–3008.
Warnes G, Bolker B, Bonebakker L *et al.* (2015) gplots: Various R programming tools for plotting data.
Weis VM (2008) Cellular mechanisms of Cnidarian bleaching: stress causes the collapse of symbiosis. *The Journal of Experimental Biology*, **211**, 3059–66.
Weis VM (2010) The susceptibility and resilience of corals to thermal stress: adaptation, acclimatization or both? *Molecular Ecology*, **19**, 1515–7.
Weis VM, Davy SK, Hoegh-Guldberg O, Rodriguez-Lanetty M, Pringle JR (2008) Cell biology in model systems as the key to understanding corals. *Trends in Ecology & Evolution*, **23**, 369–76.
Weitemier K, Straub SCK, Cronn RC *et al.* (2014) Hyb-Seq: Combining Target Enrichment and Genome Skimming for Plant Phylogenomics. *Applications in Plant Sciences*, **2**, 1400042.
Williams GC (1975) The Strawberry-Coral Model. In: *Sex and Evolution* , pp. 26–34. Princeton University Press, Princeton, New Jersey.
Wisecaver JH, Hackett JD (2011) Dinoflagellate genome evolution. *Annual Review of Microbiology*, **65**, 369–87.
Wolfowicz I, Baumgarten S, Voss PA *et al.* (2016) *Aiptasia* sp. larvae as a model to reveal mechanisms of symbiont selection in cnidarians. *Scientific Reports*, srep32366.
Wood-Charlson EM, Hollingsworth LL, Krupp DA, Weis VM (2006) Lectin/glycan interactions play a role in recognition in a coral/dinoflagellate symbiosis. *Cellular Microbiology*, **8**, 1985–1993.
Xiang T, Nelson W, Rodriguez J, Tolleter D, Grossman AR (2015) *Symbiodinium* transcriptome and global responses of cells to immediate changes in light intensity when grown under autotrophic or mixotrophic conditions. *The Plant Journal*, **82**, 67–80.
Yellowlees D, Rees TA V, Leggat W (2008) Metabolic interactions between algal symbionts and invertebrate hosts. *Plant, Cell & Environment*, **31**, 679–94.
Zhang Z, Zhang Z, Li J *et al.* (2006) KaKs_Calculator: Calculating Ka and Ks through model selection and model averaging. *Genomics Proteomics Bioinformatics*, **4**, 259–263.
Zheng Q, Wang XJ (2008) GOEAST: a web-based software toolkit for Gene Ontology enrichment analysis. *Nucleic Acids Research*, **36**, 358–363.

APPENDICES

APPENDIX A: Supplementary tables for Chapter 2

Table A1. Read coverage based genotyping of *Symbiodnium* communities harbored by anemone samples. Asterisks indicate aposymbiotic samples. The length of the sequence is given in parentheses. For the clade B cyt b and psbA sequences, polymorphisms were observed among the 10 samples at positions listed, separated by colons. The observed bases and percent of reads supporting them are shown for these markers for each sample. Presence or absence of an insertion/deletion polymorphism in cp23s is also indicated.

Clade	Marker	Average per-sample read coverage (x)									
		BM1*	BM2	HI1*	HI2	HI3	FL1	CC7	UN1	UN2	UN3
A	*COI* (1044)	0	0	0	0	0	0	17	0	27	0
	cyt b (1131)	0	0	0	0	0	0	12	0	29	0
	COIII (783)	0	0	0	0	0	0	6	0	28	0
	cp23s (1131)	0	0	0	0	0	0	12	0	68	0
	psbA (1131)	0	0	0	0	0	0	21	0	144	0
	ITS2 (1131)	0	0	0	0	0	0	1	0	18	0
B	*COI* (1044)	0	10	1	47	3	94	0	4	77	9
	cyt b Pos. 87:578:871	0 -	9 C:G:G (100%)	1 -	40 C:G:C (100%)	3 C:G:G (100%)	62 T:C:C (100%)	0 -	4 C:G:G (100%)	68 T:C:C/ C:G:G (96%/4%)	11 C:G:G/C:G:C (88%/12%)
	COIII (783)	0	7	1	31	1	47	0	4	51	6
	cp23s Pos. 193-284	0 -	8 Del.	1 -	20 Del.	5 Del.	167 Ins.	0 -	5 Del.	157 Ins.	16 Del.
	psbA Pos. 65:542	0 -	8 G:T (100%)	0 -	15 G:T (100%)	6 G-	82 G:T (100%)	0 -	3 G:T (100%)	42 A:T/ G:T (93%/7%)	14 G:C/G:T (75%/25%)
	ITS2 (1131)	0	1	0	2	0	10	0	1	28	0

Table A2. Genome-wide outlier regions. Regions were selected if at least 4 consecutive 100 kb windows (step size = 10kb) were observed that had values of heterozygosity (Hw), pairwise nucleotide diversity (π), or Tajima's D that were more than 3 SD from the mean. A list of predicted genes in each of the following regions is available with the published version of the manuscript online (Bellis *et al.* 2016).

Outlier Category	Scaffold	Start Position	End Position	Size (kb)	Tajima's D	Hw	π
High Hw (>3SD from mean)	scaffold3size1550370	1410000	1550000	140	-0.05	0.58	279
	scaffold110size576893	110000	310000	200	-0.36	0.64	272
	scaffold115size568046	50000	250000	200	-0.85	0.60	212
	scaffold142size481666	0	130000	130	-0.24	0.55	275
	scaffold162size446422	100000	240000	140	0.22	0.53	345
	scaffold397size198121	40000	190000	150	-0.92	0.55	235
	scaffold439size166312	0	130000	130	-0.47	0.55	333
High π (>3SD from mean)	scaffold8size1436206	850000	1370000	520	-0.26	0.43	851
	scaffold10size1280550	740000	1000000	260	-0.06	0.31	842
	scaffold63size817263	250000	810000	560	-0.22	0.35	860
	scaffold76size705516	120000	420000	300	-0.39	0.34	868
High Tajima's D (>3SD from mean)	scaffold3size1550370	430000	580000	150	0.73	0.39	283
	scaffold53size786922	360000	490000	130	0.74	0.38	189
	scaffold173size436934	80000	240000	160	0.58	0.31	507
	scaffold203size396098	40000	200000	160	0.56	0.41	415
Low Hw (>3SD from mean)	scaffold58size770527	150000	300000	150	-0.83	0.19	303
	scaffold311size264479	60000	210000	150	-0.26	0.21	410
Low Tajima's D (>3SD from mean)	scaffold19size1061714	350000	680000	330	-1.62	0.40	208
	scaffold33size924377	140000	310000	170	-1.70	0.28	292
	scaffold71size717949	270000	470000	200	-1.83	0.31	138
	scaffold115size568046	180000	320000	140	-1.82	0.35	157
	scaffold141size483637	150000	420000	270	-2.02	0.33	166
	scaffold149size465730	320000	460000	140	-1.83	0.35	170
	scaffold155size455307	10000	250000	240	-1.67	0.36	178
	scaffold301size296964	40000	290000	250	-1.68	0.37	243
	scaffold362size220168	40000	180000	140	-1.60	0.32	193

Table A3. Results from GO-term enrichment analysis for outlier lists. GO-terms listed in order of increasing p-value at a significance level of α=0.01. P-values were corrected for multiple comparisons using the Yekutieli method.

Ontology	GO ID	Term	Genes (#)	p-value
High π (>3SD from mean)				
Biological Process	GO:1901642	nucleoside transmembrane transport	4	9.6E-03
Cellular Component	GO:0016607	nuclear speck	13	7.8E-06
	GO:0016604	nuclear body	14	2.7E-04
	GO:0005575	cellular_component	170	1.2E-03
	GO:0005654	nucleoplasm	24	9.6E-03
Molecular Function	GO:0005415	nucleoside:sodium symporter activity	4	1.9E-04
	GO:0030246	carbohydrate binding	16	2.7E-04
	GO:0015370	solute:sodium symporter activity	6	9.6E-03
Low Hw (>3SD from mean)				
Biological Process	GO:0006821	chloride transport	4	1.1E-03
	GO:0015698	inorganic anion transport	4	2.7E-03
	GO:0007218	neuropeptide signaling pathway	5	4.4E-03
Cellular Component	GO:0034707	chloride channel complex	4	5.5E-04
	GO:0045211	postsynaptic membrane	5	4.3E-03
	GO:0034702	ion channel complex	5	6.6E-03
	GO:0097060	synaptic membrane	5	6.6E-03
Molecular Function	GO:0022824	transmitter-gated ion channel activity	3	5.5E-04
	GO:0022835	transmitter-gated channel activity	3	5.5E-04
	GO:0005253	anion channel activity	4	1.1E-03
	GO:0005254	chloride channel activity	4	1.1E-03
	GO:0015108	chloride transmembrane transporter activity	4	1.1E-03
	GO:0015103	inorganic anion transmembrane transporter activity	4	2.1E-03
	GO:0005230	extracellular ligand-gated ion channel activity	4	6.6E-03
	GO:0016934	extracellular-glycine-gated chloride channel activity	2	9.3E-03

Table A3 (Continued)

Low Tajima's D (>3SD from mean)				
Biological Process	GO:0038032	termination of G-protein coupled receptor signaling pathway	68	2.1E-121
	GO:0023021	termination of signal transduction	68	1.8E-120
	GO:0045744	negative regulation of G-protein coupled receptor protein signaling pathway	68	6.5E-113
	GO:0008277	regulation of G-protein coupled receptor protein signaling pathway	68	4.0E-100
	GO:0032321	positive regulation of Rho GTPase activity	68	2.1E-84
	GO:0048011	neurotrophin TRK receptor signaling pathway	59	4.0E-82
	GO:0032319	regulation of Rho GTPase activity	68	8.3E-82
	GO:0038179	neurotrophin signaling pathway	59	7.3E-81
	GO:0035023	regulation of Rho protein signal transduction	68	9.1E-79
	GO:0032320	positive regulation of Ras GTPase activity	68	5.2E-73
	GO:0097190	apoptotic signaling pathway	60	5.1E-70
	GO:1900117	regulation of execution phase of apoptosis	60	1.6E-69
	GO:0043065	positive regulation of apoptotic process	62	3.4E-68
	GO:0032318	regulation of Ras GTPase activity	68	9.4E-68
	GO:0043068	positive regulation of programmed cell death	62	1.3E-67
	GO:0010942	positive regulation of cell death	62	5.1E-66
	GO:0046578	regulation of Ras protein signal transduction	68	1.1E-62
	GO:0051056	regulation of small GTPase mediated signal transduction	68	4.1E-61
	GO:0043547	positive regulation of GTPase activity	68	4.6E-59
	GO:0043087	regulation of GTPase activity	68	8.9E-58
	GO:0033124	regulation of GTP catabolic process	68	9.8E-58
	GO:0007411	axon guidance	59	4.1E-57
	GO:0007264	small GTPase mediated signal transduction	60	1.5E-56
	GO:0030811	regulation of nucleotide catabolic	68	2.1E-56

Table A3 (Continued)

	GO:0033121	regulation of purine nucleotide catabolic process	68	2.1E-56
	GO:0009118	regulation of nucleoside metabolic process	68	2.3E-56
	GO:0009968	negative regulation of signal transduction	69	2.9E-54
	GO:0007409	axonogenesis	62	1.1E-53
	GO:0042330	taxis	60	1.0E-52
	GO:0006935	chemotaxis	59	4.2E-52
	GO:0023057	negative regulation of signaling	69	1.3E-51
	GO:0010648	negative regulation of cell communication	69	2.4E-51
	GO:0048585	negative regulation of response to stimulus	70	7.7E-51
	GO:0048667	cell morphogenesis involved in neuron differentiation	62	1.2E-50
	GO:0071363	cellular response to growth factor stimulus	59	7.5E-50
	GO:0051345	positive regulation of hydrolase activity	69	9.0E-50
	GO:0070848	response to growth factor stimulus	59	2.1E-49
	GO:0048812	neuron projection morphogenesis	62	3.7E-49
	GO:1900542	regulation of purine nucleotide metabolic process	68	8.6E-49
	GO:0006140	regulation of nucleotide metabolic process	68	1.0E-48
	GO:0031329	regulation of cellular catabolic process	68	2.3E-48
	GO:0031175	neuron projection development	63	1.6E-46
	GO:0009894	regulation of catabolic process	68	1.6E-46
	GO:0000904	cell morphogenesis involved in differentiation	63	3.1E-46
	GO:0007169	transmembrane receptor protein tyrosine kinase signaling pathway	59	2.5E-45
	GO:0043085	positive regulation of catalytic activity	73	8.7E-43
	GO:0048858	cell projection morphogenesis	63	3.4E-42
	GO:0048666	neuron development	64	7.9E-42
	GO:0032990	cell part morphogenesis	63	1.1E-41
	GO:0006915	apoptotic process	63	3.9E-41
	GO:0051336	regulation of hydrolase activity	69	4.8E-41

Table A3 (Continued)

	GO:0007167	enzyme linked receptor protein signaling pathway	59	6.0E-41
	GO:0035556	intracellular signal transduction	72	1.3E-40
	GO:0012501	programmed cell death	63	2.4E-40
	GO:0044093	positive regulation of molecular function	73	1.3E-39
	GO:0000902	cell morphogenesis	64	3.0E-38
	GO:0030182	neuron differentiation	64	3.0E-37
	GO:0019220	regulation of phosphate metabolic process	77	5.6E-37
	GO:0051174	regulation of phosphorus metabolic process	77	6.4E-37
	GO:0032989	cellular component morphogenesis	65	6.5E-37
	GO:0042981	regulation of apoptotic process	63	2.3E-36
	GO:0008219	cell death	63	3.8E-36
	GO:0016265	death	63	4.0E-36
	GO:0043067	regulation of programmed cell death	63	4.5E-36
	GO:0030030	cell projection organization	64	1.5E-35
	GO:0040011	locomotion	61	2.3E-35
	GO:0010941	regulation of cell death	63	3.0E-35
	GO:0007186	G-protein coupled receptor signaling pathway	61	8.6E-34
	GO:0009966	regulation of signal transduction	76	3.7E-32
	GO:0048699	generation of neurons	64	3.9E-32
	GO:0050790	regulation of catalytic activity	74	1.3E-31
	GO:0006928	cellular component movement	61	4.3E-31
	GO:0071310	cellular response to organic substance	59	1.2E-30
	GO:0022008	neurogenesis	64	2.3E-30
	GO:0048468	cell development	65	1.6E-29
	GO:0065009	regulation of molecular function	74	1.2E-27
	GO:0010646	regulation of cell communication	76	1.3E-27
	GO:0023051	regulation of signaling	76	1.4E-27
	GO:0048583	regulation of response to stimulus	78	5.7E-27
	GO:0048523	negative regulation of cellular process	81	8.1E-27
	GO:0070887	cellular response to chemical stimulus	59	3.3E-26
	GO:0009605	response to external stimulus	62	7.5E-26

Table A3 (Continued)

	GO:0007399	nervous system development	68	5.0E-25
	GO:0048519	negative regulation of biological process	82	2.2E-24
	GO:0010033	response to organic substance	61	7.8E-23
	GO:0019219	regulation of nucleobase-containing compound metabolic process	87	5.1E-22
	GO:0051171	regulation of nitrogen compound metabolic process	87	1.3E-21
	GO:0009653	anatomical structure morphogenesis	67	6.8E-20
	GO:0031323	regulation of cellular metabolic process	93	2.8E-18
	GO:0007166	cell surface receptor signaling pathway	65	7.3E-18
	GO:0030154	cell differentiation	69	1.1E-17
	GO:0048869	cellular developmental process	71	4.3E-17
	GO:0080090	regulation of primary metabolic process	91	4.4E-17
	GO:0048522	positive regulation of cellular process	71	9.1E-17
	GO:0042221	response to chemical stimulus	63	3.2E-16
	GO:0007165	signal transduction	82	3.3E-16
	GO:0019222	regulation of metabolic process	95	7.0E-16
	GO:0048518	positive regulation of biological process	72	3.8E-15
	GO:0023052	signaling	83	4.9E-14
	GO:0044700	single organism signaling	83	4.9E-14
	GO:0007154	cell communication	83	4.5E-13
	GO:0048731	system development	70	8.9E-13
	GO:0051716	cellular response to stimulus	85	1.0E-10
	GO:0048856	anatomical structure development	73	1.0E-10
	GO:0071840	cellular component organization or biogenesis	82	1.7E-10
	GO:0007275	multicellular organismal development	74	4.9E-10
	GO:0016043	cellular component organization	79	5.0E-10
	GO:0044767	single-organism developmental process	75	9.1E-10
	GO:0032502	developmental process	76	9.0E-09
	GO:0050896	response to stimulus	90	5.2E-06
	GO:0050794	regulation of cellular process	104	7.0E-06

Table A3 (Continued)

	GO:0044707	single-multicellular organism process	75	1.9E-05
	GO:0032501	multicellular organismal process	75	5.0E-05
	GO:0050789	regulation of biological process	105	1.0E-04
	GO:0065007	biological regulation	109	4.6E-04
Cellular Component	GO:0070062	extracellular vesicular exosome	63	1.2E-40
	GO:0043230	extracellular organelle	63	1.6E-40
	GO:0065010	extracellular membrane-bounded organelle	63	1.6E-40
	GO:0005829	cytosol	69	2.4E-28
	GO:0031988	membrane-bounded vesicle	66	3.9E-25
	GO:0031982	vesicle	66	1.5E-23
	GO:0044421	extracellular region part	65	3.3E-21
	GO:0005576	extracellular region	68	6.1E-13
	GO:0044444	cytoplasmic part	99	1.6E-07
	GO:0005737	cytoplasm	124	6.7E-06
	GO:0016020	membrane	107	1.3E-05
	GO:0043227	membrane-bounded organelle	124	2.6E-05
	GO:0044424	intracellular part	141	3.7E-03
	GO:0005622	intracellular	141	7.0E-03
Molecular Function	GO:0005089	Rho guanyl-nucleotide exchange factor activity	68	2.9E-92
	GO:0005088	Ras guanyl-nucleotide exchange factor activity	68	1.8E-86
	GO:0005085	guanyl-nucleotide exchange factor activity	68	2.6E-77
	GO:0005096	GTPase activator activity	68	7.4E-77
	GO:0001664	G-protein coupled receptor binding	59	4.0E-74
	GO:0005083	small GTPase regulator activity	68	4.5E-68
	GO:0008047	enzyme activator activity	68	5.5E-66
	GO:0030695	GTPase regulator activity	68	1.0E-58
	GO:0060589	nucleoside-triphosphatase regulator activity	68	2.7E-58
	GO:0030234	enzyme regulator activity	68	1.2E-42
	GO:0005102	receptor binding	61	4.8E-39
	GO:0005515	protein binding	93	1.0E-08

Table A4. Gene models in genome-wide outlier regions with Ha/Hs > 1. Number of samples considered (*n*), length of the coding region, total number of substitutions, and within-genome heterozygosity at nonsynonymous sites (Ha) relative to synonymous sites (Hs) are reported as averages across all considered samples.

Gene	***n***	**bp**	**Subs**	**Ha/ Hs**	**Description**
AIPGENE16775	1	336	6	>5	
AIPGENE22607	2	924	5	>5	Testis-specific DMRT1
AIPGENE7567	4	786	7.8	4.25	Uncharacterized protein
AIPGENE21797	3	504	6.3	3.56	
AIPGENE15560	1	1464	14	2.34	Reverse transcriptase
AIPGENE7644	2	1694	7	2.31	Uncharacterized protein
AIPGENE20061	6	756	6.8	2.14	
AIPGENE16773	1	648	7	2.04	Putative uncharacterized protein
AIPGENE22611	1	774	6	2.01	Putative uncharacterized protein
AIPGENE7575	3	1166	8.3	1.93	Uncharacterized protein
AIPGENE9404	7	939	16.1	1.93	Uncharacterized protein
AIPGENE9426	5	1878	10.2	1.92	Putative uncharacterized protein
AIPGENE7656	1	1596	6	1.80	Predicted protein
AIPGENE20733	2	2226	12.5	1.50	hypothetical protein [Nematostella vectensis]
AIPGENE21800	4	1255	10.8	1.50	Uncharacterized protein
AIPGENE2444	1	1239	5	1.50	BRO1 domain-containing protein BROX
AIPGENE21801	2	879	5	1.49	hypothetical protein [Crassostrea gigas]
AIPGENE20770	2	2301	5.5	1.38	Predicted protein
AIPGENE20151	2	714	5	1.37	Bcl-2-related ovarian killer protein
AIPGENE1620	1	3609	6	1.33	Transient receptor potential cation channel subfamily A member 1
AIPGENE22584	4	1854	9	1.28	Probable RNA-directed DNA polymerase from transposon X-element
AIPGENE16694	1	606	5	1.24	
AIPGENE2488	1	1341	14	1.21	GRB2-associated and regulator of MAPK protein-like
AIPGENE10506	1	2868	5	1.20	Uncharacterized protein
AIPGENE16595	6	654	8.5	1.18	
AIPGENE16763	3	865	8.7	1.18	Predicted protein
AIPGENE16562	2	3735	11	1.15	Uncharacterized protein

Table A4 (Continued)

AIPGENE7603	2	2126	8.5	1.12	Peptidase M20 domain-containing protein 2
AIPGENE25671	3	1926	7.7	1.11	Predicted protein
AIPGENE9411	7	576	7.6	1.08	
AIPGENE9417	1	1203	6	1.06	hypothetical protein [Crassostrea gigas]
AIPGENE16689	5	1473	9.4	1.04	LINE-1 retrotransposable element ORF2 protein
AIPGENE17747	2	672	5.5	1.04	Uncharacterized protein C17orf59 homolog
AIPGENE16765	5	3122	13.8	1.00	uncharacterized protein [Strongylocentrotus purpuratus]

Table A5. Gene models on scaffold 72, in regions with elevated heterozygosity, pairwise nucleotide diversity, or Tajima's D (>2SD from mean).

Gene	Description
Position 100,000-260,000: Hw (0.49); π (574); Tajima's D: (0.29)	
AIPGENE16026	Fibroblast growth factor receptor 3
AIPGENE16028	Potassium voltage-gated channel protein Shal
AIPGENE16030	Fibroblast growth factor receptor 4
AIPGENE16031	ATP-dependent DNA helicase PIF1
AIPGENE16035	Eukaryotic peptide chain release factor subunit 1
AIPGENE16047	Fibroblast growth factor receptor 1
AIPGENE16048	PREDICTED: uncharacterized protein LOC100212441 [Hydra vulgaris]
AIPGENE16056	Fibroblast growth factor receptor 2
AIPGENE16061	Fibroblast growth factor receptor 2
AIPGENE16071	Acid-sensing ion channel 3
AIPGENE16076	Cytosolic purine 5'-nucleotidase
Position 350,000-540,000: Hw (0.35); π (734); Tajima's D: (0.12)	
AIPGENE16015	Protein sprouty homolog 2
AIPGENE16019	Fibroblast growth factor receptor 3
AIPGENE16020	Fibroblast growth factor receptor 3
AIPGENE16021	
AIPGENE16024	Protein sprouty homolog 2
AIPGENE16025	Protein sprouty homolog 2
AIPGENE16029	predicted protein [Nematostella vectensis]
AIPGENE16032	Angiopoietin-4
AIPGENE16036	Poly(U)-binding-splicing factor PUF60
AIPGENE16037	Poly(U)-binding-splicing factor PUF60
AIPGENE16039	Protein O-linked-mannose beta-1,2-N-acetylglucosaminyltransferase 1
AIPGENE16042	Protein O-linked-mannose beta-1,2-N-acetylglucosaminyltransferase 1
AIPGENE16049	predicted protein [Nematostella vectensis]
AIPGENE16050	Fibroblast growth factor 1 (Fragment)
AIPGENE16051	Fibroblast growth factor 17
AIPGENE16065	Fibroblast growth factor 8
AIPGENE16066	Putative transmembrane protein
AIPGENE16073	RING finger protein 145
AIPGENE16077	Glutaredoxin-3

APPENDIX B: Supplementary tables for Chapter 3

Table B1. Genotyping of *Aiptasia* host strains based on six nuclear genes. Heterozygosity *(H)* is reported as the average fraction of heterozygous genotypes per polymorphic site.

Gene	Annotation	Primer sequences	Amplicon (bp)	Alignment (bp)	SNPs	*H*
AIPGENE25508	Cadherin, EGF LAG seven-pass G-type receptor 3 (CELSR3)	5'-CCAACGCTACAGGATATACG-3' 5'-ACCGTTACTATCACAGAGGC-3'	529	466	5	0.20
AIPGENE19740	Adrenergic receptor, beta 1 (ADRB1)	5'-AGTCAGAGCGCTTTTAATCC-3' 5'-TCAGTGTTGTATGCCGAATC-3'	513	348	10	0.37
AIPGENE9245	Patched-domain containing protein 2 (PTCHD2)	5'-TCACTCATGTCAGCGAAATG-3' 5'-AACCGTTATCCACAAACCAG-3'	858	760	20	0.22
AIPGENE18961	Calcium-sensing receptor	5'-CATTGGACGCATTAACAACG-3' 5'-CAGAAGTTCTCCCACCAATG-3'	843	746	13	0.35
AIPGENE19577	Atrophin-1 interacting protein 1 (AIP1)	5'-ATTTCCGTGTTTCTGGTCAG-3' 5'-TAAGCGTTAGAAAATCCGGC-3'	690	545	11	0.32
AIPGENE26625	A disintegrin and metalloproteinase with thrombospondin motifs 17 (ADAMTS17)	5'-GCTGTCCCCTCAATAGAACC-3' 5'-GGGCTTCAGTTTCTTTGGTC-3'	625	567	26	0.21

Table B2. Analysis of raw fluorescence measurements in controls. *P*-values lower than the significance threshold of 0.01 are bolded and italicized.

	Estimate	**Std. Error**	**t-value**	***P*-value**
Intercept	43.21	1.55	27.78	***<0.001***
Day				
10	0.44	0.66	0.66	0.51
13	0.76	0.67	1.15	0.25
18	-7.53	0.60	-12.60	***<0.001***
Region				
Tentacle	-6.19	1.13	-5.47	***<0.001***
Strain				
FL1	5.23	2.18	2.42	0.02
UN1	3.06	2.18	1.40	0.16
HI1	3.69	2.12	1.73	0.08
H2	3.62	2.16	1.67	0.09
FL2	-1.46	2.16	-0.68	0.50
Region:Strain				
Tentacle:FL1	-9.45	1.61	-5.88	***<0.001***
Tentacle:UN1	-9.04	1.58	-5.78	***<0.001***
Tentacle:HI1	5.36	1.74	3.08	***0.002***
Tentacle:H2	-5.81	1.61	-3.61	***<0.001***
Tentacle:FL2	-5.25	1.50	-3.49	***<0.001***

APPENDIX C: Supplementary material for Chapter 4

Sample storage and processing

Anemones were collected from Galeta between 15 July 2015 and 19 July 2015 and from sites in Bocas del Toro between 30 August 2015 and 11 September 2015. Anemones were kept alive until sample processing at Naos Island Laboratories (Panama City, Panama) or the Bocas del Toro Research Station (Colon Island, Panama) that occurred within one week of sample collection. After homogenization in 200 uL Buffer EB (Qiagen, Valencia, CA, USA) with a motorized tissue grinder and sterile polypropylene pestle, 100-uL of tissue homogenate was combined with 180 uL Buffer ATL and 20 uL Proteinase K (DNeasy Blood and Tissue Kit, Qiagen, Valencia, CA). Samples were digested at 56°C in a water bath according to the manufacturer's instructions. After digestion, tissue lysates are stable at room temperature for up to 6 months, and tissue lysates were transported from Panama to Oregon State University (Corvallis, OR, USA) before resuming the DNA extraction protocol. Extracted DNA was stored at -20°C for ~8 months before genomic library preparation.

Tissue homogenate not aliquoted for DNA extraction was used for determination of algal cell density and mitotic index. Algal cells were pelleted by centrifugation at 5,000 g for 3 minutes. Pellets were resuspended in 500 uL filtered seawater (FSW) and centrifuged once again. The algal pellet and the combined supernatant were frozen for later determination of protein content, algal cell number, and mitotic index.

Determination of algal cell density and mitotic index

Cell counts were performed following a protocol available from the Weis Lab at Oregon State University (OSU) (http://people.oregonstate.edu/~weisv/assets/cellcounts.pdf). Briefly, algal pellets were thawed and resuspended in 500 uL FSW. In most cases, an aliquot of the sample had to be further diluted with FSW to give a final concentration of ~25 cells per 1 square millimeter. A glass Pasteur pipette was used to load samples into a Bright-Line Improved Neubauer hemacytometer (Hausser Scientific, Horsham, PA, USA), rinsing the pipette three times between samples with FSW and re-mixing each sample before loading

the next replicate. Six replicate counts were performed for each sample, and the number of cells, squares counted, and dividing cells were recorded. Counts were performed on an Olympus BH-2 light microscope with the 20x objective lens (Galeta samples) or on a Nikon Eclipse E200 light microscope with the 10x objective lens (Bocas samples). Cell concentration for each replicate was calculated as follows, where *N* is the total number of cells counted:

$$\frac{N \text{ cells}}{\text{squares counted}} \; x \; \frac{\text{total vol. of } 2^{\text{nd}} \text{ dilution}}{\text{sample aliquot for } 2^{\text{nd}} \text{ dilution}} \; x \; 10 = \# \text{ cells}/\mu\text{L}$$

The cell concentration was multiplied by the total volume of the supernatant to determine the total number of cells in the pellet.

To account for differences in size among anemones, the total number of cells was normalized to total protein. Protein content in the supernatant was determined using the Pierce BCA Protein Assay according to the manufacturer's instructions (Thermo Scientific, Rockford, IL, USA). Absorbance at 562 nm was measured for all samples in duplicate using the Genesys 20 Spectrophotometer (Thermo Scientific, Rockford, IL, USA) at the STRI Bocas del Toro Research Station (Colon Island, Panama). Cell densities were analyzed using a generalized linear model with the Gamma distribution and identity link function in R.

Mitotic indices (MI) were measured as the number of dividing cells per total number of counted cells for each replicate count. MI was analyzed using a generalized linear mixed model with the binomial distribution and logit link function implemented with the 'glmer' function of the 'lme4' package in R. Site was included as the explanatory variable with a random effect of sample ID to take into account replicate counts (n=6) from the same anemone. Site was a significant predictor of MI (p<0.001, LRT for comparison of full vs. intercept only model). *Post hoc* comparisons were performed using the 'glht' function of the 'multcomp' package.

Preparation of 2bRAD libraries

Preparation of 2bRAD genomic libraries followed the protocol available from the Meyer lab at OSU (http://people.oregonstate.edu/~meyere/docs/2bRAD_25Aug2016.pdf) and described here. This protocol involves three stages: digestion of DNA with a type IIb restriction enzyme, adaptor ligation, and amplification and barcoding of libraries via PCR. DNA was quantified before digestion using the AccuBlue BroadRange dsDNA Quantitation Kit (Biotium, Inc., Fremont, CA, USA).

To perform DNA digests, 1.2 μg of DNA was concentrated into 8 μL by ethanol precipitation and combined with 4 μL of a digestion master mix comprising 1.2 μL Buffer 3.1, 0.8 μL 150 μM SAM, 0.5 μL BcgI (2 U/μL, New England BioLabs, Ipswich, MA, USA), and 1.5 μL nuclease-free water (NFW). Reactions were incubated for 4 hours at 37°C, and *BcgI* was heat-inactivated at 65°C for 20 minutes.

To ligate partially double stranded adaptors to 36 bp fragments generated by *BcgI*, 2μM adaptors were prepared by annealing oligonucleotides 5ILL-NN (5'-CTA CAC GAC GCT CTT CCG ATC TNN-3') and anti-ILL (5'-AGA TCG GAA GAG C[inverted dT]-3') or 3ILL-NN (5'-CAG ACG TGT GCT CTT CCG ATC TNN-3') and anti-ILL. Adaptors were annealed for 10 minutes at room temperature before combining 10 μL of digested DNA with 40 μL of the ligation master mix comprising 1 μL 10 mM rATP, 4 μL 10x T4 ligase buffer, 5 μL Adaptor 1, 5 μL Adaptor 2, 1 μL T4 ligase (400 U/μL, New England BioLabs, Ipswich, MA, USA), and 24 μL NFW. Ligations were performed overnight at 16°C.

Individual libraries were then amplified and barcoded during PCR. Dual barcodes were introduced using sample specific oligonucleotides (5'-CAA GCA GAA GAC GGC ATA CGA GAT[BC]GTG ACT GGA GTT CAG ACG TGT GCT CTT CCG AC-3' and 5'-TGA TAC GGC GAC CAC CGA GAT CTA CAC[BC]ACA CTC TTT CCC TAC ACG ACG CTC TTC CGA TCT-3') and ligation products were amplified by combining 5 μL of each barcoded oligonucleotide with 40 μL ligation product and 50 μL PCR master mix comprising 23 μL NFW, 2 μL 10 mM dNTPs, 2 μL each of the universal primers ILL-Lib1 (10 μM, 5'- AAT GAT ACG GCG ACC ACC GA-3') and ILL-Lib2 (10 μM, 5'-CAA GCA GAA GAC GGC ATA CGA-3'), 20 μL 5x Q5 buffer, and 1 μL

Q5 High-Fidelity Polymerase (New England BioLabs, Ipswich, MA, USA). Amplification was performed for 18 cycles using the following profile: 98°C for 5 s, 60°C for 20 s, 72°C for 10 s. PCR products were run on a 2% agarose gel in a 1x sodium borate buffer containing 1 mM EDTA at 220 V for 60 minutes. The target band of 166 bp was cut from the gel and extracted with 40 μL of NFW added to the microcentrifuge tube containing the gel slice. Gel slices were incubated overnight at -80°C and then centrifuged for 20 minutes at 4°C at max speed, and the supernatant extracted while pushing the gel slice against the wall of the tube with a pipet tip.

Individual libraries were quantified via qPCR with the SensiFast SYBR Hi-Rox Kit (Bioline, London, UK) and pooled at equimolar quantities. The pooled library was concentrated with the QiaQuick PCR Purification Kit (Qiagen, Valencia, CA, USA) and sequenced as a single-end 37 bp run in high output mode on the NextSeq 500 at the University of Oregon Genomics and Cell Characterization Core Facility (Eugene, OR).

Genotyping

Genotype calling was performed for 2bRAD data as previously described (Wang *et al.* 2012) using scripts available from the Meyer lab at OSU except where indicated (https://github.com/Eli-Meyer/2brad_utilities/tree/v2.0). Reads were trimmed from 38 bp to 36 bp to remove adaptor sequence with 'fastx_trimmer' (http://hannonlab.cshl.edu/fastx_toolkit). To enable comparisons with previously studied lab strains, we also performed *in silico* digestion of 100 bp paired-end reads previously generated for low-coverage whole genome sequencing of 10 *Aiptasia* strains (Bellis *et al.*, 2016; BcgIDigestFastq.pl script from https://github.com/em-bellis/PanamaPopGen/). Reads for which less than 83% of called bases had Phred quality scores less than 28 were removed with 'fastq_quality_filter' (http://hannonlab.cshl.edu/fastx_toolkit). Phred quality scores were consistently low at the six invariant bases of the *BcgI* recognition site ($[N_{10}]CGA[N_6]TGC[N_{12}]$); the fastq filtering parameters allowed for low quality at the six invariant bases of the recognition motif, but required high quality at all remaining 30 sites in the read. Low quality at the six invariant sites was associated with a substantial number of miscalled bases at positions 15, 22, and 23 in the read, where median quality

was lowest. To improve mapping of reads with miscalled bases at the recognition site, we masked bases at positions 13-15 and 22-24 by bioinformatically changing them to the correct recognition sequence if the correct bases were observed at positions 13 and 14 or at positions 13 and 24. Reads that didn't meet these criteria were left unaltered (FixBcgIRecognitionSites.pl from https://github.com/em-bellis/PanamaPopGen/). Before masking, an average of 10.9% of reads from each sample matched the recognition motif exactly. Masking increased the number of reads with exact matches to the recognition motif to 82.7%

After read processing and filtering, reads were aligned to the set of 44,428 *BcgI* recognition sites present in the *Aiptasia* reference genome v1.0 (Baumgarten *et al.* 2015). Mapping was performed using Shrimp v2.2.2, and alignments were filtered to remove ambiguous alignments or weak matches (alignment length < 32 bp or < 30 matching bases). Samples were genotyped as heterozygotes if the minor allele frequency (MAF) at the locus exceeded 30% or as homozygotes if the minor allele frequency at the locus was less than 5%; genotypes with MAF between 5% and 30% or coverage below the thresholds of 5x, 10x, or 15x were not called. Sample BTCA44 was excluded from the final dataset due to low sequencing coverage. Samples CAPG1 and CAPGB4 were also excluded because very few reads from these individuals (<1%) mapped to the reference with high confidence. Sites were excluded if they were not polymorphic in at least 4 individuals (MinPolyFilter.pl from https://github.com/em-bellis/PanamaPopGen/), if there were more than 2 polymorphisms observed within the same 36 bp tag, or if they were genotyped in less than 80% of individuals.

Individuals identified as *E. brasiliensis* were confirmed by sequencing a 3164 bp region of mitochondrial DNA that included the 16S ribosomal RNA (*16S rRNA*) and cytochrome c oxidase subunit III (*COIII)* genes. The region was amplified using oligonucleotides MslrRNA-F (5'-CTGGAAACTGAAACATCTAAGTACC-3') and ApCOI_5-R (5'-TCATTCCAGAACCTATTCCAAA-3') each at a final concentration of 0.4 μM in a 50 μL reaction volumes containing 1 μL DMSO, 10 μL reaction buffer, and 0.25 μL MyTaq DNA Polymerase (Bioline, London, UK). A PCR cycling protocol optimized for amplification of long DNA products was used: 10 cycles of 92°C for 10 s,

55°C for 20 s, and 60°C for 10 m followed by 25 cycles of 92°C for 10 s, 55°C for 20 s, and 60°C for 10 m + 10 s/cycle. PCR products were sequenced on the ABI 3730 capillary sequencer at the Center for Genome Research and Biocomputing at Oregon State University (Corvallis, OR) with oligonucleotides MslrRNA-F, ApCOI_5-R, and internal sequencing primers ApCOIII-R (5'-AGACCTTGGAAAGTTGCCTCT-3') and AplRNA-R (5'-AAGCTCACCTTCGTTACCTTT-3'). Phylogenetic trees were inferred using the Maximum Likelihood method and the General Time Reversible model assuming uniform substitution rates in MEGA5 with 1,000 bootstrap replications.

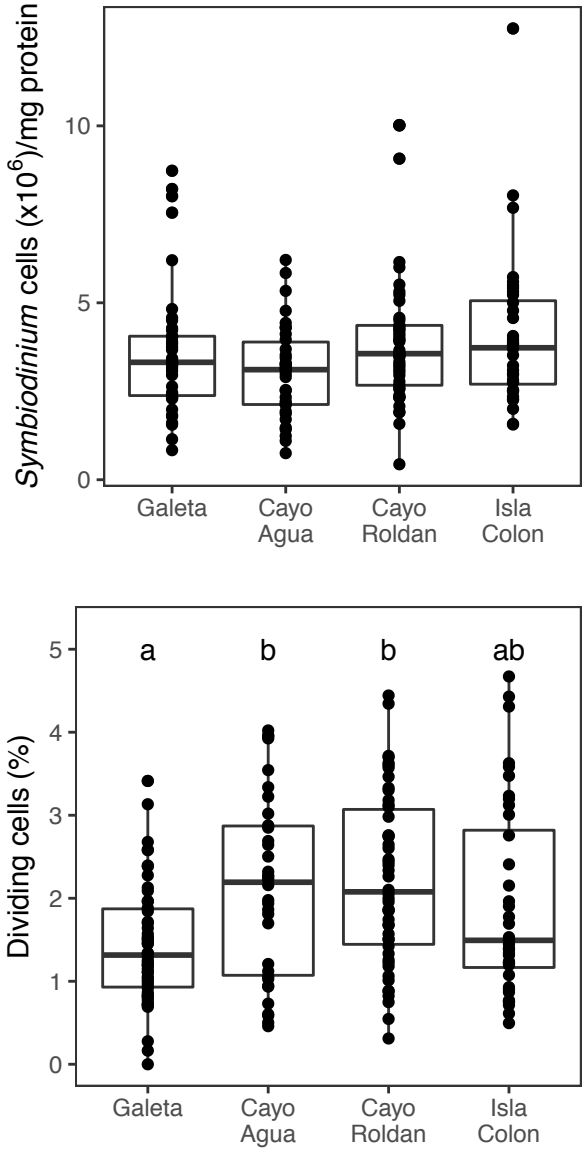

Fig. C1. Differences in *Symbiodinium* cell density and mitotic index among sites. Strong evidence for significant differences in *Symbiodinium* density (top) among sites was not observed (P=0.08, GLM). In contrast, site was a significant predictor of mitotic index (bottom panel, P<0.001, GLMM), with evidence for lower *Symbiodinium* division rates in anemones from Galeta compared to Cayo Roldan (P<0.001, Tukey HSD) and Cayo de Agua (P=0.014, Tukey HSD).

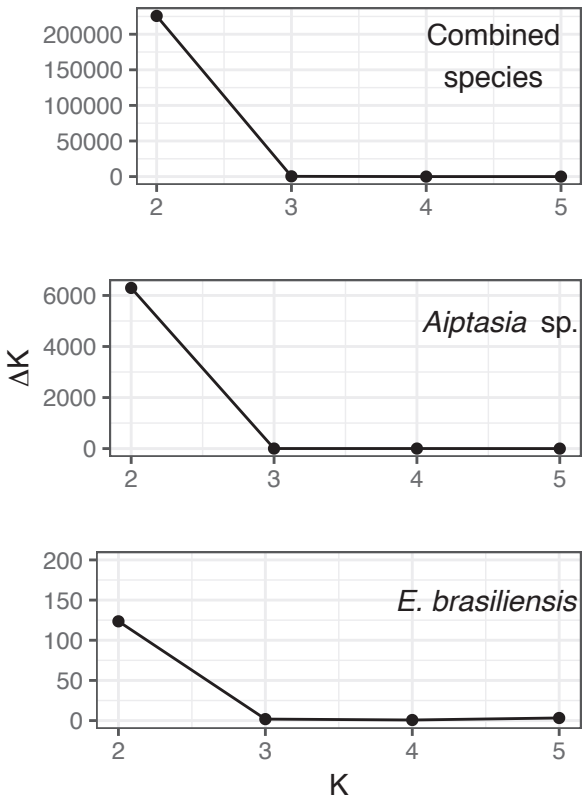

Fig. C2. Optimal K value for STRUCTURE analyses via the Evanno method. Shown are analyses from the 10x SNP dataset.

Table C1. Summary of SNP callsets. Number of individuals genotyped (*N*) and SNPs passing all quality filters is given, as well as the proportion of SNPs present in introns, coding DNA sequence (CDS), five-prime untranslated regions (5'UTR), and three-prime untranslated regions (3'UTR).

Callset	*N*	SNPs	SNPs in introns	SNPs in CDS	SNPs in 5'UTR	SNPS in 3'UTR
Combined sp.						
15x	162	1474	360 (24%)	627 (43%)	50 (3%)	97 (7%)
10x	162	2991	731 (24%)	1223 (41%)	114 (4%)	187 (6%)
5x	162	5391	1399 (26%)	2042 (38%)	224 (4%)	357 (7%)
***Aiptasia* sp.**						
15x	127	1160	360 (31%)	462 (40%)	44 (4%)	106 (9%)
10x	127	2538	730 (29%)	849 (33%)	96 (4%)	194 (8%)
5x	127	4640	1384 (30%)	1412 (30%)	198 (4%)	346 (7%)
E. brasiliensis						
15x	35	715	181 (25%)	265 (37%)	31 (4%)	51 (7%)
10x	35	1257	336 (27%)	448 (37%)	53 (4%)	84 (7%)
5x	35	2035	558 (27%)	712 (35%)	86 (4%)	137 (7%)

Table C2. Gene models containing SNPs highly differentiated between *Aiptasia* global and Bocas-specific populations (95th percentile of F_{ST} values in 5x dataset).

Scaffold	Position	F_{ST}	Annotation
scaffold31size936128	720251	0.84	Elongation_factor_Tu_GTP-binding_domain-containing_protein_1
scaffold10size1280550	1258482	0.83	Myoferlin
scaffold40size871389	594914	0.81	Putative_uncharacterized_protein
scaffold90size632433	396456	0.81	Laminin_subunit_gamma-1
scaffold227size359198	50641	0.80	Peptide-N(4)-(N-acetyl-beta-glucosaminyl)asparagine_amidase
scaffold60size753757	564146	0.79	Cytoplasmic_FMR1-interacting_protein_2
scaffold30size940304	213507	0.76	N-acetyl-beta-glucosaminyl-glycoprotein_4-beta-N-acetylgalactosaminyltransferase_1
scaffold432size172134	42801	0.76	Photoreceptor-specific_nuclear_receptor
scaffold280size295080	116748	0.75	Lactadherin
scaffold453size156515	106895	0.74	Diencephalon/mesencephalon_homeobox_protein_1-B
scaffold46size824853	59254	0.74	EGF-like_repeat_and_discoidin_I-like_domain-containing_protein_3
scaffold125size537866	76178	0.74	Oxysterol-binding_protein-related_protein_8
scaffold3size1550370	50411	0.74	Orexin_receptor_type_1
scaffold2size2342127	893481	0.72	von_Willebrand_factor_A_domain-containing_protein_5A
scaffold663size70006	48177	0.72	Putative_uncharacterized_protein
scaffold40size871389	450609	0.72	Mitochondrial_assembly_of_ribosomal_large_subunit_protein_1
scaffold341size236075	116893	0.72	Tensin
scaffold74size710114	523138	0.71	Metabotropic_glutamate_receptor_4
scaffold58size770527	178714	0.71	Probable_G-protein_coupled_receptor_133
scaffold16size1115347	9732	0.71	E3_ubiquitin-protein_ligase_RNF25
scaffold39size882683	520493	0.71	Formate_acetyltransferase_2
scaffold101size600899	516091	0.71	Substance-K_receptor
scaffold20size1056720	751284	0.71	Uncharacterized_protein
scaffold551size110876	15960	0.70	Thyrotropin-releasing_hormone_receptor
scaffold105size588288	237954	0.69	Disintegrin_and_metalloproteinase_domain-containing_protein_9
scaffold161size448273	297389	0.69	GDP-D-glucose_phosphorylase_1
scaffold33size924377	893709	0.68	Neuropilin-2
scaffold74size710114	611125	0.68	Probable_ATP-dependent_RNA_helicase_DHX34
scaffold10size1280550	1240651	0.67	Uncharacterized_protein
scaffold13size1176135	996795	0.67	Brain-specific_angiogenesis_inhibitor_3
scaffold2756size2234	418	0.67	Predicted_protein_(Fragment)
scaffold425size176235	85710	0.67	Tenascin-X
scaffold38size893299	659214	0.66	V-type_proton_ATPase_116_kDa_subunit_a_isoform_1

Table C2 (Continued)

scaffold119size550493	433316	0.66	Putative_adenosylhomocysteinase_3
scaffold457size153498	132984	0.66	PR_domain_zinc_finger_protein_13
scaffold95size625746	198238	0.66	Putative_uncharacterized_protein
scaffold74size710114	403803	0.66	Kinesin-like_protein_FLA10
scaffold235size354650	129978	0.66	Capsule_biosynthesis_protein_CapA
scaffold14size1146941	1134617	0.65	BRCA2_and_CDKN1A-interacting_protein
scaffold364size252640	178306	0.64	Uncharacterized_protein
scaffold549size113263	53076	0.64	C3_and_PZP-like_alpha-2-macroglobulin_domain-containing_protein_8
scaffold15size1141927	273790	0.64	Titin
scaffold121size546648	359869	0.63	Zinc_finger_protein_ZIC_1
scaffold31size936128	667943	0.62	Helicase-like_transcription_factor
scaffold237size353065	154289	0.62	Noggin
scaffold23size1048345	150279	0.62	Probable_serine_incorporator
scaffold2size2342127	1595437	0.61	Ribonuclease_Oy
scaffold36size913768	395839	0.61	Pre-mRNA_3'-end-processing_factor_FIP1
scaffold309size265292	177100	0.61	Potassium_voltage-gated_channel_subfamily_A_member_5
scaffold93size630182	99433	0.61	Nematocyst_outer_wall_antigen
scaffold237size353065	192071	0.60	Uncharacterized_protein
scaffold255size330100	113121	0.60	Fibrous_sheath-interacting_protein_1
scaffold236size353755	249846	0.59	Armadillo_repeat-containing_protein_4
scaffold104size796845	423511	0.58	Arginine_kinase
scaffold113size572466	135083	0.58	Sodium/potassium-transporting_ATPase_subunit_alpha
scaffold309size265292	34012	0.58	Ankyrin_repeat_and_SOCS_box_protein_7
scaffold7size1443125	1291447	0.58	Retrovirus-related_Pol_polyprotein_from_transposon_TNT_1-94
scaffold69size1084271	382368	0.58	SWI/SNF-related_matrix-associated_actin-dependent_regulator_of_chromatin_subfamily_E_member_1
scaffold52size862905	81855	0.57	Dedicator_of_cytokinesis_protein_1
scaffold309size265292	34198	0.57	Ankyrin_repeat_and_SOCS_box_protein_7
scaffold66size737514	255991	0.57	Phosphatidylinositide_phosphatase_SAC2
scaffold241size349998	275972	0.57	Phosphopantothenate--cysteine_ligase
scaffold368size290937	274556	0.57	Major_facilitator_superfamily_domain-containing_protein_12
scaffold182size421695	188340	0.57	Sushi,_von_Willebrand_factor_type_A,_EGF_and_pentraxin_domain-containing_protein_1
scaffold227size359198	80820	0.56	Sushi,_von_Willebrand_factor_type_A,_EGF_and_pentraxin_domain-containing_protein_1
scaffold97size618721	393983	0.56	Armadillo_repeat-containing_protein_6
scaffold357size223317	178503	0.56	Uncharacterized_protein

Table C2 (Continued)

scaffold368size290937	257780	0.55	Synapsin-3
scaffold8size1436206	41371	0.55	Uncharacterized_protein_C17orf97_homolog
scaffold9size1394036	1132244	0.55	Hemicentin-1
scaffold34size915982	806855	0.55	Protein_transport_protein_Sec31A
scaffold46size824853	714818	0.55	N-acetyl-beta-glucosaminyl-glycoprotein_4-beta-N-acetylgalactosaminyltransferase_1
scaffold391size200042	164868	0.54	Mucin-17
scaffold64size745175	575103	0.54	Usher_syndrome_type-1G_protein
scaffold15size1141927	75970	0.53	Alpha-1,6-mannosylglycoprotein_6-beta-N-acetylglucosaminyltransferase_A
scaffold66size737514	703121	0.53	Sterile_alpha_motif_domain-containing_protein_9-like
scaffold15size1141927	269446	0.52	Titin
scaffold41size867863	683737	0.52	Tiggy-winkle_hedgehog_protein
scaffold139size486224	301576	0.52	Contactin-associated_protein_1
scaffold74size710114	437598	0.52	Golgi-associated_plant_pathogenesis-related_protein_1
scaffold50size812239	613083	0.52	Tetratricopeptide_repeat_protein_28
scaffold473size145179	40026	0.52	Predicted_protein
scaffold182size421695	187663	0.52	Sushi,_von_Willebrand_factor_type_A,_EGF_and_pentraxin_domain-containing_protein_1
scaffold287size288319	110487	0.52	SERTA_domain-containing_protein_2
scaffold423size179430	86854	0.51	Low-density_lipoprotein_receptor-related_protein_4
scaffold35size915306	121570	0.51	Xaa-Pro_aminopeptidase_1
scaffold225size362265	189670	0.51	Double_zinc_ribbon_and_ankyrin_repeat-containing_protein_1
scaffold369size229073	167592	0.51	Activating_signal_cointegrator_1_complex_subunit_3
scaffold318size259462	207392	0.51	Substance-P_receptor
scaffold101size600899	300223	0.50	Tyrosinase
scaffold285size292703	129780	0.50	Golgi-associated_plant_pathogenesis-related_protein_1
scaffold1size1833262	804109	0.50	Ubiquitin-conjugating_enzyme_E2_H
scaffold5size1497922	788153	0.50	Synaptonemal_complex_protein_3
scaffold4389size1185	323	0.49	Predicted_protein
scaffold33size924377	761290	0.49	Versican_core_protein
scaffold41size867863	679809	0.49	Tiggy-winkle_hedgehog_protein
scaffold90size632433	100854	0.49	Complement_C3_(Fragment)
scaffold59size754371	377381	0.48	Lactadherin
scaffold304size274614	121864	0.48	Tetratricopeptide_repeat_protein_28
scaffold255size330100	296532	0.48	Predicted_protein
scaffold4050size1311	1275	0.48	Guanine_deaminase
scaffold74size710114	609742	0.48	Probable_ATP-dependent_RNA_helicase_DHX34
scaffold241size349998	295073	0.48	Phosphopantothenate--cysteine_ligase
scaffold28size967684	719528	0.47	Gamma-glutamyl_hydrolase

Table C2 (Continued)

scaffold32size935796	161937	0.47	A_disintegrin_and_metalloproteinase_with_thrombospondin_motifs_6
scaffold75size706631	366636	0.47	Fibrillin-1
scaffold322size257171	12177	0.47	Translation_initiation_factor_IF-2
scaffold368size290937	252338	0.47	Tissue_inhibitor_of_metalloproteases
scaffold23size1048345	340249	0.47	Transient_receptor_potential_cation_channel_subfamily_A_member_1
scaffold75size706631	100658	0.47	Nuclear_protein_MDM1
scaffold46size824853	273776	0.47	Potassium_voltage-gated_channel_subfamily_F_member_1
scaffold291size284740	200631	0.46	Nematocyte_expressed_protein_6
scaffold335size243503	183555	0.46	Myotubularin-related_protein_5
scaffold162size446422	374819	0.45	LD08471p
scaffold60size753757	347830	0.45	Krueppel-like_factor_12
scaffold904size24990	19619	0.44	Protein_Jumonji
scaffold50size812239	439485	0.44	Latrophilin-1
scaffold8size1436206	1336982	0.44	RNA-dependent_RNA_polymerase_2
scaffold317size260744	241229	0.44	WD_repeat-containing_and_planar_cell_polarity_effector_protein_fritz_homolog
scaffold41size867863	771487	0.44	Protein_rolling_stone
scaffold1698size6018	1118	0.44	Neuronal_acetylcholine_receptor_subunit_alpha-9
scaffold823size33281	20465	0.44	Predicted_protein
scaffold238size352562	153728	0.44	Unconventional_myosin-XV
scaffold320size257358	147389	0.44	G-protein_coupled_receptor_126
scaffold331size247803	85991	0.44	Endothelin-converting_enzyme_1
scaffold374size211550	134246	0.43	Uncharacterized_GTP-binding_protein_YGR210C
scaffold32size935796	123333	0.43	A_disintegrin_and_metalloproteinase_with_thrombospondin_motifs_6
scaffold566size105323	49015	0.43	Predicted_protein
scaffold260size320762	76967	0.43	von_Willebrand_factor_A_domain-containing_protein_3A
scaffold190size412162	164440	0.43	Synaptotagmin-C